Towards new treatments for hereditary photoreceptor degeneration: Pharmacological and genetic approaches to restore Ca^{2+} homeostasis and Pde6a function

Dissertation
zur Erlangung des Grades eines Doktors der Naturwissenschaften
der Mathematisch-Naturwissenschaftlichen Fakultät und der Medizinischen Fakultät
der Eberhard-Karls-Universität Tübingen

vorgelegt von
Soumyaparna Das
aus Kolkata, Indien

Tübingen
December 2020

Tag der mündlichen Prüfung: 24.03.2021

Dekan der Math-Nat. Fakultät: Prof. Dr. Thilo Stehle
Dekan der Medizinischen Fakultät: Prof. Dr. Bernd Pichler

Berichterstatter 1: Prof. Dr. François Paquet-Durand
Berichterstatter 2: Prof. Dr. Bernd Wissinger

Prüfungskommission:
Prof. Dr. François Paquet-Durand
Prof. Dr. Bernd Wissinger
Prof. Dr. Thomas Euler
Prof. Dr. Marlies Knipper

Erklärung/ Declaration

Ich erkläre dass ich die zur Promotion eingereichte Arbeit mit dem Titel "Towards new treatments for hereditary photoreceptor degeneration: Pharmacological and genetic approaches to restore Ca^{2+} homeostasis and Pde6a function" selbständig verfasst, nur die angegebenen Quellen und Hilfsmittel benutzt und wörtlich oder inhaltlich übernommene Stellen als solche gekennzeichnet habe. Ich versichere an Eides statt, dass diese Angaben wahr sind und dass ich nichts verschwiegen habe. Mir ist bekannt, dass die falsche Abgabe einer Versicherung an Eides statt mit Freiheitsstrafe bis zu drei Jahren oder mit Geldstrafe bestraft wird.

I hereby declare that I have produced the work entitled "Towards new treatments for hereditary photoreceptor degeneration: Pharmacological and genetic approaches to restore Ca^{2+} homeostasis and Pde6a function", submitted for the award of a doctorate, on my own (without external help), have used only the sources and aids indicated and have marked passages included from other works, whether verbatim or in content, as such. I swear upon oath that these statements are true and that I have not concealed anything. I am aware that making a false declaration under oath is punishable by a term of imprisonment of up to three years or by a fine.

Tübingen, den 15.12.2020 (Datum/ Date)

(Unterschrift/ Signature)

Happiness is a journey, not a destination

Abstract

Retinitis pigmentosa (RP) is a rare hereditary retinopathy that begins with the loss of peripheral vision and gradually progresses towards the centre causing blindness. The responsible factor behind this pattern is the primary degeneration of rod photoreceptors (rods) followed by the secondary degeneration of cone photoreceptors (cones). About 1 in 4,000 individuals are affected worldwide with no effective cure currently available. RP is genetically very heterogeneous with about 65 causative genes and numerous underlying mutations. In this study, two different RP causing mutations have been investigated to understand the cell death mechanisms and explore possible therapeutic interventions. This work focuses on mutations in phosphodiesterase-6 (PDE6) enzyme, which leads to the elevated accumulation of intracellular cGMP in photoreceptors and in-turn is responsible for high Ca^{2+} influx into the photoreceptors. One of the considered consequences of high Ca^{2+} is photoreceptor degeneration by the activation of Ca^{2+}-dependent cysteine type proteases, calpain. Primarily two approaches were employed to investigate the consequences of the PDE6 mutations: (1) interfering with the downstream cascade following a *Pde6b* mutation. This was achieved by targeting Cyclic Nucleotide Gated Channels (CNGC) and the lowering of intracellular Ca^{2+} concentration and (2) by editing the mutant mRNA of *Pde6a* via site-directed RNA editing to restore functional PDE6A subunit of PDE6 enzyme.

Earlier studies have highlighted that the high Ca^{2+} influx in RP is caused via CNGC, suggesting it as the target candidate for reducing the intracellular Ca^{2+} concentration. This study applied the possibility of reducing intracellular Ca^{2+} concentration by: (A) targeting CNGC using pharmacological inhibition (diltiazem enantiomers and cGMP analogues) and (B) designing Antisense Oligonucleotides (ASO) to down-regulate *Cngb1*. Diltiazem is a well known hypertension drug where L- and D-cis-diltiazem are known to

target CNGC and Voltage Gated Calcium Channels (VGCC) respectively, the two important channels responsible for Ca^{2+} influx in the photoreceptors. To understand the downstream effects of Ca^{2+} channel inhibition, the activity of calpain and Poly(ADP-ribose) Polymerase (PARP) were investigated. Activated PARP uses Nicotinamide Adenine Dinucleotide (NAD^+) and generates Poly (ADP-Ribose) (PAR) polymer as a response to DNA damage during cell death. Thus, PAR was also investigated with the treatment conditions. Further the blocking of VGCC with D-cis-diltiazem showed a lowering of the PARP activity in *rd1* however, blocking CNGC with L-cis-diltiazem increased the PARP activity in wild-type (wt). These indicate that level of intracellular Ca^{2+} could modulate the PARP activity. Lowering of the Ca^{2+} influx via CNGC (L-cis-diltiazem) showed elevated calpain-2 in wt to the level of *rd1* retina but did not change the calpain activity. The inhibition of photoreceptor Ca^{2+} influx via VGCC showed lowered calpain-2 in *rd1*, however showed no change in the calpain activity. Moreover, the photoreceptor degeneration got elevated on CNGC inhibition using L-cis-diltiazem and cGMP analogue (DF156). Thus, the CNGC blocking and inhibition of Ca^{2+} influx via CNGC did not prevent or slow the course of photoreceptor degeneration. Consequences of mutation in PDE6 can also be prevented by replacing it with a functional PDE6. The restoration of functional PDE6A in animal model *Pde6a* V685M was achieved with site-directed RNA editing on the mouse retinal explant cultures. The editing was achieved by using ASO that exploits naturally occurring enzymatic activity of Adenosine Deaminase that acts on RNA (ADAR) in the cell. It acts on the primary transcript (mRNA) to perform site-directed editing and is highly targeted and reversible approach with reduced off-target effects. Site-directed RNA editing in *Pde6a* V685M retinal explants showed expression of PDE6A in retinal histological sections, indicating a possible functional restoration of PDE6A. NAD^+ consumption leads to energy depletion and Glucose transporters help in meeting the energy demand of photoreceptors. The localisation of Glucose Transporter 3 (GLUT 3), a neuronal glucose transporter, was investigated to indicate its possible role in the degeneration. GLUT 3 showed a continuous, but likely a structurally independent expression between OS and IS across the adult mouse retina. Their active role is unclear. Retinal degeneration resulting due to exogenous factors such as, malarial parasite (*Plasmodium berghei*) was investigated on the wt retina. Infiltration of the malarial parasites were found in the neuroretina by crossing the blood-retinal-barrier. Müller cells are likely to play an important role during parasitaemia indicated by their co-localisation with the parasites.

Therefore in the cell death pathway, PARP activity was found to be modulated by Ca^{2+} concentration and photoreceptor degeneration in *rd1* does not appear to be directly influenced by the CNGC Ca^{2+} influx. Importantly, the pharmacological inhibition of CNGC was not protective for degenerating the rod photoreceptors, providing a new insight on *rd1* cell death mechanisms.

Contents

Outline of the Thesis

This thesis is dedicated to investigate: (1) the effects of blocking Cyclic Nucleotide Gated Channels (CNGC) on the photoreceptor degeneration. This has been elucidated by studying downstream components of the degeneration pathway mediated by the high cGMP and the overactivation of CNGC. (2) restoration of functional PDE6A by the site-directed RNA editing, (3) the co-localisation of Glucose Transporter 3 (GLUT 3) expression and (4) murine malarial retinopathy. The outline of the thesis is as follows:

Chapter 1 gives an introduction about the mouse retina and retinal dystrophies leading to retinal degeneration. It discusses one common hypothesis surrounding the degeneration and the existing gap in knowledge, leading to the motivation of our study.

Chapter 2 shows the detailed experimental protocols, methods of analysis and statistical tests followed to obtain the results discussed in the following chapters.

Chapter 3 lays out the effect of Ca^{2+} channel inhibition on the mouse retina and its immediate effect on the Ca^{2+}-dependent cysteine proteases, calpain. Here, two strategies were used to inhibit Ca^{2+} influx via CNGC in the photoreceptors: (1) Antisense Oligonucleotide (ASO) mediated down-regulation of *Cngb1* and (2) pharmacological inhibition of CNGC. It gives the detailed approach taken to design ASO for the down-regulation of *Cngb1* and the challenges in that approach. Pharmacological inhibition was achieved using the enantiomers of diltiazem (D and L). Initially, the inhibition efficacy of D- and L-cis-diltiazem were tested on CNGC subunits and then their effects were assessed on the light-induced cone Ca^{2+} response. Further, the effect of Ca^{2+} channel inhibition on calpain activity and photoreceptor degeneration is discussed. The effect on photoreceptor degeneration was further evaluated with cGMP analogues. This chapter highlights

some key points regarding the role of Ca^{2+} in the photoreceptor degeneration in RP and addresses the reason behind the existing controversy in the literature regarding the block of Ca^{2+} channels in photoreceptors.

Chapter 4 shows the effect of diltiazem enantiomers on Poly (ADP-Ribose) Polymerase (PARP) activity and PARylation. The effect of the modulating intracellular Ca^{2+} concentration in photoreceptors has been shown.

Chapter 5 shows the expression and localisation of GLUT 3 in the adult mouse retina using fluorescent microscopy and Electron Microscopy (EM). The images highlight the localisation of GLUT 3 with respect to other retinal structures to obtain a closer understanding of its probable function in the retina.

Chapter 6 shows the results of ASO application designed for RNA editing to correct a point mutation in *Pde6a* V685M animals using the recruitment of Adenosine Deaminases that act on RNA (ADAR) as a possible therapeutic approach for a specific retinitis pigmentosa mutation. This is the first demonstration of RNA editing in tissue cultures of mouse retina.

Chapter 7 shows activation of Müller cells in malarial retinopathy even after 12 days of administration of anti-malarial treatment. The evidence for malarial parasites in the neuroretina and their interaction with Müller cells is also shown.

Chapter 8 discusses the effectiveness of Ca^{2+} inhibition using diltiazem enantiomers. In wt retina, L-cis-diltiazem was found to reduce light-induced Ca^{2+} responses and Ca^{2+} base level. The possible cellular response that could lead to such effect has been discussed. Further, it examines the possible underlying event that may connect the calpain activity and photoreceptor degeneration in wt and mutant animal models, after blocking the Ca^{2+} permeable channels (CNGC and VGCC). It discusses the effects of such a block on the PARP activity, another major component of photoreceptor degeneration. Finally, the usefulness of targeting the Ca^{2+} channels as a therapeutic strategy for RP has been analysed and puts forth the advanced understanding of the photoreceptor degeneration pathway.

1 Introduction

Inherited retinal degeneration is one of the major causes of blindness with 5.5 million people are expected to be affected worldwide, without any effective cure [Hanany *et al.* 2020]. Retinitis Pigmentosa (RP) is a rare hereditary retinopathy that leads to progressive loss of vision. This thesis explores the effects of degeneration in animal models of RP and addresses disease causing mutations using different therapeutic strategies.

1.1 Organisation of the mouse retina

The retina is a light-sensitive sensory tissue present at the back of the eye, which is arranged in different units based on their functional specialisation. It is an immune privileged structure in the eye with a strong Blood Retinal Barrier (BRB) comparable with the Blood Brain Barrier (BBB) [Trost *et al.* 2016]. This barrier is formed by tight junctions in the Retinal Pigment Epithelium (RPE) cells and Bruch's membrane located below the choriocapilaris, shown in Figure 1.1. The functional units are arranged in three nuclear layers called the Outer Nuclear Layer (ONL), the Inner Nuclear Layer (INL) and the Ganglion Cell Layer (GCL). Two plexiform layers are the Outer Plexiform Layer (OPL) and the Inner Plexiform Layer (IPL) [Hoon *et al.* 2014].

The ONL comprises light-sensitive neurons called photoreceptors, which are the first-order neurons. The INL is composed of Bipolar Cells (BC), Horizontal Cells (HC), and Amacrine Cells (AC) which are second-order neurons. This is followed by ganglion cells located in the GCL, the third-order neurons. The OPL forms the neuronal network between the photoreceptors, bipolar cells and horizontal cells. The INL comprise connection between BC, AC and GCL. Müller glial cells span the retina from the outer limiting membrane to the inner limiting membrane. These cells support the survival of photoreceptors by supplying end products of anaerobic metabolism, phagocytosis of

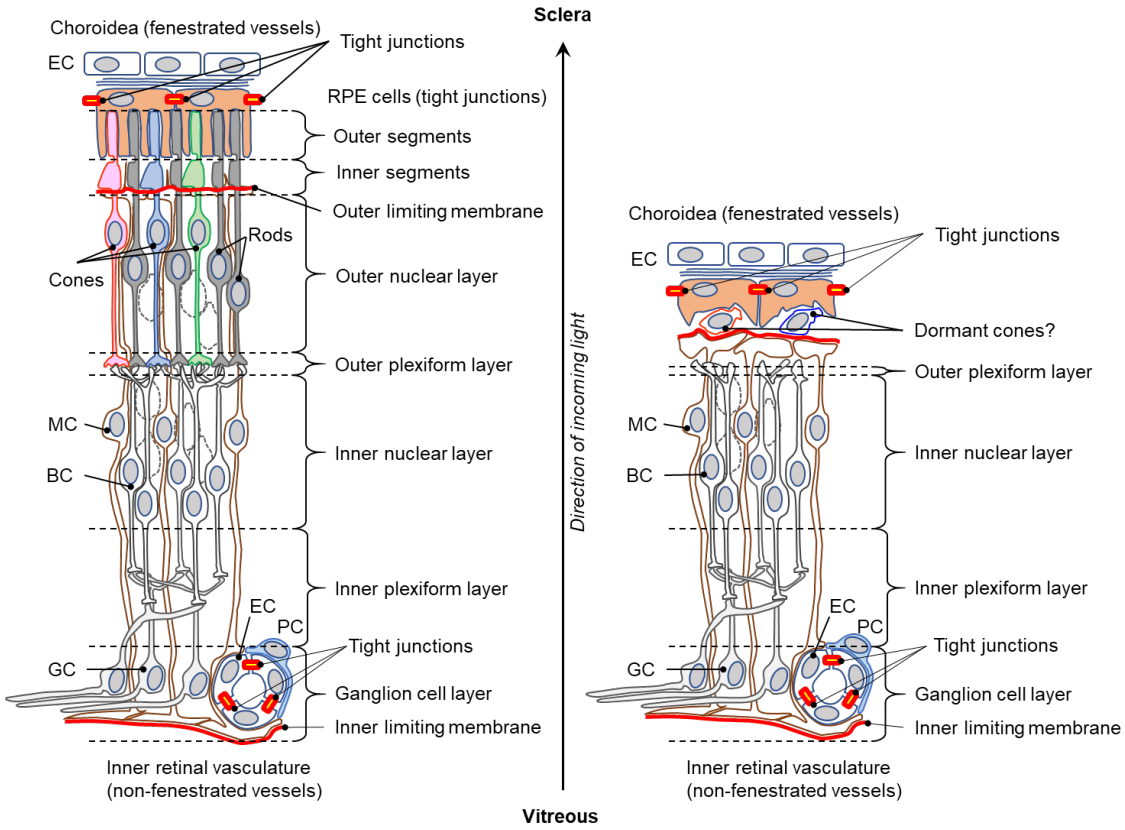

Figure 1.1: **Organisation of retinal layers in healthy and degenerating retina:** The left panel shows the illustration of healthy retina while the right panel shows a degenerated retina. The names of all the retinal layers are labelled on their right and the major cells types are on their left. In the outer retina, fenestrated and choroidal blood vessels are lined up by Endothelial Cells (EC). Retinal Pigment Epithelium (RPE) is present below EC, connected to each other by tight junctions. At the base of the Inner Segment (IS), apical end of Müller cells are present forming the outer limiting membrane. Horizontal Cells (HC), Müller Cells (MC), Bipolar Cells (BC) and Amacrine Cells (AC) are in the INL. The Ganglion Cell Layer (GCL) is located below INL. Adapted from [Power, Das *et al.* 2020].

neural debris, release of neuroactive chemicals and controlling homeostasis of K^+ distribution, to name a few [Reichenbach *et al.* 1995]. A detailed overview is given in Figure 1.1. Photoreceptors are of two different types, rods and cones. Rods are responsible for low light vision and cones are responsible for the bright light and colour vision. In human, cones are classified into three types: red, blue, and green whereas, in mice cones are of two types: blue and green that sense different wavelengths of light in the visual spectrum.

Photoreceptors are highly specialised neurons. Moving from the apical to basal side, they are divided into functional compartments namely the Outer Segment (OS), Inner Segment (IS), cell body, and the synaptic terminal. Microvilli of RPE holds and stabilizes OS of the photoreceptors. These are highly specialised structures with stacks of membranous disks. Disks in the OS are very dynamic structures designed for phototransduction and are recycled constantly by the RPE. A very specialised primary cilium called connecting cilium connects the OS and the IS, which acts as a gateway of transportation for metabolites from the cell body via IS to the OS. The IS of the photoreceptors are rich in mitochondria, endoplasmic reticulum and golgi bodies. These are believed to be metabolically very active structures [Hoon *et al.* 2014]. The outer limiting membrane of the retina formed by tight junctions between the Müller cells and photoreceptors. Müller cells are immunoreactive for Glial Fibrillary Acidic Protein (GFAP) which are highly up-regulated during the degeneration or infection, [Hiscott *et al.* 1984] shown in Figure 7.1. The end-feet of Müller cells are at the basal side of the retina that also has the axons of ganglion cells forming the inner limiting membrane of the retina.

Photoreceptors respond to light via the phototransduction cascade. In dark condition, photoreceptors are in a depolarised state. The Phototransduction cascade is initiated by light (photon) and takes place in the OS photoreceptor disk. Rhodopsin in rods and opsin in cones are the first component of this cascade. Light activates rhodopsin (in rods) converting 11-cis-retinal into all-trans-retinal. The activated rhodopsin further activates transducin. The Phosphodiesterase 6 (PDE6) is further activated by the active transducin in the cascade. PDE6 hydrolyses Cyclic Guanosine MonoPhosphate (cGMP), which in turn closes the Cyclic Nucleotide Gated ion Channels (CNGCs). Closure of CNGC stops the cation influx in photoreceptors (Ca^{2+} and Na^{+}) and results in hyperpolarisation [Burns *et al.* 2014].

1.2 Retinal dystrophies

Among all retinal cell types, photoreceptors are known to be the most vulnerable to genetic aberrations resulting in retinal dystrophies. There are several forms of retinal dystrophies among which Retinitis Pigmentosa (RP) is a rare form of hereditary retinopathy. RP is genetically and clinically very heterogeneous in nature having 1 out of every 4,000 people affected worldwide [Hanany *et al.* 2020]. More than 65 genes (Retinal Information Network database - information retrieved on December 12, 2020) are known to be associated with RP. The associated mutations can be either autosomal dominant, autosomal recessive, or X-linked. All the different mutations affect different components of the photoreceptor degeneration pathway. Moreover, different mutations in one single

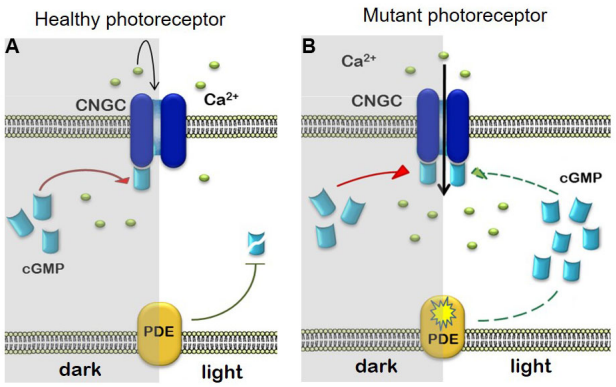

Figure 1.2: **Phototransduction cascade:** Illustration of phototransduction in healthy (A) and mutant (B) situation. (A) shows healthy photoreceptor in darkness (on the left) where cGMP binding has activated CNGC. On the right, it shows the activated PDE in light hydrolysis cGMP. (B) shows mutant photoreceptor with dark situation on the left and light on the right with high accumulation of cGMP. Figure adapted from [Power, Das *et al.* 2020].

gene can result in two different types of retinal dystrophies, as shown in Figure 1.3 [Berger *et al.* 2010]. This level of complexity pose challenges in the way of understanding the disease pathway and further complicates the therapeutic intervention of such diseases.

Mutations in *Pde6b* are reported to be about 4% of all the autosomal recessive RP in North America, and result in the disruption of phototransduction cascade [McLaughlin *et al.* 1995]. cGMP plays a very important role as a second messenger in the phototransduction cascade. In darkness, cGMP mediated activation of CNGC induce depolarisation of the cells. cGMP upregulation or excessive accumulation of cGMP has been highlighted [Power, Das *et al.* 2020, Paquet-Durand *et al.* 2019] as a major factor associated with photoreceptor degeneration in RP. cGMP concentration is regulated by two components in the photoreceptors: (1) phosphodiesterase (PDE) enzyme that hydrolyses cGMP and (2) Guanylyl Cyclase (GC) that synthesise cGMP. The balance between the activation of GC and PDE maintains the physiological concentration of cGMP, they are connected with a feedback loop that inhibits each other in order to maintain the balance. Guanylyl Cyclase Activating Protein (GCAP) activates GC. The resulting sythesis of cGMP activates the CNGC by opening them. Opening of CNGC leads to Ca^{2+} influx in the photoreceptors. The increased concentration of intracellular Ca^{2+} in turn inhibits the activity of GC [Koch *et al.* 1988]. The depletion of intracellular cGMP concentration occurs when PDE gets activated in the presence of light. Activated PDE hydrolyses

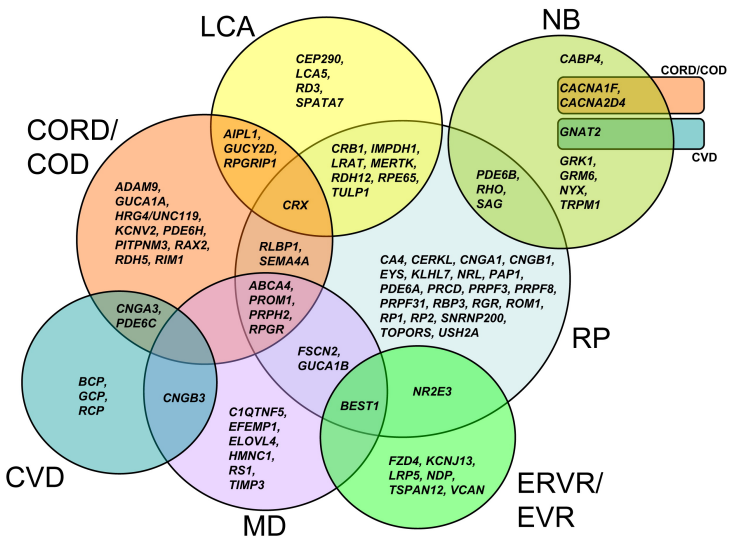

Figure 1.3: **Complex genetic heterogeneity of different retinal dystrophies:** Different circles are represented by different colours, represents a type of retinal dystrophy and the genes known to be associated with it. The figure also represents the genes which overlap between two (*e.g.*, *PDE6B*) or three (*e.g.*, *ABCA4*) different retinal dystrophies. For example, *PDE6B* is a gene responsible for both Retinitis Pigmentosa (RP) and Night Blindness (NB). *ABCA4* is known to be associated with RP, Macular Degeneration (MD) and Cone Rod Dystrophy (CORD/ COD). LCA refers to Leber Congenital Amaurosis and CVD refer to Cone Vision Defect. Adapted from [Berger *et al.* 2010].

cGMP that leads to the closure of CNGC. The depletion in intracellular Ca^{2+} concentration activates GC to produce more cGMP. In addition, intracellular Ca^{2+} concentration of the OS also modulates Ca^{2+} permeability of the CNGC with the help of calmodulin (CaM) more strongly in cones than in rods [Picones *et al.* 1997]. In higher Ca^{2+} concentration the affinity of CNGC decreases for cGMP as its β subunit binds to CaM. During constant light, at lower Ca^{2+} concentration, CaM dissociates from the channel increasing the affinity of CNGC for cGMP, making it more permeable [Hsu *et al.* 1993]. In healthy photoreceptors, the variable activity of GC, PDE, and CNGC maintains the physiologically accurate concentration of intracellular cGMP and Ca^{2+} during the light or darkness. Mutations in the components of the phototransduction cascade, such as subunits of PDE, leads to high accumulation of cGMP. This activates the CNGC that in turn leads to high influx of Ca^{2+} in the OS. Photoreceptors have been shown to follow a non-apoptotic form of cell death [Arango-Gonzalez *et al.* 2014] and rod photoreceptors show a primary degeneration followed by a secondary degeneration of cones.

1.3 Mechanisms of hereditary retinal degeneration

Two of the most studied cell death mechanisms are apoptosis and necrosis. Apoptosis is a caspase-dependent degeneration mechanism which can be activated by two different pathways, namely extrinsic (via FAS and FADD; FAS Associated Death Domain) and intrinsic (via mitochondrial leakage of cytochrome C mediated by *Bcl 2* Associated X protein (BAX)/ Bak-associated Apoptosis-activated Channel (BAC) forming pores on mitochondrial membrane) [Galluzzi *et al.* 2018]. Classical necrosis, unlike apoptosis, is a non-regulated cell death mechanism. It is known for the loss of cell membrane integrity and lysosomal release into cytosol leading to the cellular degeneration in an uncontrolled fashion affecting neighbouring cells at the same time. It is believed to be initiated by reactive oxygen species, Ca^{2+} overload, calpains and several other stress situations.

Earlier it has been believed that photoreceptors undergo either apoptotic death [Portera-Cailliau *et al.* 1994] (DNA fragmentation) or necrosis (activation of calpains) during the photoreceptor degeneration in retinal dystrophies. Later it has been shown across various animal models that photoreceptors follow a non-apoptotic cell death mechanism during the retinal degeneration [Arango-Gonzalez *et al.* 2014]. More recently with the advancement in the understanding of cellular mechanisms, newer regulated cell death pathways have been discovered. Keeping in mind the observed markers during the photoreceptor degeneration, most relevant degeneration pathways could be the Mitochondrial Permeability Transition (MTP)-driven necrosis and parthanathos [Galluzzi *et al.* 2018]. Parthanathos is characterised by the increased activation of Poly (ADP-ribose) Polymerase (PARP) and is mediated by Poly (ADP-ribose) (PAR) polymer binding to Apoptosis Inducing Factor (AIF). PAR availability for binding to AIF is regulated by: (1) PAR binding protein ring finger 146 (RNF146), if it is bound to PAR, PAR cannot bind to AIF and (2) polyADP-Ribosyl Hydrolase (ARH) 3, which degrades unbound PAR polymer [Mashimo *et al.* 2013]. The release of AIF from mitochondria to the cytoplasm is mediated by the interaction with PAR. Cytoplasmic AIF can translocate to the nucleus for DNA fragmentation and promotes nuclear translocation of macrophage Migration Inhibitory Factor (MIF), that in-turn catalyses DNA fragmentation [Wang *et al.* 2016]. Hexokinase-I is also believed to be associated with parthanathos [Andrabi *et al.* 2014]. MTP-driven necrosis is known to be initiated by Ca^{2+} calmodulin-dependent protein kinase-II (CaMK-II) on β adrenergic receptors. The cascade leads to an osmotic breakdown of mitochondrial membrane by the release of mitochondrial Permeability Transition Pore Complex (PTPC) situated between the Inner Mitochondrial Membrane (IMM) and the Outer Mitochondrial Membrane (OMM). This was also reported due to overload of Ca^{2+} and activation of Mitochondrial Ca^{2+} Uniporter (MCU) and Mitochondrial Ca^{2+} Uptake-I (MICU-I).

1.4 cGMP-dependent photoreceptor degeneration

CNGC is one of the important components of phototransduction cascade. During the darkness, in a healthy situation, Na^+ and Ca^{2+} enter photoreceptors via activated CNGC. Cation influx maintain photoreceptors in the depolarised state during the dark and the continuous release of glutamate. Photoreceptors are special as compared to other neurons in this case, because these release neurotransmitters in the off state. Hydrolysis of cGMP and the subsequent closure of CNGC, stops the influx of Ca^{2+} thereby hyperpolarising the cell, shown in Figure 1.2 and ceasing in the glutamate release.

In mutant conditions, such as mutation of PDE in RP, the mutation disables the PDE to hydrolyse cGMP. This results in pathological accumulation of cGMP in the photoreceptors. In cGMP-dependent degeneration PKG, calpain and PARP are found to be elevated. High accumulation of cGMP activates its targets downstream which are CNGC and PKG in photoreceptors following two parallel pathways. The activation of PKG is thought to activate HDAC in its downstream and may further lead to the activation of PARP [Arango-Gonzalez *et al.* 2014].

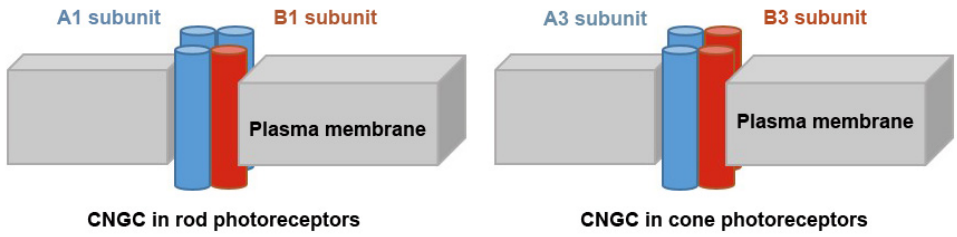

Figure 1.4: **Heterotetrameric arrangement of CNGC in photoreceptors:** Shows a cartoon of heterotetrameric CNGC in (A) rods with 3 subunits of A1 and 1 subunit of B1 and (B) in cones with 2 subunits of A3 and 2 subunits of B3. Cone channels are also reported to have 3 A3 to 1 B3 subunits by certain studies [Kaupp *et al.* 2002, Peng *et al.* 2004].

The overactivation of CNGC further leads to high Ca^{2+} influx which increases the intracellular Ca^{2+} concentration. It is believed to cause photoreceptor degeneration due to the activation of several downstream events. A general hypothesis suggests that high cGMP leads to overactivation of Ca^{2+} channels. The increased Ca^{2+} is reported to activate the downstream cascade by the activation of Ca^{2+}-dependent proteases calpain [Orrenius *et al.* 2003, Fox *et al.* 1999]. Ca^{2+} regulation in the intracellular environment is

very critical for the survival of neurons [Yamashima 2004]. Therefore Ca^{2+} channels have been studied as a potential candidate for RP therapeutic approach for last two decades.

Thus, CNGC is present in an inter-phase between the healthy and the diseased state of photoreceptors making it very interesting as a candidate. Photoreceptor OS, having CNGC, are very dynamic in nature. RPE connecting to photoreceptors by OS (see Figure 1.1) plays a very important role in the visual cycle and the renewal of OS. In healthy adult mammalian retina the rate of renewal is about 10% in one day [Goldberg *et al.* 2016]. CNGCs are transmembrane cation channels present in the photoreceptor OS with 6 (S1-S6) transmembrane domains, a pore region between S5 and S6, and a Cyclic Nucleotide Binding Domain (CNBD). These channels activated by cyclic nucleotides such as cGMP and are responsible for a major percentage of Ca^{2+} influx in the OS. Rod CNGC are heterotetrameric in nature having subunits A1 and B1 (see Figure 1.4) assembled in 3:1 ratio. In cones, the assembly of the subunits A3 and B3 are reported to be in the ratio of 1:1 and 1:3 [Kaupp *et al.* 2002, Peng *et al.* 2004]. CNGB1 in rods have a unique bipartite structure on a protein level. It is encoded by 33 exons and two different proteins are formed by alternative splicing of the exons. N-terminal forms GARP which is a structural component of the OS. C-terminal forms the $\beta 1$ subunit of CNGC. CaM binding region is present at the N-terminal of CNGB1 and CNBD at the C-terminal [Ardell *et al.* 2000, Kaupp *et al.* 2002, Körschen *et al.* 1995]

Healthy photoreceptors in dark condition are continuously undergoing two major processes which involve Ca^{2+} (1) dark current: CNGC are activated by binding of cGMP resulting influx of Na^{+} and Ca^{2+} in the OS. The excessive Na^{+} and Ca^{2+} are being continuously extruded by NCKX which are regulated by Na^{+} gradient across the membrane. The Na^{+} gradient is in turn maintained by NKX, which extrudes Na^{+} by ATP hydrolysis. The photoreceptor is maintained at a partial depolarised state which is -40 mV. (2) Ca^{2+} mediated glutamate release: deactivated PDE enables cGMP to bind to and activate CNGC resulting in influx of Ca^{2+}. This influx results signal propagation via membrane and Ca^{2+} influx via synaptic VGCC maintains the continuous release of glutamate. The NCKX channel which is also present in the OS continues to extrude Ca^{2+} during the darkness to balance the Ca^{2+} concentration in the OS. NCKX has low affinity for Ca^{2+} and inactivated in lower Ca^{2+} concentration. Thus, in light, the continuous function of NCKX helps to lower the intracellular Ca^{2+} concentration. PMCA present in the inner segment and cell body has high affinity for Ca^{2+} and extrudes Ca^{2+} from the cell body in ATP-dependent manner.

1.5 Motivation

Ca^{2+} channels have been studied as a therapeutic target for more than past two decades. However, till date there remains some controversy and gap in our knowledge regarding the inhibition of Ca^{2+} channels for delaying photoreceptor degeneration. A delay in photoreceptor degeneration was reported by using the Ca^{2+} channel blocker (D-cis-diltiazem) that is commonly used in treating hypertension [Frasson *et al.* 1999]. This was the first study indicating the impact of Ca^{2+} channel inhibition on the retinal degeneration. The controversy arose when the follow-up studies could not replicate the protective effect suggested in the above study questioning the effectiveness of Ca^{2+} block [Barabas *et al.* 2010]. In the meantime, another study showed the use of L-cis-diltiazem protective for photoreceptor survival [Pawlyk *et al.* 2002]. This discrepancy could be possibly explained as diltiazem is found as two different enantiomers, *i.e.*, D-cis-diltiazem and L-cis-diltiazem. D-cis-diltiazem is known to inhibit VGCC and L-cis-diltiazem blocks CNGC. Diltiazem occurs as a racemic mixture of both the enantiomers. A pure enantiomer of diltiazem was difficult to obtain. Thus, commercially available D-cis-diltiazem could be a racemic mixture of both L-cis and D-cis enantiomers. Therefore, the treatment effect reported with D-cis-diltiazem could result from L-cis-diltiazem, showing a protective effect [Frasson *et al.* 1999].

This hypothesis was further supported by the results of two important knockout studies later performed in this context, which were *Cngb1* and *Cacna1f* knockout. *Cngb1* is an RP causing gene (see Figure 1.3) [McLaughlin *et al.* 1993]. When these animals were cross-bred with *rd1* animals, another animal model for RP, very surprisingly the double mutants were found to have a strongly delayed peak of degeneration and improved retinal function [Paquet-Durand *et al.* 2011]. On the other hand, $Cacna1f^{-/-}$ [Specht *et al.* 2009] animals, lacking the $\alpha 1$ subunit of VGCC, on cross-breeding with *rd1* showed no significant delay in the photoreceptor degeneration. Mutation in *Cacna1f* causes congenital stationary night blindness in humans [Regus-Leidig *et al.* 2014]. These results were also reflected in an earlier study with a knockout of $\beta 2$ subunit of VGCC [Read *et al.* 2002]. All these results highlighted CNGC as a potential target to delay the rod photoreceptor degeneration in RP mediated by the pathological accumulation of cGMP and overactivation of CNGC.

To address the apparent contradiction and understand the role of Ca^{2+} influx via CNGC in the photoreceptor degeneration in *rd1* and *rd10* animal models, this study explores the possibility of CNGC inhibition using pharmacology as well as ASO. The possibility of targeted functional loss of CNGC would be explored by ASO mediated down-regulation of b1a subunit of CNGC. D-cis-diltiazem L-cis-diltiazem would be used to inhibit VGCC and CNGC respectively. It would also help to understand the differ-

ential block effect of the two major Ca^{2+} sources in rod photoreceptors. Some novel cGMP analogues would be used to specifically block CNGC. Block efficiency of diltiazem enantiomers would be assessed on heterologously expressed channel subunits to understand their inhibition effect, and the light-induced Ca^{2+} response would be measured. To further explore the effect of Ca^{2+} inhibition downstream, some of the key downstream components such as calpain and PARP-1 would be studied to understand the mechanism of cell death. The expression of GLUT 3 would be localised in the retina to understand its role concerning ATP depletion and retinal degeneration. In addition to that, the possibility of restoring functional PDE6a in *Pde6a* V685M mice via RNA editing approach would be explored. Altogether, the combination of all these approaches would give a better understanding of the photoreceptor degeneration pathway in RP and help the development of treatments.

2 Experimental Procedure

2.1 Animal models

Phosphodiesterase 6 (PDE6) hydrolyses cGMP in the OS of photoreceptors during the phototransduction cascade. Hydrolysis of cGMP leads to the closure of CNGC and a stop of Ca^{2+} influx into the photoreceptors. This results in hyperpolarisation of cells and transmission of visual signals to higher-order neurons in the retina. PDE6 is a heterotetrameric enzyme comprising α, β and γ subunits in the rod photoreceptors. Mutation in these subunits leads to the disruption of the phototransduction cascade and degeneration of photoreceptors. To study the underlying problems in this thesis, the following animal models were used for the experiments: (1) C3H *rd1* that is *Pde6b* mutant with its corresponding, (2) C3H wild-type (wt), (3) *rd1*- TN-XL, a *Pde6b* mutant with Troponin C-XL (TN-XL) calcium biosensor, (4) *rd10* that is another *Pde6b* mutant and (5) *V685M* that is a *Pde6a* mutant. All the animals used in this work was as per the German law of animal protection.

2.1.1 *Pde6a* V685M

Mutation in *Pde6a* is a mutation variant found in the patients of retinitis pigmentosa. *Pde6a* V685M mutant mouse models were used in this study. *Pde6a* V685M mouse mutants have been generated by N-ethyl-N-nitrosourea (ENU) mutagenesis (described in [Sakamoto *et al.* 2009]). Afterwards a human RP patient was identified compound heterozygous for the c.1684C>T/p.Arg562Trp and c.2053G>A/p.Val685Met mutations in *PDE6A* [Sothilingam *et al.* 2015].

2.1.2 *Pde6b rd1* and *rd10*

rd1 was first described in 1927 having rodless retina (r). This mouse line was lost in the World War II [Keeler 1927] and in 1951 it was rediscovered as retinal degeneration mouse model (*rd*) [Brückner 1951]. Mutation in the β subunit of PDE6 causes autosomal recessive retinitis pigmentosa in patients. *Pde6b* can be further broken down into 22 exons and 21 introns. A reduced catalytic activity of PDE6B subunit in *rd1* is caused due to two different genetic mutations: a nonsense codon in exon 7 and an intronic insertion of a retroviral element [Bowes *et al.* 1993]. *rd1* is an extensively studied mouse model showing a rapid degeneration of photoreceptors and therefore ONL. In humans, *PDE6b* is located on 4p16 and on chromosome 5 in *rd1* mouse models. Human *PDE6b* is often mutated in the patients of retinitis pigmentosa [Bowes *et al.* 1990, Sidman *et al.* 1965, Pittler *et al.* 1993].

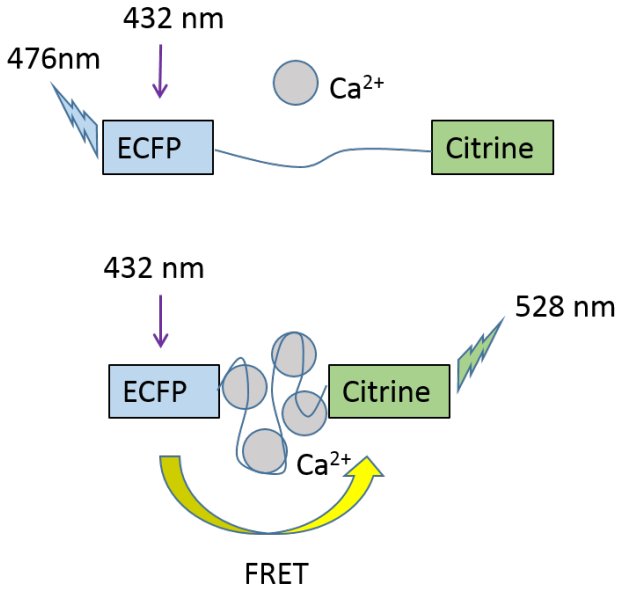

Figure 2.1: **FRET based mechanism of TN-XL Ca^{2+} biosensor:** Shows a representation of TN-XL molecule in the lower Ca^{2+} concentration (on the top). In this state when ECFP receives violet light (432 nm) it emits blue light (476 nm). At increased concentration of Ca^{2+} (at the bottom), the Troponin C binds to Ca^{2+} bringing ECFP and Citrine close to each other and activating FRET. In this state, the energy received by ECFP via violet light (432 nm) gets transferred to Citrine emitting green light (528 nm). This green signal gives the indication of light-induced Ca^{2+} response (Ca^{2+} biosensor described in [Mank *et al.* 2006]).

The *rd1*- TN-XL is a mouse model that carries the same set of mutations as *rd1*. The mouse line has been modified with a transgenic insertion of the Ca^{2+} biosensor TN-XL. It is a Ca^{2+} biosensor based on Fluorescence Resonance Energy Transfer (FRET) in which extra-large Troponin C is flanked by ECFP and Citrine on either its end, shown in Figure 2.1. Troponin C, has a very high affinity for Ca^{2+}. Increase in the intracellular Ca^{2+} concentration leads Ca^{2+} to bind to Troponin C bringing ECFP and Citrine close to each other and activating FRET [Wei *et al.* 2012]. The light-induced Ca^{2+} responses were determined using *rd1*-TN-XL [Kulkarni *et al.* 2015]

The *rd10* mouse is another model for RP. It also carries the mutation in the β subunit of PDE6 gene however as compared to *rd1* it shows a later onset and slower degeneration of photoreceptors. The missense mutation in *rd10* is in exon 13 of β subunit of *Pde6* and maps to mouse chromosome 5. It is an autosomal recessive mutation that corresponds to human RP patients [Chang *et al.* 2000].

2.2 Histology

2.2.1 Histological preparation of the eye

This is a procedure to preserve and study the histology of the eye. The eyes from the mice were enucleated and incubated in 4% Paraformaldehyde (PFA) for 45 minutes. These were then subsequently incubated in 10%, 20% and 30% sucrose for cryoprotection for about 10 minutes, 20 minutes and 2 hours respectively. Finally, these were embedded in TissueTek (Sakura Finetek Europe B.V.) using liquid N_2.

2.2.2 Organotypic retinal explant culture

This is a highly specialised method of culturing retinal tissue in serum-free condition [Caffé *et al.* 2002]. The explants were prepared on early post-natal day (P) and were cultured for about 5 to 8 days [Caffé *et al.* 1989]. The culturing period for *rd1* and *rd10* were from P5-P11, P9-P17 respectively. For V685M the culturing period was from P5 to P13. To prepare the explants, animals were sacrificed using an appropriate method, such as decapitation for P5. To keep the experimental conditions sterile, the animal parts were cleaned with 70% ethanol before extraction of eyeballs under the stereoscope. To keep the tissue alive after extraction, it was transferred to basal medium and incubated for 5 minutes. The eyeballs were further incubated in Proteinase K solution for 15 minutes. To stop Proteinase K activity, the eyes were treated with serum solution [1 (FBS/FCS): 4 (basal medium)] for 5 minutes. After the incubation time, the eyes were kept into a fresh basal medium for final wash and preparation of explants. In sterile condition the lens and

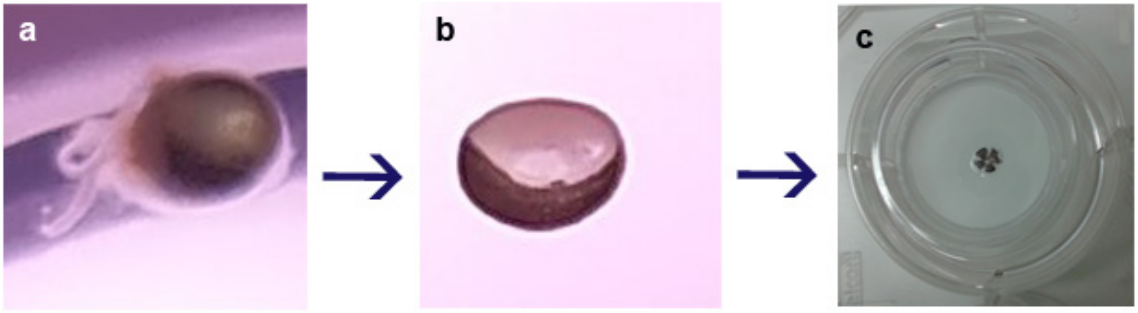

Figure 2.2: **The explantation procedure:** The eyeball was enucleation from the young animal. (a) Shows the freshly enucleated eye having all the ocular tissues. Other ocular tissues in the eye ball such as sclera, were removed by incubation with Proteinase K for 15 minutes. (b) shows the isolated retina with RPE. The isolated retina is given cuts on its four sides to give a clover-leaf shape. The retina is then transferred to a polycarbonate membrane by a tip broadly cut at the base (tissue-saver tip) (c) for culturing and supplemented with complete medium.

the sclera were separated to isolate retina from the eyecup. The isolated retina was given a small cut from four sides to give it a clove-leaf shape (see Figure 2.2). The explant so prepared was placed on the membrane by pipetting (wide cut 1 ml tip) on 6-well culture plate and supplemented with complete medium [Belhadj, Tolone, Christensen, Das *et al.* 2020]. Complete medium was replaced every 48 hours.

2.2.3 Fixing and embedding of explant cultures

For fixing the mice retinal explant cultures 4% paraformaldehyde was used as a fixative. Two different incubation timings were followed namely 15 minutes and 45 minutes depending on the further intended analysis of the samples. After fixation the tissues were washed with PBS incubation for 5 minutes and cryopreservation procedure was followed by incubating in 10%, 20% and 30% sucrose for 10 minutes, 20 minutes and 2 hours or overnight respectively. Followed by cryopreservation, these tissues were embedded in TissueTek (OCT) in aluminium cubes and preserved by freezing in liquid N_2.

2.2.4 TUNEL staining for cell death analysis

Cell death is detected by an assay called Terminal deoxynucleotidyl transferase dUTP Nick End Labelling (TUNEL) to detect the DNA fragmentation as a marker of cell death [Gavrieli *et al.* 1992]. It is done with the help of an *in situ* cell death detection kit (Roche

Diagnostics, Mannheim, Germany; 12156792910). As its name suggests, the enzyme terminal deoxynucleotidyl transferase is a special type of DNA polymerase that uses 3′ overhang of DNA as a template and nucleotide to the 3′ nick ends. This enzyme attaches fluorescently labelled tags to the broken ends of DNA as a marker of cell death. Tissue sections fixed with 4% paraformaldehyde and embedded in TissueTek were marked with hydrophobic pen (Dako, Denmark and Glostrup, Denmark) and hydrated in Phosphate Buffer Saline (PBS; 0.1 M) for 15 minutes. They were then were incubated with 0.01% Proteinase K in pre-warmed Tris-buffer (TBS; 0.05 M) for 5 minutes at 37°C followed by 3× wash with TBS each for 5 minutes. Further, these were incubated with ethanol acetic acid solution for 5 minutes followed by 3× wash with TBS each for 5 minutes. Then the sections were incubated with TUNEL blocking solution (10% NGS, 1% BSA, 1% fishgelatin in 0.03% PBST) for 1 hour. The sections were further incubated with TUNEL reaction mixture (50% TUNEL block, 45% Label solution and 5% enzyme) for 1 hour at 37°C or overnight at 4°C. Finally, the sections were washed with PBS 2× 5 minutes each and mounted using Vectashield with DAPI (Vector Laboratories Inc, Burlingame, CA, USA).

2.2.5 Immunostaining

The cryosectioned slides were dried for 30 minutes at 37°C and hydrated for 15 minutes. Then the sections were then incubated with blocking solution (10% NGS, 1% BSA and 0.3% PBST) for 1 hour. The primary antibody was diluted in the blocking solution and incubated overnight at 4°C. After incubation, the sections were rinsed with PBS 3× for 10 minutes each and incubated with secondary antibody at RT for 1 hour. Secondary antibody (AlexaFluor) was diluted in PBS (1:500). Followed by the incubation, the sections were rinsed with PBS 3× for 10 minutes each and mounted using Vectashield with DAPI (Vector Laboratories). Primary antibodies with their respective details are listed in Table 2.1.

2.2.6 Calpain activity assay

This assay allows to resolve the calpain activity *in situ*, on unfixed tissue sections [Paquet-Durand *et al.* 2006]. Retinal tissue sections were incubated and rehydrated for 15 minutes in Calpain Reaction Buffer (CRB) (5.96 g HEPES, 4.85 g KCl, 0.47 g $MgCl_2$, 0.22 g $CaCl_2$ in 100 ml ddH_2O; pH 7.2) with 2 mM dithiothreitol (DTT). The tissue sections were incubated for 2 hours at 37°C in CRB with tBOC-Leu-Met-CMAC (5 μM; Molecular Probes) [Ekström *et al.* 2014]. Afterwards, the tissue sections were washed twice with PBS (5 minutes) and mounted using Vectashield mounting medium (Vector Laboratories) for immediate visualisation under the microscope (Zeiss Apotome-2).

Antibodies	Animal	Dilution	Company	Catalogue no.
CNGB1	rabbit	1:1000	Sigma-Aldrich	HPA039159
Calpain-2	rabbit	1:300	Abcam	ab39165
PAR	mouse	1:200	Enzo	ALX-804-220
PDE6a	rabbit	1:400	Novus Biologicals	NBP1-87312
PNA	Alexa 488 conj.	1:100	Molecular Probe	L21409
Rhodopsin	mouse	1:400	Chemicon	MAB 5316
GLUT 3	rabbit	1:100	Abcam	ab41525
Gt335	mouse	1:1500	Enzo	ab804-885-C100
GFAP	rabbit	1:400	Sigma	G 3893
GFP	rabbit	1:200	Millipore	ab3080

Table 2.1: **List of antibodies:** Gives detailed information about the primary antibodies used during the experiments. The second column give the names of the host animal. In the third column the dilutions used, in the fourth column the names of the company and in the fifth column the catalogue numbers of the orders are given.

2.2.7 PARP activity assay

The tissue sections were incubated with PARP reaction mixture (PARP reaction buffer, 1 mM DTT and 5 μM of 6-Biotin-17-NAD). These were incubated at 37°C for 2 hours and 30 minutes for optimum enzymatic activity in physiological conditions. Following that, the sections were washed 3× for 5 minutes with PBS (0.1 M) and incubated with Avidin (conjugated with Alexa Fluor 488) diluted 1:800 in PBS for 1 hour. This step had to be performed in dark conditions. As the last step, the slides were washed 3× for 5 minutes with PBS and mounted with Vectashield containing DAPI, which is a nuclear stain [Bakondi *et al.* 2002].

2.2.8 PAR staining

Sections were rehydrated with PBS for 5 minutes. Further, the sections were incubated with PBS and 0.1% Triton (PBST) containing quenching solution (30% H_2O_2, methanol, PBS with 0.1% Triton) for 20 minutes. These were washed 3× for 5 minutes with PBS and incubated with blocking solution (10% normal goat serum in 0.1% PBST) for 30 minutes. Following the blocking, the slides were incubated with mouse anti-PAR (ALX-804-220, 1:200, Enzo, Farmingdale, NY, USA) at 4°C overnight and the slides were washed 3× for

10 minutes with PBS. The biotinylated secondary horse anti-mouse antibody (PK-6102, 1:150, Vector Laboratories, Burlingame, California, USA) was applied in the sections and incubated for 2 hours at room temperature and were washed 3× for 10 minutes with PBS. As the next step, the vector ABC (Vector Laboratories, Burlingame, California, USA) was prepared 30 minutes before these were applied to the slides. The vector ABC is composed of Avidin and biotinylated horseradish peroxidase. The further washing steps were done with Phosphate Buffer (PB). Finally, the slides were incubated in a 3,3′-Diaminobenzidine (DAB) (DCS-Inovative, Hamburg, Germany) solution containing 20% glucose (Sigma-Aldrich, Hamburg, Germany), 0.4% NH_4Cl (Sigma-Aldrich, Hamburg, Germany) and 1% Nickel ammonium sulphate (Sigma-Aldrich, Hamburg, Germany), where Glucoseoxidase (Calbiochem, Merck, Darmstadt, Germany) was added at last to start the reaction for 2 minutes and 30 seconds. Following a microscopic inspection, the slides were washed 3× for 5 minutes with PB and mounted with Aquatex mounting medium (Merck, Darmstadt, Germany).

2.2.9 Imaging and analysis

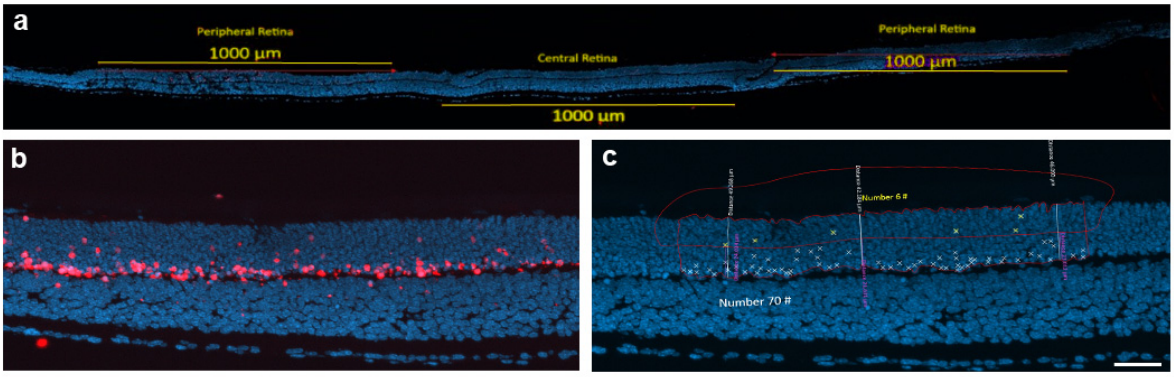

Figure 2.3: **Analysis of explant images:** (a) shows a tiled image (3,000 μm long) of complete explant culture. The portions of the explant sections analysed were divided across as central and peripheral retina (1,000 μm each). The data from the central and peripheral retina are pooled together in the observation. (b-c) show the quantification strategy used for the analysis of the localisation shift. The length of the ONL was divided into half and distribution of the cells were manually counted in each of the halves (upper and lower). The percent positive cells localised close to OPL, were analysed by comparing cell count in the lower half of ONL with respect to the total positive cells in the ONL. Scale bar; a = 1,000 μm, b = 40 μm.

The images of the sections from *ex-vivo* retina and organotypic explant cultures were

captured using a Zeiss Imager Z.2 fluorescence microscope, equipped with ApoTome2, an Axiocam 506 mono camera, and HXP-120V fluorescent lamp (Carl Zeiss Microscopy, Oberkochen, Germany) after performing the above-mentioned assays. The excitation [$\lambda_{Exc.}$]/ emission [$\lambda_{Em.}$] characteristics of the filter sets used for the different fluorophores were as follows (in nm): DAPI ($\lambda_{Exc.} = 369$ nm, $\lambda_{Em.} = 465$ nm), AF488 ($\lambda_{Exc.} = 490$ nm, $\lambda_{Em.} = 525$ nm), and AF562 ($\lambda_{Exc.} = 578$ nm, $\lambda_{Em.} = 603$ nm). The images were taken as Z-stack, or both tiled and z-stack using 20× or 63× magnification and were analysed using Zen 2.3 blue edition (.NET Framework Version 4.0.30319.18063) software. The data were collected from 7 to 9 different sections obtained from 3 to 5 individual animals. Sections of 12 μm thickness were analysed using 8-12 Apotome Z-planes. For analysing percent positive cells in the ONL of the tissue sections, the area of the ONL was outlined and the positive cells were counted manually. The percent positive cells were calculated with respect to the total number of cells in the given area using an average cell (nucleus) size. All the values are normalised with respect to the untreated considering that the number of positive cells are 100% in untreated condition, unless otherwise mentioned. Every experimental group was individually normalised with respect to its internal experimental control. For analysing the thickness of ONL and length of OS, the line perpendicular to the OPL and IS respectively were considered. To analyse the localisation shift of positive cells in the ONL toward the outline of OPL, the relative localisation of positive cells within the ONL was assessed by dividing the width of the ONL horizontally into two equal halves (*i.e.*, upper and lower half). The distribution was manually quantified by counting the distribution of positive cells in each of the halves. The chance level for cell distribution was 50%. The percent of degenerating photoreceptors localized close to OPL, were analysed by comparing cell count in the lower half of ONL with respect to total positive cells in the ONL (see Figure 2.3).

2.2.10 Statistical analysis

Data were analysed with GraphPad Prism 8.4.3 (June 10, 2020; GraphPad Software LLC) and JMP 15.2.0 (466311, SAS Institute Inc, Cary, NC, USA). Figures were prepared using Photoshop CS5 (Version 12.0 ×64). Linear mixed-effects models (calculated using JMP) were fitted by restricted maximum likelihood estimation (REML), to assess the significance of the effects in explaining the variations of the dependent variables. Variance inflation factors (VIF) of the predictor variables were calculated and assured to fall well below the common threshold value, indicating no collinearity between them. The residuals were confirmed visually to follow a normal distribution, while homoscedasticity (homogeneity of the residual variances) was tested using the Brown–Forsythe test and reported in case of violations. Figures were prepared using Photoshop CS5 (Adobe, San Jose, CA, USA).

2.3 Molecular biology

2.3.1 Design of Antisense Oligonucleotides (ASOs)

ASO are small nucleic acid molecules complementary to the targeted sequence in the gene of interest. The designs of ASOs were aimed towards down-regulation of CNGB1 by mediating exon skipping that could lead to nonsense-mediated decay of the primary transcript of CNGB1 (pre-mRNA) or ribonuclease H mediated degradation. There are two aspects of designing an ASO, selecting the sequence and adding a background modification. For the selection of an optimum sequence, several parameters such as sequence alignment, single strand (ss) count, Tm, 3D accessibility, off-target in the genome, splice motifs and free energy were analysed [Aartsma-Rus *et al.* 2009]. A detailed designing procedure will be discussed in Chapter 3.

2.3.2 Primer design

Both PCR and cloning primers were designed using the Primer3Plus, a web interface to Primer3 [Untergasser *et al.* 2007] considering GC content, Tm and self-annealing properties of the primers.

2.3.3 Isolation of total RNA from mouse retina and retinal explants

To analyse the expression of CNGB1 transcript in cell lines and mouse retina, total RNA was extracted from the cell lines, *ex-vivo* single retina, *ex-vivo* pooled retina (3 animals), single explants and 4 explants pooled together. The extraction was done using Peq Gold Total RNA kit from Peqlab.

Ex-vivo retinae were extracted and kept in RNA later solution at 4°C overnight and then transferred to -80°C for further storage. For isolating total RNA from cell lines, the harvested cells were stored in -20°C. Total RNA from explants were isolated from freshly cultured explants and the samples were always kept on the ice.

The tissue or cell samples were transferred to the homogeniser column (MP biomedicals lysing matrix tubes) with 400 μl of RNA lysis buffer T placing them on the ice. The tissue was homogenised using Precellys24 (Bertin Instruments, P000669-PR240-A) at 5,500 rpm for 20 seconds (with intermittent chilling in the case of multiple required cycles). The samples were then centrifuged for 2 minutes at 7,000 rpm and the lysate were transferred to DNA removing columns (green) using 100 μl filter tips and centrifuged for another minute at 10,000 rpm. An equal volume (400 μl) of freshly prepared

of 70% ethanol added to the flow-through and mixed well by pipetting. The mixture was transferred to RNA columns (orange) and centrifuged for 1 minute at 9,000 rpm. The flow-through was discarded and washed with 500 μl of RNA Wash Buffer at 9,000 rpm for 15 seconds. Another washing was done by adding 600 μl of RNA Wash Buffer II to the column and centrifuged at 9,000 rpm for 15 seconds. Then the columns were dry-centrifuged for 2 minutes at 9,000 rpm and placed in RNase Free vial. 40 μl of RNase free water was added to it and incubated for 3 minutes at RT. To elute total RNA the vials were centrifuged for 1 minute at 4,500 rpm and stored in -80°C. Concentration was measured using the NanoDrop (PeqLab Biotechnologies, ND-1000).

2.3.4 cDNA synthesis

To ensure the cDNA free from DNA contamination, the synthesis from total RNA was done in two different steps. The first step DNase digestion and the second step reverse transcription.

The enzyme used for DNase digestion was Deoxyribonuclease I (Sigma-Aldrich). A reaction mixture was prepared with 1.5 μg RNA, 1 μl of 10× reaction buffer, 1 μl DNase I (1U/μl) and RNase free water was added to make the final volume to 10 μl. The reaction mixture was incubated for 15 minutes at room temperature and added 1 μl stop-buffer (50 mM EDTA) with incubation for 10 minutes at 70°C to stop the digestion. The concentration of RNA was measured using NanoDrop. Depending on the nature of further experiments with total RNA, the DNase digestion step could be avoided as heat inactivation of the enzyme may also be harmful for the RNA.

Reverse transcription or RT-PCR was done using Transcriptor High Fidelity cDNA Synthesis Kit by Applied Biosystems. The reaction mixture was prepared with 1 μg DNase I digested RNA, 2 μl Random-Hexamer (600 pmol/μl) and RNAse free H_2O to make a final volume of 11.4 μl and incubated for 10 minutes at 65°C. It was stored on the ice immediately after the incubation. 4 μl of 5× reaction buffer, 0.5 μl Protector RNase Inhibitor (40 U/μl), 2 μl dNTPs (10 mM), 1 μl DTT (0.1 M), and 1.1 μl Transcriptase (9 U/μl) were added to it. The reaction was incubated for 30 minutes at 50°C and 5 minutes at 85°C. The cDNA was stored in 4°C.

2.3.5 Polymerase Chain Reaction (PCR) for *Cngb1*

PCR is one of the most common molecular biology technique used in labs for several purposes. It comprises 3 basic steps namely denaturation of the DNA strands, annealing of the primers to them and extension for amplification of a DNA fragment using desired primers. Taq DNA polymerase from and ATII buffer (in house buffer) was used to prepare

Temperature	Time	Cycles	Remarks
94°C	2 minutes		denaturation
94°C	30 seconds	-	denaturation
58°C	30 seconds	35	annealing
72°C	30 seconds	-	extension
72°C	2 minutes		final extension
4°C	store		hold

Table 2.2: PCR condition for amplification of *Cngb1*.

the reaction mixture. Reaction mixture for one sample contained 50-100 ng cDNA, 2.5 μl of 10× ATII buffer, 1 μl dNTP, 1 μl forward primer (5 μm), 1 μl reverse primer (5 μm), 0.4 μl of Taq polymerase and ddH_2O to make a total volume of 25 μl. PCR for *Cngb1* from cDNA (conditions as shown in the Table 2.2) were used for the analysis of CNGB1 expression in the mouse retina and cell lines.

2.3.6 Transfection

The cell line B16F10 (CL13-00037) was cultured in DMEM added with 1% Penicillin/ streptomycin, 10% FCS and 1% sodium pyruvate and was used for the screening of ASO. The cells were seeded in a 12 well plate with 2×10^6 cells per well. The cells were transfected with master mix prepared with OptiMEM (100 μl) (Gibco), liposome (3 μl) (Fugene) and ASO (0.5 μM).

To test the ASO mediated RNA editing on the retina, the retinal explants were transfected with ASO using the transfection agent RNAimax. RNAimax (5 μl) was incubated with OptiMEM (3 μl) for 5 minutes. Then the mixture of ASO (300 pmol) and optiMEM (volume calculated as per the stock concentration of ASO) were added to RNAimax-OptiMEM master mix to make a final volume of 30 μl for each retina and incubated for 20 minutes. The transfection mix was applied to the tissue with freshly supplemented complete medium and cultured as per the above-mentioned protocol.

3

Effect of Cyclic Nucleotide Gated Channel Inhibition

Ion exchange across the membrane is a key phenomenon that mediates light responses in photoreceptors and transmits them via the changes in membrane potential from the outer segment to the synaptic terminal. In darkness, the photoreceptors are in a state of depolarisation. The resting membrane potential is -40 mV. Depolarisation happens mainly due to the influx of K^+ and Ca^{2+} in the cell via CNGC mediated by cGMP binding. Other ion channels in the outer segment such as Na^+, Ca^{2+} exchanger (NCKX) extrudes Ca^{2+} and intakes Na^+ maintaining the dark current [McNaughton 1990]. The Na^+, K^+ ATPases (NKX) extrudes of Na^+ from the IS consuming about 50% of the metabolic energy. It is responsible for regulating the Na^+ gradient across the membrane, indirectly regulating the activity of NCKX [Wetzel *et al.* 1999]. The influx of Ca^{2+} in the outer segment leads to change in the membrane potential leading to the Ca^{2+}-dependent release of glutamate at the synapse in darkness [Bech-Hansen *et al.* 1998]. Thus, the major source of Ca^{2+} influx in the Outer Segemnts (OS) of photoreceptors are Cyclic Nucleotide Gated Channels (CNGC) and in the synaptic terminal is Voltage Gated Calcium Channels (VGCC). In the physiological condition, rod CNGC is found to behave differently than that of cones, having more percent of total ion channels present in the active state as compared to rods. This also allows cones to be more adaptive to respond to different wavelengths of light which is not the case for cones. Mutation in *Pde6b* corresponds to around 4% of the total RP situation [McLaughlin *et al.* 1995] in North America. The mutant possesses a dysfunctional PDE6B which is not able to hydrolyse cGMP resulting in a pathological elevation of intracellular cGMP concentration. High cGMP is leading to the activation of a higher number of CNGC as compared to the physiological condition resulting in high concentration of intracellular Ca^{2+}. This elevated Ca^{2+} influx is believed to drive the photoreceptor degeneration mediated by the high cGMP. CNGC is thus believed to play an important role in cGMP-dependent photoreceptor degeneration (see Chapter 1). This study evaluated the role of Ca^{2+} via

CNGC in contrast to another major channel VGCC. To access their roles, the effect of two different diltiazem enantiomers (a well-known drug for hypertension) were investigated on: (1) heterologously expressed CNGC from both rods and cones, (2) cone Ca^{2+} dynamics in the retina, (3) calpain activity downstream of Ca^{2+} and (4) photoreceptors degeneration. Moreover, the effect of cGMP analogue specific for CNGC inhibition were also evaluated on cell death.

3.1 Existing controversy

The hypothesis surrounding the RP degeneration suggests, high levels of Ca^{2+} is the main disease driver and hence the lowering of Ca^{2+} influx via Ca^{2+} channels would be a potential therapeutic approach [Fox *et al.* 1999]. Therefore, a large number of studies over the last two decades have assessed the protective potential of Ca^{2+}-channel blockers on the photoreceptors [Takano *et al.* 2004]. A seminal study by Frasson and colleagues [Frasson *et al.* 1999] showed that inhibition of Ca^{2+} channels using D-cis-diltiazem, which is a blocker of VGCC, rescue photoreceptor degeneration *in-vivo*. Follow-up studies by several groups could not reproduce the protective effect on degenerating photoreceptors [Barabas *et al.* 2010]. In the meantime, another study showed a protective effect on the photoreceptor degeneration using L-cis-diltiazem, which is known to block CNGC [Fox *et al.* 2003]. Later knockout studies by cross-breeding *Cngb1* and *rd1* animal models, a double mutant *rd1* $\times$ *Cngb1*$^{-/-}$, showed prolonged viability of rods and improved retinal function *in-vivo* [Paquet-Durand *et al.* 2011]. On the other hand, knockout of *Cacna1f* for VGCC showed no effective delay in photoreceptor degeneration [Schön *et al.* 2016, Read *et al.* 2002]. Interestingly both the above knockout animal models show a significant reduction in the calpain activity.

Despite the controversy, all the above studies highlighted that Ca^{2+} influx in photoreceptors are playing a major role in its degeneration. The dose-dependent inhibition of CNGC might be beneficial for photoreceptor survival in RP. In this study, the gap in present knowledge was addressed by understanding the role of Ca^{2+} via the major Ca^{2+} channels in degeneration and explore further on the effect of blocking those channels.

3.2 Expression of CNGC during development and degeneration in *rd1*

A mouse model that shows rapid photoreceptor degeneration is *rd1* having a peak of cell death between P10 and P12. The pattern of CNGC expression in the degeneration model *rd1* was important to be determined. This would help to understand the window

available for the study.

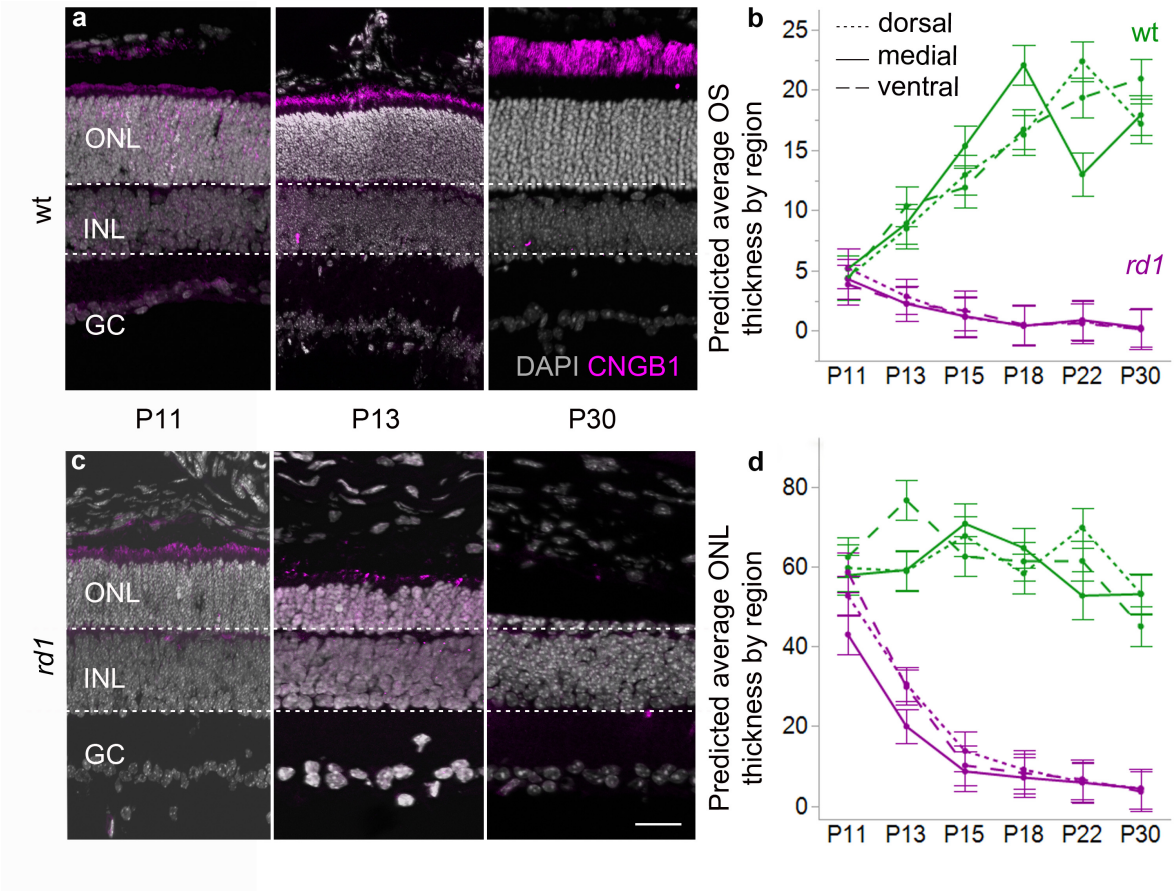

Figure 3.1: **Spatiotemporal expression of CNGB1 in *rd1* and wt**: Immunostaining for CNGB1a (magenta), that labelled the photoreceptor OS, was performed at different postnatal (P) days in wt and *rd1* retina (a, c). The nuclear counterstain (DAPI, grey) indicates ONL, INL, and GCL. Dotted, solid and dashed lines in the graph represent dorsal, medial, and ventral mouse retina respectively (b,d). (a) In wt retina, CNGB1a grew longer from P11 to P30. (c) In *rd1* retina, CNGB1a were detectable at P11 and P13 but disappeared by P30. (d) The thickness of the ONL in wt retina (green) remained approximately constant between P11 and P30, while in *rd1* (magenta) ONL thickness sharply reduced after P11. (b) OS in wt retina grew longer from P11 to P24 until reaching a plateau at a length of approximately 20 μm. In contrast, *rd1* OS, while still comparable to wt at P11, had reduced to nearly 0 μm by P24. Retinal sections from 4-5 different animals per time-point and genotype were quantified for analysis. Scale bar = 30 μm.

	OS length n = 109, $R^2_{adj.}$ = 0.96		**ONL thickness** n = 109, $R^2_{adj.}$ = 0.93	
Fixed effect	*F*-statistic	*p*-value	*F*-statistic	*p*-value
genotype	F(1, 25.25 = 0.0078)	0.9304	F(1, 25.99) = 2.6450	0.1159
Time-point	F(5, 24.7) = 4.4213	0.0052	F(5, 24.77) = 15.1946	< 0.0001
Retinal position	F(2, 48.36) = 0.2982	0.7435	F(2, 49.39) = 2.9380	0.0623
genotype x time-point	F(5, 24.7) = 13.2699	< 0.0001	F(5, 24.77) = 12.0885	< 0.0001
genotype x retinal position	F(2, 48.36) = 0.3245	0.7245	F(2, 49.39) = 0.9156	0.4070
Time-point x retinal position	F(10, 47.94) = 3.8401	0.0007	F(10, 48.41) = 2.0258	0.0508
genotype x time-point x retinal position	F(10, 47.94) = 4.2248	0.0003	F(10, 48.41) = 1.3344	0.2397

Figure 3.2: **Effects explaining the variability of the length of OS with respect to ONL thickness in *rd1* and wt**: Results of the linear mixed-effects models with the dependent variables OS length and ONL thickness. The residuals of the model followed a normal distribution, while the Brown-Forsythe test indicated a violation of the assumption of homoscedasticity for both models. However, linear mixed-effects models estimates have been shown to be robust against such violations

The photoreceptor OS are highly dynamic in nature, replaced at the rate of around 10% per day in the mammalian retina [Goldberg *et al.* 2016, LaVail 1976]. In *rd1*, the retinal degeneration coincides with the retinal development. To determine the expression of CNGC in *rd1* retina in the relevant time window (the turnover rate of OS), immunostaining was performed in a spatiotemporal manner for the CNGB1a channel subunit on retinal tissue sections collected at six different time-points (see Figure 3.1). Degeneration in *rd1* spans around P10 to P12 with a peak at P11 [Sahaboglu *et al.* 2013]. The immunohistochemistry was done from P11 to P30 with a focus on the peak of degeneration. The expression of CNGB1 was analysed after every 48 hours interval, starting from P11. This also helped to delineate the therapeutic window for OS using the *rd1* mouse model. Our data reflect central to peripheral pattern of mouse retinal degeneration, illustrated earlier in the literature, in the ONL which is not present in the disappearance of OS.

Linear mixed-effects models were used to determine statistically significant effects of genotype and post-natal day to explain the variability of OS length and ONL thickness data. A Brown-Forsythe test indicated heterogeneity of variance of the fitted model residuals, however, this was not deemed to significantly affect results since linear mixed-effects models have been shown to be robust against this violation. A post hoc test using custom contrasts was used to compare between wt and *rd1* retina. Least-square (LS) means difference between post-natal day P11 to 18, for OS length (wt: 13.73 $\pm$ 2.05 μm; F (1, 25.25) = 44.6828; p $<$ 0.0001, *rd1*: 3.99 $\pm$ 2.03 μm; F (1, 24.44) = 3.8582; p = 0.0610) showed that the length of OS quadrupled between P11 and P30 in wt, while

it sharply decreased in *rd1*. The thickness of ONL was compared with respect to the photoreceptor degeneration with LS means difference between post-natal day P11 to 18 (wt: 1.46 ± 5.25 μm; F (1, 25.99) = 0.0780; p = 0.7822) *rd1*: 43.31 ± 5.13 μm; F (1, 24.18) = 71.1854; p < 0.0001) 3.2. The ONL was found to be fairly stable in wt at this postnatal day, however in *rd1* it reduced significantly. The data also reflect that the development of ONL in wt retina attains stability during the maturation of OS. On the other hand in *rd1*, degeneration of ONL, as well as OS, follows the peak of degeneration. At P22 when most of the photoreceptors have disappeared to a significant level, from around 50 μM in P11 to around 10 μM in P22, there are still some remaining OS which could be contributed by cones. Importantly, the development of ONL as well as OS till P11 is same in wt and *rd1*. During the onset of the *rd1* degeneration ($\sim$ P10), CNGC expression, as assessed via OS length, was still comparable to that in wt animals (average P11 OS length LS means difference between wt and *rd1* 0.18 ± 2.05 μm, F (1, 25.25) = 0.0078; p = 0.9304). This highlights that the best study or the therapeutic window is about P11 *in-vitro*.

3.3 CNGC knockdown: antisense technology

Antisense technology is a very powerful for biological research as well as novel therapeutic strategies. The idea of antisense technology dates back to early 1980s with the discovery of a unique phenomenon of translational inhibition by the complementary RNA transcript by [Mizuno *et al.* 1984]. Later the mechanism of RNA interference received much attention after the breakthrough by Mello and group in 1998 [Fire *et al.* 1998]. Today antisense technology has moved to the clinical trials for many diseases [Bennett 2019] among which are Duchenne Muscular Dystrophy [Vita *et al.* 2019], Usher syndrome [Wolfrum *et al.* 2018] and Leber Congenital Amaurosis (LCA) [Cideciyan *et al.* 2019]. About four decades of research has seen much evolution in the idea and the mechanism of this approach gaining understanding about ASO mechanism of action, identification of relevant target sequence and improving the intracellular half-life. However, many more including cell specific internalisation and uptake mechanisms are yet to be understood. In this section of my project, the targeted down-regulation of *Cngb1* has been attempted by exploiting the available knowledge of ASO. This approach might help us understanding the mechanism of cGMP-dependent photoreceptor degeneration downstream of Ca^{2+} influx after specific ASO mediated down-regulation.

3.4 ASO mediated down-regulation of *Cngb1*

As described in Chapter 1, CNGCs are one of the major sources of Ca^{2+} in photoreceptor OS and the degeneration resulted due to the pathological accumulation of cGMP [Fesenko

et al. 1985]. Studies have shown improved rod viability and cone function in *Cngb1a*$^{-/-}$ × *rd1* double mutant animal models [Paquet-Durand *et al.* 2011]. CNGCs are an important functional factor for the healthy survival of photoreceptors. The knockout of *Cngb1a* has shown improved retinal function but gene knockout cannot be practised in the clinic for treating patients. ASO is an emerging field for therapeutic development [Dhuri *et al.* 2020]. Motivated by the above-mentioned study, the effect of ASO mediated targeted down-regulation of the CNGC subunit was evaluated on photoreceptor degeneration.

Mutant animal models showing the features of RP, such as *rd1* have the resultant mutation in rod photoreceptors. CNGC in rods are composed of CNGA1 and CNGB1 (see Chapter 1). The assembly of a functionally efficient heterotetrameric CNGC in rods require the single unit of CNGB1, therefore down-regulation of *Cngb1* might be the most effective way of lowering the expression of the functional channel in the rod OS. For controlled and selective down-regulation of *Cngb1* two different types of ASOs were designed: (1) ASO inducing splice modulation for exon skipping in this case and (2) RNase H mediated degradation using gapmer ASOs (illustrated in the following page).

RNase H mediated degradation

RNase H is a ribonuclease enzyme (RNase HI and RNase HII in eukaryotes) which use DNA/RNA hybrid as a substrate to degrade RNA strand [Murante *et al.* 1998], illustrated in Figure 3.3. It is a ubiquitous enzyme evolutionarily conserved across the species [Bin-Guang *et al.* 2008]. RNase H can recognise DNA-RNA hybrid which can be an useful tool to target matured mRNA. Targeting matured mRNA for down-regulation of a gene has certain advantages, some of which are mentioned as follows: (1) it is present in the cytoplasm of the cell before the translation which makes it highly accessible, (2) matured mRNA possesses 5′ cap and polyA tail at its 3′ end which makes it highly stable in the cytoplasm. The increased stability increases the probability of its interaction with ASO and thereby mediating an RNase H mediated cleavage and (3) the translating machinery ribosomes recognise and bind to the 5′ end of the mature mRNA sequence. The rest of the sequence is available for the interaction with ASO. To form a DNA/RNA heteroduplex by ASO binding and get recognisable for RNase H, the construction of ASO needs to be a gapmer. A gapmer is a single-stranded oligonucleotide sequence with a central block of DNA, about 8-10 ntds long flanked by the chemically modified RNA sequence. The flanking RNA sequence and its chemical modification help to increase its binding affinity to the mRNA of interest and enhance its stability by protecting it from the cytoplasmic nuclease degradation. The backbone modification O-me has been extensively studied and O-me chemistry on flanking RNA has shown to make very stable heteroduplex [Masaki *et al.* 2010]. The flanking RNA sequence of the gapmers were 2′-O-methyl (O-me) modified. It is a US Food and Drug Administration approved

modification used in RNase H-dependent antisense drug Mipomersen [Hair *et al.* 2013]. Matured mRNA targeted via this approach can either prevent translation by binding to the mRNA sequence if it gets failed to be recognised by the RNase H enzyme or induce degradation by the recruitment of RNase H enzyme.

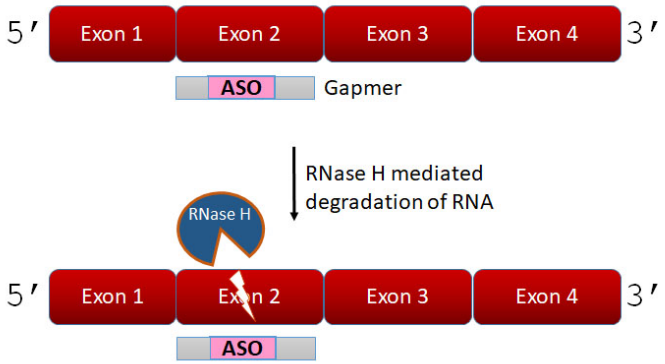

Figure 3.3: **Mechanism overview of RNase H in the presence of ASO:** Shows a schematic representation of the condition for RNase H activity which can target mature mRNA forming a DNA/RNA heteroduplex. The ASO designed as a gapmer (DNA block flanked by RNA sequences on its both ends) with O-me modification. The DNA/RNA hybrid is recognised by the RNase H leading to the cleavage of mature mRNA.

Exon skipping

In the mammalian genome exons are interspaced by the intron sequences. A pre-mRNA comprises three important sequence structures for splicing its consecutive exons. Composition of intron-exon with canonical splice sites at 5′ and 3′ end and branch point site are shown in Figure 3.4. These sequences are splice site acceptor, splice site donor and branch point. During the splicing event, the splicing machinery recognise these sequences as the guideline to splice out the intron and join to consecutive exons for the formation of mature mRNA. The splicing machinery first attach to the splice donor site and subsequently with the branch point sequence (present within an intron) and then to splice acceptor site for the completion of the splicing event [Green 1986]. Exon skipping by splice modulation is a phenomena in which the normal splicing of pre-mRNA gets interrupted by the binding of ASO during the formation of a matured mRNA. These ASOs are also called Splice-Switching Oligonucleotides (SSO) [Bauman *et al.* 2009]. The design of SSO was aimed to prevent the binding of splicing machinery to the targeted sequence of interest, which is pre-mRNA *Cngb1* to induce exon skipping. Figure 3.4 shows a schematic representation of the possible phenomena of exon skipping mediated

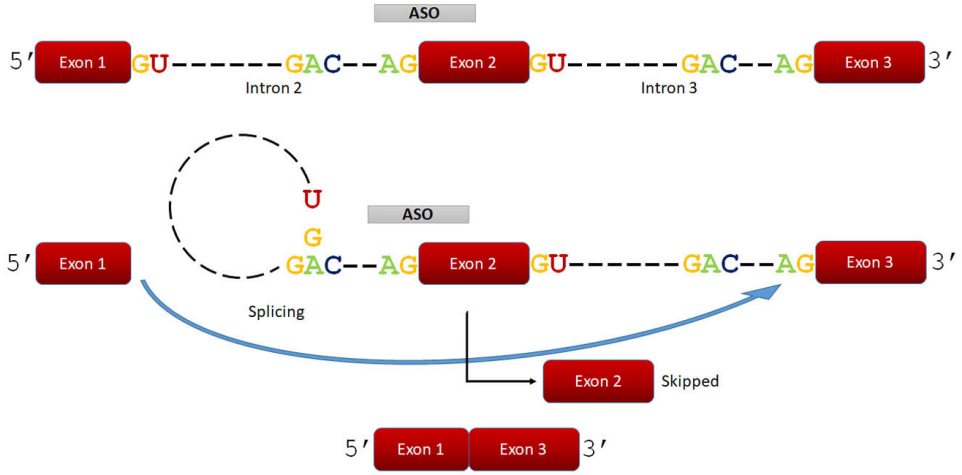

Figure 3.4: **Schematic overview of exon splicing:** Shows a schematic representation of 3 exons interspaced by 2 introns comprising splice acceptor site, donor site and branch point. Binding of an exemplary ASO at splice acceptor site shows the possible exon skipping mediated by the binding of ASO. The donor site of intron 2 joins to the branch point of intron 2 as usual. The presence of ASO in the acceptor site of intron 2 makes it target the acceptor site of intron 3 resulting in the skipping of exon 2.

by the binding of ASO. This can further lead to a frameshift mutation in the target sequence gaining a premature stop codon and activate Nonsense Mediated Decay (NMD) of the mRNA. To design ASO that can successfully induce the splice modulation in the target pre-mRNA, consideration of certain factors have been suggested to be very important [Aartsma-Rus *et al.* 2009]. These factors are: (1) splice enhancer motifs, (2) Single Strand (ss) count, (3) free energy of the sequence and (4) the off-target effects. Apart from these, length of ASO, % GC content in the target sequence and position to the exon border were also considered.

Backbone chemistry of ASO has come a long way showing less toxicity and high stability [Dhuri *et al.* 2020]. As a backbone modification for SSO, the combination of first and second generation of backbone modification were used for a stable preliminary validation. Phosphorothioate (PS) modification is the first generation of ASO backbone chemistry where the non-bridged O of the phosphate group is replaced by the S forming a PS-bond. This is a very stable modification and is resistant to nuclease degradation [Eckstein 2014]. This has been combined with O-me modification discussed above.

3.4.1 Sequence design

CNGB1 is a rod specific CNGC subunit. Mutation in *rd1* is homologous to human autosomal recessive RP. ASOs were designed aiming its clinical application as a therapeutic strategy. Therefore, sequences were identified that are conserved between *Mus musculus* (*Mm*) mouse and *Homo sapiens* (*Hs*) human to make the transition from mice to human therapeutically easier and applicable. The *Cngb1* comprise 33 exons and 32 introns. The sequence was screened for the conserved region using EditSeq (Dnastar). Table 3.2 shows in details the conserved sequences between the *Mm* and *Hs*. Exons 13, 19, 21, 24, 27, 28 and 29 were found to have conserved sequences in donor and acceptor splice sites. Exon 13 was not considered for the ASO design because *Cngb1* has been shown to have a unique bipartite structure that encodes for GARP (N-terminal) via alternative splicing [Ardell *et al.* 2000, Körschen *et al.* 1995]. To induce the skipping of the targeted exon and introduce a frameshift mutation, the number of nucleotide in each of the exons were taken under consideration. As a codon is composed of 3 nucleotides, a frameshift mutation and a Pre-mature Termination Codon (PTC) can be introduced by breaking a codon. Thus, the introduction of PTC via exon skipping can lead to Nonsense Mediated Decay (NMD) of the primary transcript. Table 3.1 gives a list of all the exons with the number of nucleotides and the number of nucleotides divided by their codons. Exon 1, 14, 18, 20, 22, 23, 25, 29 and 31, were found to be exactly divisible by 3 or a codon. Thus, a frameshift mutation cannot be introduced in the pre-mRNA by skipping any of these exons. Figure 3.5 gives a brief overview of exon and intron distribution in *Mm* with respect to *Hs* highlighting the possible exons that could be targeted for the exon skipping, which were exon 19, 21, 24, 27 and 28.

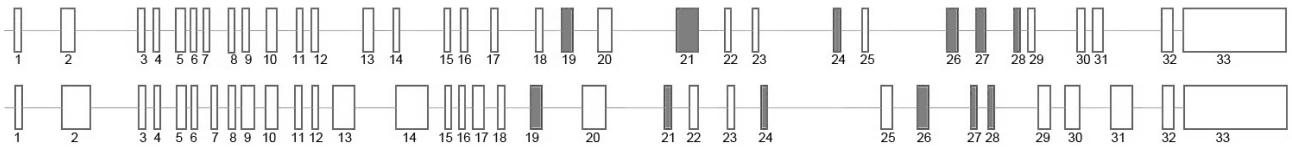

Figure 3.5: **Schematic representation of Human and Mouse (pre-mRNA) *Cngb1*:** Human (top) and mouse (below) (pre-mRNA) *Cngb1* showing the total number of 33 exons with a relative lengthwise comparison between human and mouse. Exons highlighted in grey are the exons considered for analysis and having conserved sequences.

Exonic Splicing Enhancers (ESEs)

Exonic Splicing Enhancers (ESEs) in a sequence are set of nucleotides which are specific to splicing machinery and increase the splicing efficiency. To modulate the splicing and

induce exon skipping, the ESEs present in the screened sequences were listed. Special attention was given to the sequences specific for strong ESEs such as SC35, SRp40, SRp45, SRp55 and SF2/ASF (see Figure 3.6). The strength of the enhancer motifs are denoted by scores correlate with the higher specificity. The ESE scores and motifs to the sequences were determined by using the online tool ESEfinder [Cartegni *et al.* 2003]. The enhancer motifs were considered with respect to their strength and the length of the sequence they span. The acceptor sequence of exon 19 (19a) was found to span across 9 nucleotides with a score of 80.92 to 83.59. The donor site of exon 19 (19d) spanned across 37 nucleotides with a score of 80.06 to 89.98. In exon 21 no considerable high scored ESEs were found within the conserved sequence. In the acceptor site of exon 27 (27a), ESE spanning 7 nucleotides were found with score 80.92 to 83.87 and donor site of 27 (27d) spanned across 8 nucleotides with score 80.96 to 82. Exon 28 was found to have ESE spanning across 15 nucleotides with score 80.92 to 84.61. The results show that the donor site of exon 19 (19d) and acceptor site of exon 28 has the highest score and span of ESE across the sequence of interest. Arranging them in the order of their ESE strength, 19d, 85.02 > 28, 82.7 > 19a, 82.2 > 27d, 81.4 > 27a, 82.3 were found. The average score of ESEs was between 81.4 to 85.02 for all the exons. Exon 19, 27 and 28 were considered for further analysis excluding the exon 21.

Species	Exon	ntds	no. of codons	Species	Exon	ntds	no. codons
Hs	1	53	17.6	*Mm*	1	54	18
...	2	167	55.6	...	2	269	89.6
...	3	58	19.3	...	3	58	19.3
...	4	73	24.3	...	4	67	22.3
...	5	91	30.3	...	5	115	38.3
...	6	31	10.3	...	6	43	14.3
...	7	46	15.3	...	7	34	11.3
...	8	76	25.3	...	8	76	25.3
...	9	49	16.3	...	9	40	13.3
...	10	178	59.3	...	10	148	49.3
...	11	76	25.3	...	11	76	25.3
...	12	37	12.3	...	12	37	12.3
...	13	160	53.3	...	13	160	53.3
...	14	87	29	...	14	276	92
...	15	88	29.3	...	15	88	29.3
...	16	163	54.3	...	16	121	40.3
...	17	163	54.3	...	17	163	54.3
...	18	108	36	...	18	108	36
...	19	158	52.6	...	19	158	52.6
...	20	156	52	...	20	156	52
...	21	209	69.6	...	21	209	69.6
...	22	51	17	...	22	51	17
...	23	87	29	...	23	87	29
...	24	65	21.6	...	24	65	21.6
...	25	123	41	...	25	123	41
...	26	142	47.3	...	26	142	47.3
...	27	160	53.3	...	27	160	53.3
...	28	98	32.6	...	28	98	32.6
...	29	84	28	...	29	84	28
...	30	119	39.6	...	30	119	39.6
...	31	147	49	...	31	147	49
...	32	220	73.3	...	32	220	73.3
...	33	2118	706	...	33	2437	812

Table 3.1: **List of exon length:** Listed are the exon length (in number of nucleotides) with their respective number of codons in human (*Homo sapiens*) and mouse (*Mus musculus*). Sequence information retrieved from the Ensemble database. The list highlights that both human and mouse have 33 exons for encoding CNGB1. Moreover, for both human and mouse exon 1, 14, 18, 20, 22, 23, 25, 29 and 31, the number of codons are divisible by 3. This indicates that skipping these exons would not introduce a frameshift mutation and a Pre-mature Termination Codon (PTC) in the mature mRNA.

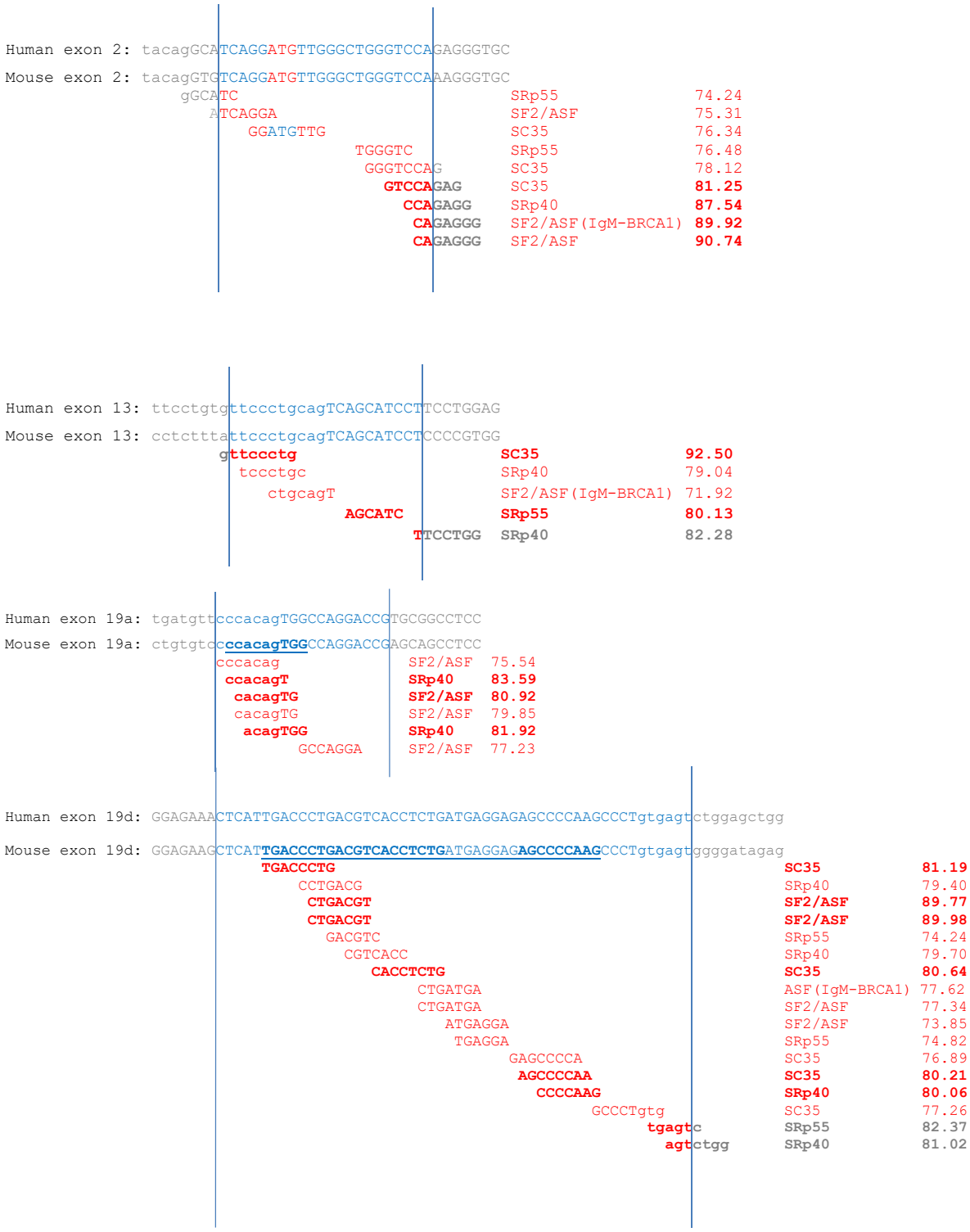
Human exon 2: tacagGCATCAGGATGTTGGGCTGGGTCCAGAGGGTGC
Mouse exon 2: tacagGTGTCAGGATGTTGGGCTGGGTCCAAAGGGTGC
gGCATC SRp55 74.24
ATCAGGA SF2/ASF 75.31
GGATGTTG SC35 76.34
TGGGTC SRp55 76.48
GGGTCCAG SC35 78.12
GTCCAGAG SC35 81.25
CCAGAGG SRp40 87.54
CAGAGGG SF2/ASF(IgM-BRCA1) 89.92
CAGAGGG SF2/ASF 90.74
Human exon 13: ttcctgtgttccctgcagTCAGCATCCTTCCTGGAG
Mouse exon 13: cctctttattccctgcagTCAGCATCCTCCCCGTGG
gttccctg SC35 92.50
tccctgc SRp40 79.04
ctgcagT SF2/ASF(IgM-BRCA1) 71.92
AGCATC SRp55 80.13
TTCCTGG SRp40 82.28
Human exon 19a: tgatgttcccacagTGGCCAGGACCGTGCGGCCTCC
Mouse exon 19a: ctgtgtccccacagTGGCCAGGACCGAGCAGCCTCC
cccacag SF2/ASF 75.54
ccacagT SRp40 83.59
cacagTG SF2/ASF 80.92
cacagTG SF2/ASF 79.85
acagTGG SRp40 81.92
GCCAGGA SF2/ASF 77.23
Human exon 19d: GGAGAAACTCATTGACCCTGACGTCACCTCTGATGAGGAGAGCCCCAAGCCCTgtgagtctggagctgg
Mouse exon 19d: GGAGAAGCTCATTGACCCTGACGTCACCTCTGATGAGGAGAGCCCCAAGCCCTgtgagtggggatagag
TGACCCTG SC35 81.19
CCTGACG SRp40 79.40
CTGACGT SF2/ASF 89.77
CTGACGT SF2/ASF 89.98
GACGTC SRp55 74.24
CGTCACC SRp40 79.70
CACCTCTG SC35 80.64
CTGATGA ASF(IgM-BRCA1) 77.62
CTGATGA SF2/ASF 77.34
ATGAGGA SF2/ASF 73.85
TGAGGA SRp55 74.82
GAGCCCCA SC35 76.89
AGCCCCAA SC35 80.21
CCCCAAG SRp40 80.06
GCCCTgtg SC35 77.26
tgagtc SRp55 82.37
agtctgg SRp40 81.02

Figure 3.6: **List of splice enhancer motifs:** pre-mRNA sequence alignment (grey) of exons (capital) and introns (small) in *Hs* (above) and *Mm* (below). The pre-mRNA sequence is aligned with respect to the ESE motif sequence (red) and their respective scores. Strong motifs are highlighted in bold. The conserved sequence with enhancer motifs is highlighted in bold and underlined.

Name	intron-exon boundary sequence	exonic sequence	exon-intron boundary sequence
Int1 Ex2 Int2	...	TCAGGATGTTGGGCTGGGTCCA	...
Int2 Ex3 Int3	...	...	...
Int3 Ex4 Int4	...	...	...
Int4 Ex5 Int5	...	...	...
Int5 Ex6 Int6	...	...	...
Int6 Ex7 Int7	...	...	...
Int7 Ex8 Int8	...	GAGCAGAATCTGGAAA	...
Int8 Ex9 Int9	...	...	...
Int9 Ex10 Int10	...	...	...
Int10 Ex11 Int11	...	...	...
Int11 Ex12 Int12	...	...	...
In12 Ex13 In13	ttccctgcagTCAGCATCCT	...	...
Int13 Ex14 Int14	...	...	...
Int14 Ex15 Int15	...	...	...
Int15 Ex16 Int16	...	...	...
Int16 Ex17 Int17	...	...	...
Int17 Ex18 Int18	...	GAGTCCCCAGTGGTTGCCTGGTC	...
In18 Ex19 In19	cccacagTGGCCAGGACCG	GACCGGCTCCAGGAGCTGGTGAAG	CTCATTGACCCTGACGTCACCTCTGATGAGGAGAGCCCCAAGCCCTgtgagt
Int19 Ex20 Int20	...	TGCGACATGCTCTGCTGCAAGTTCAA	...
Int20 Ex21 Int21	...	GTGCGCTGGGCCTTCCC,TCCTGGACATCACCGTGTTCCAGA,CGCCTGCAGTTTGTCA	AGGCGGGGACATCATTgtgagtca
Int21 Ex22 Int22	...	AATAACTACCTGAAGTCTCGCCG	...
Int22 Ex23 Int23	...	GCCTCCTGCCCTTGGA	...
Int23 Ex24 Int24	agTACATGGCCTTCTT	CCATCCTCAGCAAAGCCTACGT	...
Int24 Ex25 Int25	...	TCGGCTCCACTCACTGGGTTTACGA	...
Int25 Ex26 Int26	...	ACCCTCATCACCATCGG, ATTGTCTTCCAGCTGCTGAA, GTCTTTGCTTTCTCTGTGATGAT	...
Int26 Ex27 Int27	ccagATGAGAGATGTGGT	CAGACCTACTACCGCAGCTGCATGGACAGCAC, TTCTACAAGATCCCCA	TCGCAAGGCATGCTGGgtaaga
Int27 Ex28 Int28	cagATGAGTCAGAGCTGATGGT	...	...
Int28 Ex29 Int30	cagGGCTGTGACCGGCAGATGATCTT	...	GTGTTTGGAGAAATAAG

Table 3.2: **List of conserved sequences for *Cngb1*:** Shown all the sequences conserved for *Cngb1* between *Mm* and *Hs*. The genomic sequence information retrieved from the Ensemble database. The first column of the table shows the name of the exon with flanking introns on its either side. The second column shows the conserved sequence in the splice acceptor site. The third column shows the conserved sequence in the exonic region and the fourth column shows the sequence conserved in the donor site.

Single strand count and 3D accessibility

In the cellular environment, pre-mRNA is not present as linear but forms a 3D conformational structure. The 3D structure is dependent on the length and the sequence of the strand. Therefore, the sequence composition of each strand results in the formation of a structure which is unique and dynamic in nature. As the 3D conformation of the strand shows a dynamic nature of the folding, the target sequence for the binding of ASO might be inaccessible. For an efficient interaction and stable binding of the ASO, single-strand (ss) count is another aspect for developing ASO. Composition and length of the sequence being an important factor, each stretch of the target sequence were subdivided into increasing order nucleotide (from 1,000 to 2,000 nucleotides). The ss count of every nucleotide from the donor and acceptor regions of exon 19, 27 and 28 were calculated using mfold web server (The RNA Institute, College of Arts and Sciences, University at Albany, State University of New York) [Zuker 2003]. It was done in two different ways mentioned as follows. (1) The software provided a score of ss count based on its probability to pair with its complementary nucleotide of the same sequence and free energy. Each of the scores were listed against the base pair of the nucleotide sequence and a colour-coded map was prepared for every simulation. (2) The software also provided with a simulation of a number of possible 3D conformation. This helped with the visualisation of the sequence and compare the ss count with 3D accessibility. Based on the simulation and the colour-coded map of the sequences, each sequence was given a score for further evaluation. Figure 3.7 shows the comparative evaluation of colour-coded map with 3D simulation of exon 19 donor sequence as an example for both *Mm* and *Hs*. The score showed exon 19 acceptor has about 22.5%, ±0.72 SD, exon 19 donor site 39.6%, ±1.81 SD, exon 27 acceptor site 38.14% ±0.98 SD, exon 27 donor site 46.3% ±1.74 SD and exon 28 acceptor site 46.9 % ±2.9 SD, the chance of having a single-strand structure and accessibility to ASO.

Arranging in the decreasing order of ss count score, exon 28 (46.9%) > exon 27 donor (46.3%) > exon 19 donor site (39.6%) > exon 27 acceptor site (38.14%) > exon 19 acceptor (22.5%) were found. Also increased SD was observed with a higher percentage of ss count, for exon 28, 27 donor site and exon 19 donor sequences. Cross-referencing with heatmap showed that in the majority of the cases the hairpin loop structure is shown as the combination of highest and lowest scores for the loop and pin respectively. This resulted in a high average ss score but with increased SD. Exceptionally for exon 19 the donor site was found to have relatively high accessibility of the target sequence in 3D simulation supporting the ss count score, shown in Figure 3.7. The 3D structure of the target pre-mRNA sequence showed conformational variability on interaction with the ASO. To ensure a stable interaction, the bifold structures of the interaction of the target sequence with ASO were further evaluated.

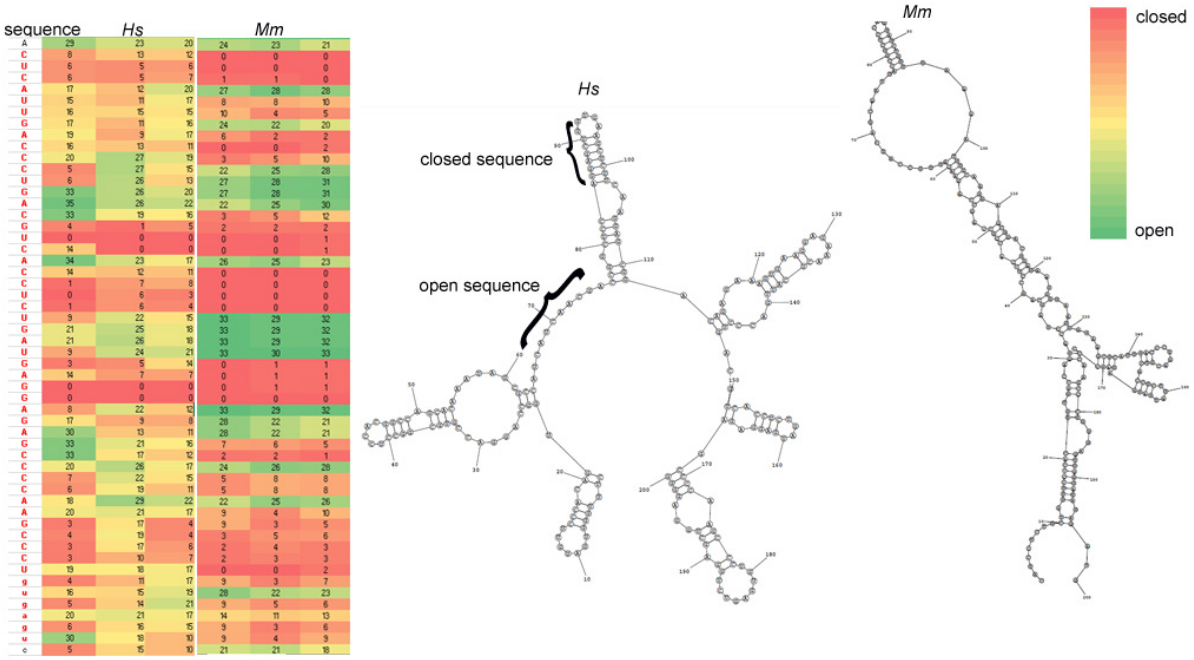

Figure 3.7: **Comparison of ss count score and 3D RNA folding simulation:** Shows the heat map score of ss count (left) and simulation of 3D conformation (right) for exon 19 donor sequence in *Mm* and *Hs*. The numerical value against each nucleotide is denoted by the colour code, represented in the form of a heat map. The red on the heat map denotes closed and green denotes open sequence.

Off-target effect

The off-target effects of the sequences were screened using a customised software cc-Top (group of Prof. Wissinger). The sequences of probable ASOs were individually screened for their off-targets against the entire *Hs* and *Mm* genome. The hits were based on number of mismatches up to 1, 2 or 3 nucleotide mismatches and the off-target hits in the exonic, intronic, or intergenic region. Mismatches of 1, 2 or 3 nucleotides were considered as in the order of their strength because the increased mismatch decreased the efficacy of ASO binding. So 3 mismatches were the least effective and 2 mismatches were lesser effective as compared to 1 mismatch. Similarly, hits against the exonic region were most effective which were lesser for the intronic region and the least for the intergenic region. In mice, a hit with 1 mismatch was found in the intergenic region of *Olfr267* (as shown in Figure 3.8). Olfr267 codes for the olfactory receptor in the mouse which were found to express in the primary visual cortex of the brain but not in the retina [Bastian *et al.* 2020]. This suggests that it has no potential off-targets in *Mm*. An exonic off-target

with 1 mismatch was found at *WWC2-AS2* in human. It was found to be a putative uncharacterised protein in human [UniProt 2018]. Although the chance of effectiveness for this off-target is high, the potential risk of such off-target is unknown.

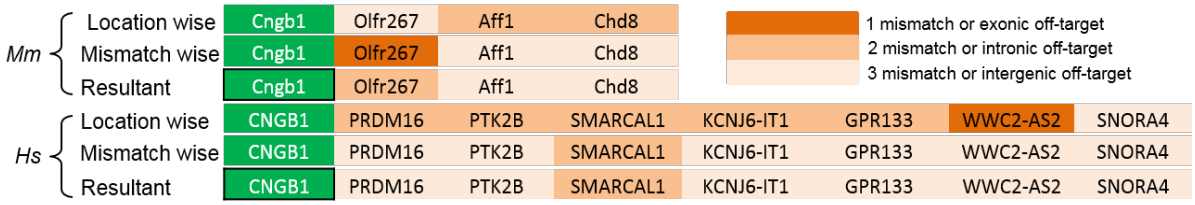

Figure 3.8: **Off-target map in *Hs* and *Mm*:** Shows the potential off-targets of ASOs after screening for the down-regulation of *Cngb1a*. The colour code denotes the effectiveness of the off-target in correlation with 1, 2 or 3 mismatches or hits in the exonic intronic or intergenic region. Against each colour, the name of the associated protein is indicated.

3.4.2 Validation of ASO

Considering all the above-described parameters two ASOs were designed for exon skipping and four ASOs for RNase H mediated degradation. The designed ASOs are listed in Table 3.3. The ASOs were screened on mouse skin melanoma cell line B16F10, found to have an endogenous expression of *Cngb1*. The successful ASO was further tested on organotypic retinal explant cultures. Figure 3.9 shows the results obtained from these experiments. The samples were obtained from the lysate of respectively transfected B16F10 cells. The untransfected cells were evaluated as the experimental controls. The amplified *Cngb1* PCR product of the B16F10 cell line was also compared against *Cngb1*, found in the wt mouse retina for accuracy. The expected size of the PCR product was 445bp. With SSO2, a smaller PCR product for *Cngb1* was found indicating successful exon skipping on the mouse cell line B16F10. Also with ASO1 and ASO4, no PCR product was found on B16F10 transfected cells when amplified for *Cngb1*. This might depict the possible degradation of the *Cngb1* primary transcript mediated by RNase H.

To check the effect of SSO efficacy on *rd1* mouse retina, it was further tested on retinal explant cultures. The amplification product of the SSO was compared with *rd1* retina and wt retina without SSO. Hypoxanthine-guanine phosphoribosyltransferase (*Hprt*) was used as a housekeeping control. No change in the product size was found to support the splice-switching in the tissue culture for SSO1. There exist certain challenges which might play a role behind the unsuccessful results in the tissue culture system: (1) The splice-switching and thereby the down-regulation efficacy of the SSO was unknown. In

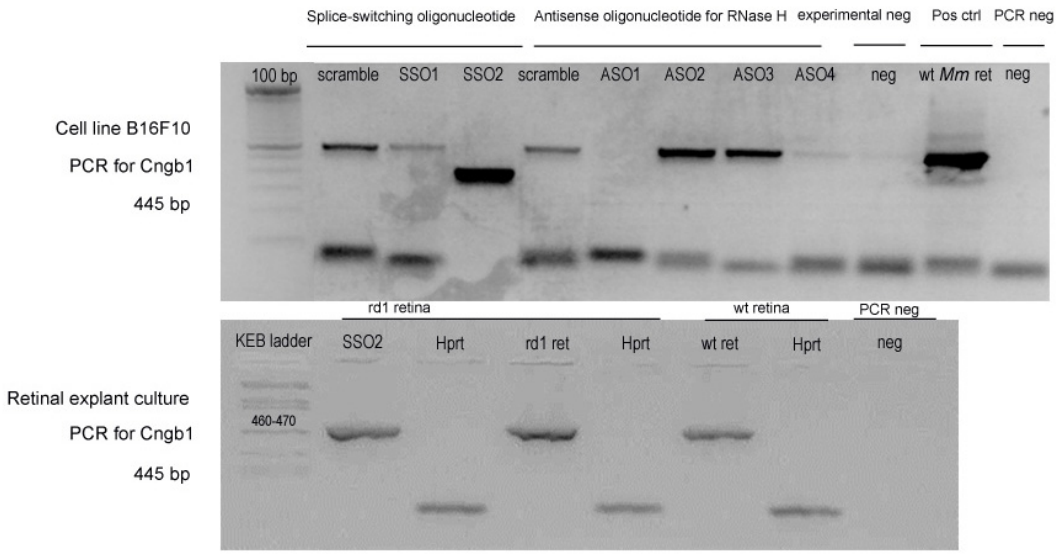

Figure 3.9: **Preliminary confirmation of successful design:** Shows *Cngb1* PCR product on gel as validation for the efficacy of ASO. SSO2, ASO1 and ASO4 indicate successful splice-switching and RNase H mediated degradation. The PCR product *Cngb1* from the cell line is compared against wt *Mm* retina. Hprt is a housekeeping control.

Denotation	ASO sequence	Backbone chemistry
SSO1	CUUCACCAGCUCCUGGAGCC	2′OmeRNA+PS
SSO2	CAUCAGAGGUGACGUCAGGG	2′OmeRNA+PS
ASO1	CAUCAGAGGUGACGUCAGGG	2′OmeRNA+PS, DNA+PS, 2′OmeRNA+PS
ASO2	CCGAUGGUGAUGAGGGU	2′OmeRNA+PS, DNA+PS, 2′OmeRNA+PS
ASO3	CAGCUGCGGUAGUAGGUCUG	2′OmeRNA+PS, DNA+PS, 2′OmeRNA+PS
ASO4	UUACCCAGCAUGCCUUGCG	2′OmeRNA+PS, DNA+PS, 2′OmeRNA+PS

Table 3.3: **List of designed antisense oligonucleotides:** Gives the sequences and backbone modifications of the designed antisense oligonucleotides for splice-switching and RNase H mediated degradation. The denotation gives the names by which these are referred to in the text.

B16F10 a lowered size of *Cngb1* PCR product was found suggesting skipping of exon in the cell line. However, the degree of down-regulation in terms of percentage could

not be measured. So the lower percent of down-regulation might be undetectable in the tissue. (2) The number of target cells in the retinal tissue are lower as compared to the cell culture system. In B16F10, all the transfected cells contribute to the resultant outcome. Whereas in the retina only rod photoreceptors express *Cngb1*. This constitute only about 40% of the cell population in the whole retina. (3) The delivery of SSO to the targeted retinal cell population was uncertain. Unlike cells, the retina is a complex tissue which has different cellular layers connected to each other, adding to its complexity. The amount of SSO actually reaching photoreceptors and more specifically to the rod photoreceptors could not be determined. (4) More sensitive readouts are helpful for the detection of a negative signal on a positive background. All these reasons might have been a contributing factor towards inconclusive result in the tissue culture. The problem can be addressed with targeted delivery of the SSO to photoreceptors.

3.5 Diltiazem: effect on channels and calcium dynamics

The pharmacological inhibition was used as an alternative approach to ASO mediated *Cngb1* downregulation, for studing the effects CNGC Inhibition on the retina. The pharmacological inhibition was mainly achieved using D and L enantiomers of diltiazem, a common drug used for the treatment of hypertension. The blocking effect of the compounds were tested on Ca^{2+} channels by measuring the differential current across the frog oocyte membrane after the heterologous expression of CNGC subunits (in collaboration with Dr. Nache's lab, University of Jena). The blocking effect on the heterologous expression system was tested with 25 μM and 100 μM. Further, the light-induced Ca^{2+} response in cones were measured under the two-photon microscope (in collaboration with Prof. Euler's lab, CIN, Tübingen). Both D- and L-cis-diltiazem with 25 μM, 50 μM and 100 μM were tested for understanding the effect on the light-induced Ca^{2+} response.

3.5.1 Differential effects of D- and L-cis-diltiazem on photoreceptor CNGC

For the direct assessment of the effects of D- and L-cis-diltiazem on retinal CNGC, the heterotetrameric rod CNGA1:B1a and cone CNGA3:B3-channels were expressed in *Xenopus* oocytes. These were examined for their functional characteristics in inside-out membrane patches and concentration-activation relationship using electrophysiological recordings. The measurement of heterotetrameric CNGC for cones showed that neither D-cis nor L-cis-diltiazem exhibit any block at physiological cGMP concentration at -35 mV when compared to the normalised cGMP-triggered current amplitudes. But

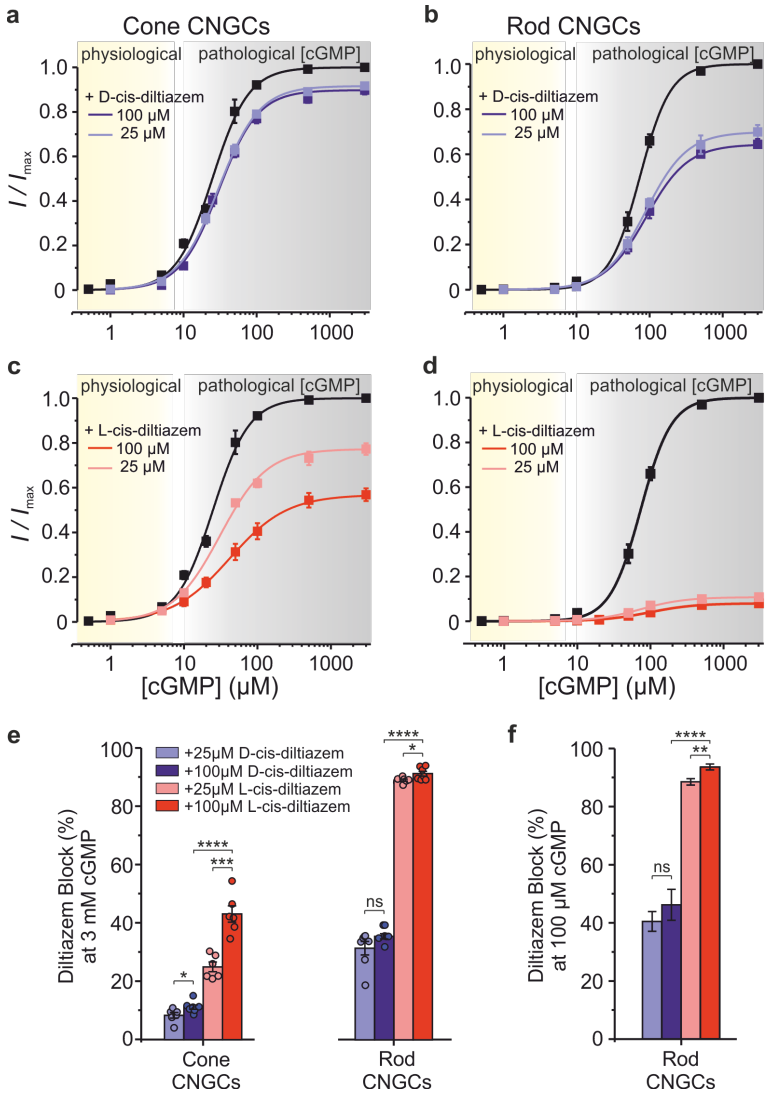

Figure 3.10: **Effects of diltiazem enantiomers on rod and cone CNGC activity:** (a-d) show the concentration-activation relationships for heterotetrameric cone (a, c) and rod (b, d) CNGCs measured at -35 mV. Black curve shows the normalised cGMP-triggered current amplitudes in the absence of diltiazem, used as a control. Blue and red curves represent data obtained in the presence of D-cis-diltiazem (a, b) and L-cis-diltiazem (c, d), respectively. The lighter and darker colour shades denote lower and higher concentrations, respectively. D- and L-cis-diltiazem - block (%, ±SEM) of CNGCs in the presence of 3 mM (e) and 100 μM cGMP (f), respectively. Contributed by Dr. Vasilica Nache and her group members.

when the concentration of cGMP is increased from physiological to pathological level, L-cis-diltiazem showed a concentration-dependent partial block which is about 25% at 25 μM and 45% at 100 μM. D-cis-diltiazem did not show any blocking effect on the heterotetrameric cone CNGC. The application of D-cis-diltiazem on rod CNGC showed no blocking effect on the heterotetrameric rod CNGC at physiological cGMP concentration. At higher concentration of cGMP (pathological concentration) D-cis-diltiazem showed a partial block which is about 40-50%. L-cis-diltiazem showed a complete block in all concentrations (25 μM and 100 μM) as compared to cGMP-triggered current amplitudes (see Figure 3.10).

L-cis-diltiazem was shown to be strongly selective for heterotetrameric rod channels which is highlighted by its stronger effect on rod CNGCs than on cone CNGCs. Under physiological conditions (at -35 mV and $\sim$ 5 μM cGMP) both D- and L-cis-diltiazem did not influence the CNGC activity at any concentration (25-100 μM). Under pathological cGMP concentration, however the inhibitory effect of both D- and L-cis-diltiazem were differential on both rods and cones CNGC. L-cis-diltiazem showed a stronger block on the rod CNGC than cone. D-cis-diltiazem showed a partial block rod CNGC at higher concentration which is nearly insignificant for cone CNGC.

In addition, the gating kinetics of the CNGC were characterised by measuring the activation and deactivation time courses for cone and rod CNGC in the presence and absence of the blocker. When both ligand and blocker were applied simultaneously the blocking effect took place only after the channel activation, which implies that either diltiazem can block the channels that are already opened or that the blocking mechanism is very slow and reaches a maximum only after the channel activation. A delay in the channels deactivation was also observed when both cGMP and diltiazem were simultaneously removed. The channel activation during the change in cGMP concentration from physiological to pathological and *vice versa* remained unaffected by the blocker whereas the deactivation of the channel was delayed. Thus, diltiazem was found to prevent the closure of the channels which indicates the pore blocking mechanism of diltiazem. Only the deactivation kinetics of rod and cone CNGC were found to be influenced by diltiazem and the effects triggered by the two diltiazem enantiomers were comparable.

3.5.2 Light-induced Ca^{2+} response

Using two-photon Ca^{2+} imaging, the light-induced cone responses were recorded in retinal slices from adult transgenic mice that had a wild-type (wt) background and expressed a fluorescent Ca^{2+} biosensor (TNXL) [Wei *et al.* 2012, Kulkarni *et al.* 2016]. Here, the relative Ca^{2+}-levels with ECFP-Citrine ratio (see Figure 2.1) were measured in the cone photoreceptor synapses. In the model, the Ca^{2+} biosensor is not expressed in the OS,

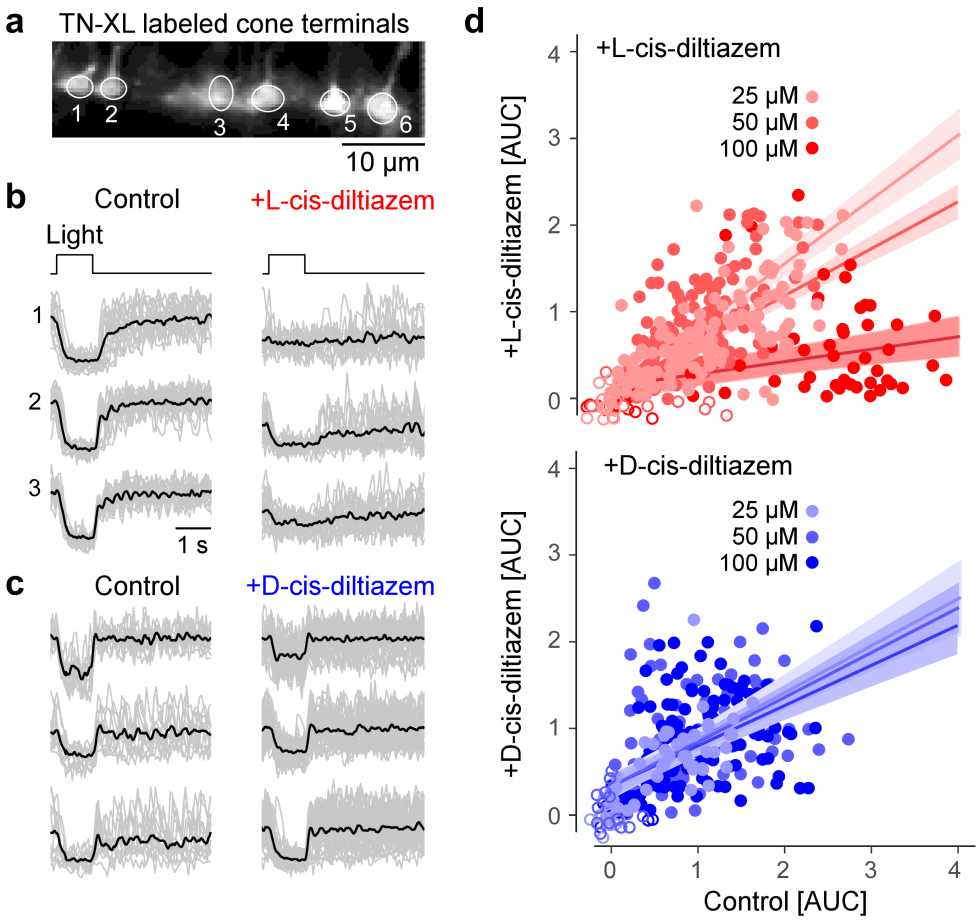

Figure 3.11: **Light-evoked cone Ca^{2+}-responses are reduced by L- but not D-cis-diltiazem**: AUC represents the total effect of the compounds on the light-induced Ca^{2+} response at a given time. (a) Recording light-evoked Ca^{2+}-responses from cone photoreceptor terminals in retinal slices prepared from a transgenic mouse that expresses the fluorescent Ca^{2+} sensor TN-XL in cones. (b,c) Exemplary Ca^{2+} responses before (control) and in the presence of 100 μM L- (b) or D-cis-diltiazem (c) (z-scored traces; grey, single trials; black, mean of n trials, with control in (b), n = 13; control in (c), n = 19; L-cis-diltiazem, n = 19; D-cis-diltiazem, n = 38). (d) Scatter plot of response size (as area under the curve, AUC) for both L-cis (blue; 25/50/100 μM n = 137/138/61 cells) and L-cis-diltiazem (red; 25/50/100 μM n = 62/140/162 cells; each data point represents a cell). Fits show mean predictions and standard errors from a multivariate linear model. L-cis-diltiazem (red) shows concentration-dependent lowering of light-induced Ca^{2+}-response. The experiments were done by Dr. Michael Power and the data analysis by Dr. Luke Rogerson and Prof. Dr. Thomas Euler.

therefore synaptic Ca^{2+} signals in the cone terminals were recorded 3.11, that indirectly show the Ca^{2+} dynamics in the OS for changes in membrane potential caused by the light-dependent modulation of CNGCs in the OS. Retinal slice preparations from *rd1*-TNXL animals were used to measure the baseline and the light-induced Ca^{2+} responses. A series of one second flashes of light were presented and the change (decrease) in terminal Ca^{2+} were measured. The responses were quantified using Area Under the Curve (AUC) in the presence of both diltiazem enantiomers at different concentrations (25, 50, and 100 μM), and in absence marked as control.

A multivariate linear model was used to identify factors (*i.e.*, enantiomer, concentration) that are significant for predicting the response of a cell after drug treatment. The analysis showed that L-cis-diltiazem induced a concentration-dependent lowering of the light-induced Ca^{2+} response. At the highest concentration (100 μM) of L-cis-diltiazem, the light-induced Ca^{2+} response was found to be almost close to zero. D-cis-diltiazem, on the other hand, did not show any change in the light-induced Ca^{2+} responses at cone synapses at any concentration (see Figure 3.11). A tendency towards the lowering of the Ca^{2+} baseline was found with the L-cis-diltiazem treatment in the cones as compared to the untreated, shown in 3.11 b exemplary responses on the left as compared to the right. The lowering of Ca^{2+} baseline was not found with D-cis-diltiazem treatment. The data suggest that the treatment with L-cis-diltiazem (essentially at higher concentrations) lowers Ca^{2+} concentration at the synapses which mimics a prolonged hyperpolarisation or a constant light situation. Thus, when the retina was exposed to light with L-cis-diltiazem treatment, these were unable to respond. The effect of L-cis-diltiazem was found to be stronger on rod CNGC than cone CNGC 3.10. The light-induced cone Ca^{2+} suggests that L-cis-diltiazem would likely have stronger response effect on light-induced rod Ca^{2+} response. Our data infers that L-cis-diltiazem efficiently blocks CNGC resulting in prolonged hyperpolarisation of the photoreceptors thereby reduces the light-induced Ca^{2+} response to a large extent.

3.6 Effect of diltiazem on calpain

The influx of Ca^{2+} via CNGC is believed to drive the degeneration process via activation of different Ca^{2+} dependent cysteine-type proteases, the calpains. Calpain gets activated by the increased concentration of intracellular Ca^{2+}. Upon activation, these are believed to be involved in various proteolytic activities leading to the cellular degeneration. After determining the differential effect of L-cis- and D-cis-diltiazem on the channel activity and on the light-induced Ca^{2+} response, their downstream effect on the calpain activity in the retina were further investigated. This was analysed on organotypic retinal tissue cultures from mutant and wt animals treated with L-cis-diltiazem (CNGC blocker) and

D-cis-diltiazem (VGCC blocker) respectively. In contrast to the light-induced Ca^{2+} response measurements, in which the incubation of the retina with the compounds were only for few a minutes, these were cultured for 7 days to obtain their effect on the degenerating retina. The activity of calpains was analysed by two independent experiments: (1) measurement of total calpain activity on unfixed tissue sections and (2) quantification of cleaved calpain-2 as a result of calpain activity on fixed retinal samples. The calpain activity assay gave the resultant activity of μ and m calpain in the retina with and without treatment of the compounds [Power *et al.* 2020].

The calpain activity has been shown to increase during the *rd1* degeneration [Paquet-Durand *et al.* 2006]. A least-square mean effects model was used to determine the statistically significant effect between the genotype and treatment. In *rd1* retina, the calpain activity was found unaltered on treatment with either D-cis-diltizem or L-cis-diltiazem (100 μM) with respect to the untreated situation. In the wt, the activity of calpain was found to be significantly lower than the *rd1* retina, treatment with either D-cis-diltiazem or L-cis-diltiazem did not show any effect on the calpain activity (3.12 m). Calpain activity in *rd1* has been shown to activate and cleave calpain-2 [Power *et al.* 2020]. The resultant of calpain activity was further assessed with the immunostaining of calpain-2, as shown in Figure 3.12. Our results showed that the LS means of calpain-2 positive cells had no effect of D-cis-diltiazem treatment (50 μM) on either of the genotypes but a statistically significant effect of L-cis-diltiazem treatment (F (1, 11.87) = 14.7372; p = 0.0024) on *rd1* and wt. The model showed the significant effect of L-cis-diltiazem treatment irrespective of the genotype 3.15, 3.16. The effect of cleaved calpain-2 were further analysed individually in each of the genotypes (wt and *rd1*)using one-way ANOVA 3.13. The analysis showed significant elevation of calpain-2 positive cells with L-cis-diltiazem treatment in wt retina, as compared to the untreated. In *rd1* retina, L-cis-diltiazem shows a likelihood towards the increase but it is not statistically significant. However with D-cis-diltiazem treatment, *rd1* retina showed a significant decrease in calpain-2 positive cells in the ONL. Our results show that the inhibition of Ca^{2+} influx via CNGC can elevate the calpain-2 positive cells in wt (about 2%) to the level of *rd1* retina. Additionally, inhibition of VGCC with D-cis-diltiazem reduces calpain-2 activation. Thus, the Ca^{2+} influx into the photoreceptors via OS CNGC is less likely to be responsible for the activation of calpain-type proteases that may result in photoreceptor degeneration in *rd1*.

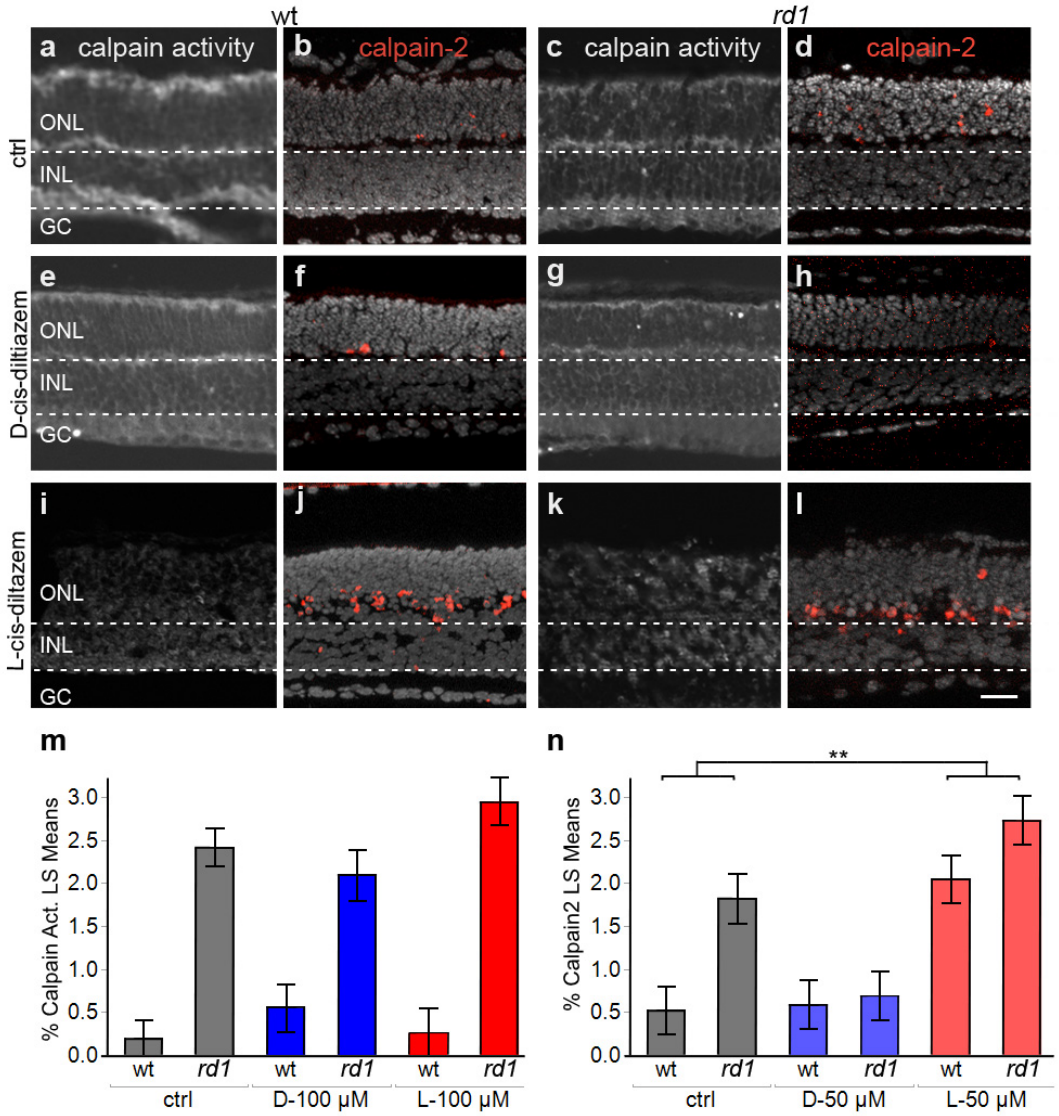

Figure 3.12: **Effects of diltiazem treatment on calpain activity:** Shows calpain-activity assay and immunostaining for activated calpain-2 in wt and *rd1* retina. Untreated retina (ctrl; a-d) was compared with D-cis diltiazem (e-h) or L-cis diltiazem (i-l) treatment. The bar graphs show the least-square (LS) means percentages of cells positive for calpain activity (m) and activated calpain-2 (n) in wt and *rd1* retina, compared to the untreated control (ctrl). Asterisks indicate a statistically significant difference from a contrast test performed between control and 50 μM L-cis-diltiazem treatment (L-50 μM). Error bars represent SEM; $** = p < 0.01$. Scale bar = 30 μm.

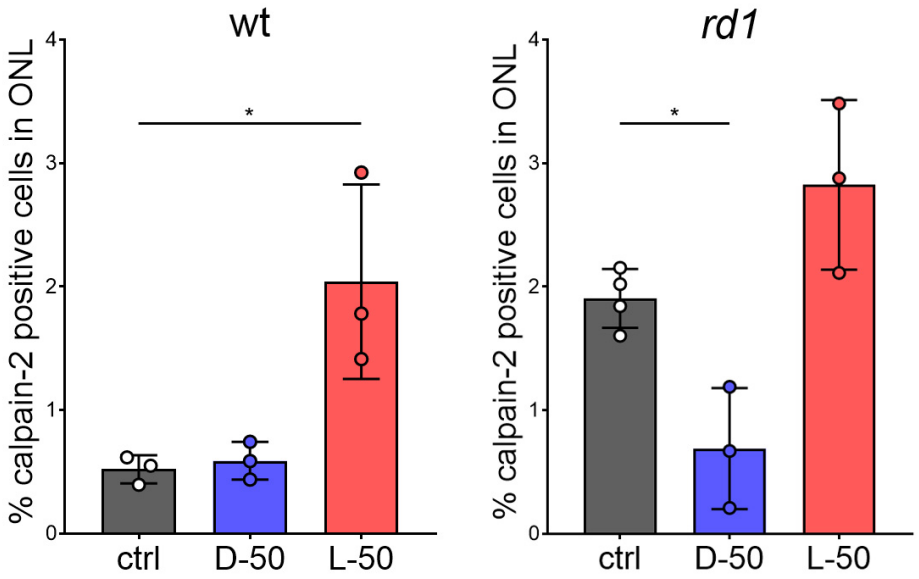

Figure 3.13: **Calpain-2 between *rd1* and wt:** A comparison between *rd1* and wt is shown for calpain-2 in respective retinal tissue. The y-axis shows the percent positive cells of calpain-2 for control or untreated (black), D-cis-diltiazem (blue) and L-cis-diltiazem (red), and the x-axis shows the respective treated animal model.

3.7 Effect of diltiazem on photoreceptor degeneration

Photoreceptor degeneration was investigated further after testing the inhibition effectiveness of the compounds on the CNGC channel subunits and the intracellular Ca^{2+} calpain activation level, which is the component of downstream Ca^{2+} interaction. The hypothesis surrounding the photoreceptor degeneration suggests that high Ca^{2+} concentration leads to high calpain activity resulting in the retinal neurodegeneration. Therefore efficient lowering of Ca^{2+} and subsequent lowering of calpain could prevent or delay the photoreceptor loss in a mutant situation. On this note, to further understand the blocking effect of D-cis-diltiazem and L-cis-diltiazem on the rod degeneration. The percent of degenerating photoreceptors were investigated in the ONL. To investigate, we used D-cis and L-cis-diltiazem for treating the retinal cultures in three different animal models *rd1*, its corresponding wt and *rd10* for the three different examined concentrations (25, 50 and 100 μM respectively) and accessed with TUNEL assay.

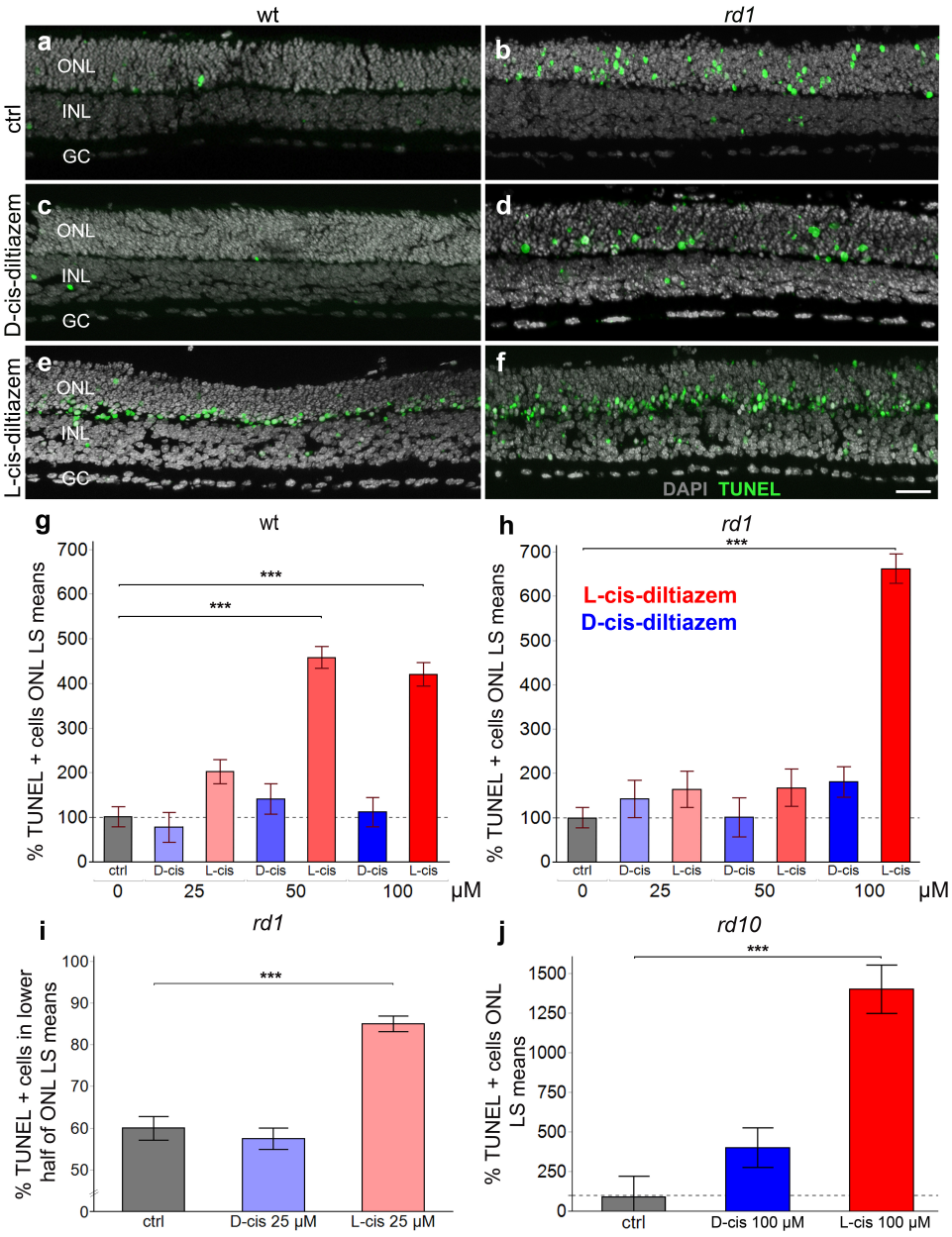

Figure 3.14: **Effect of diltiazem on *rd1* photoreceptor degeneration:** (a-f) show the images of wt and *rd1* retinal sections with TUNEL assay obtained from the retinal explant cultures of (a, b) untreated (c, d) treatment with D-cis-diltiazem 50 μM and (e, f) L-cis-diltiazem 50 μM. The retinal sections are delineated with ONL, INL and GC with nuclear staining DAPI (grey) and TUNEL (green). The quantification shows the percent TUNEL positive cells in wt (g) and *rd1* (h) treated with D-cis-diltiazem (25, 50, 100 μM) and L-cis-diltiazem (25, 50, 100 μM). (j) shows the treatment effect of untreated (black), D-cis-diltiazem 100 μM (blue) and L-cis-diltiazem 100 μM (red) on *rd10*. (i) shows the localisation percentage of dying photoreceptors near OPL in the ONL with both the treatment conditions. Scale bar = 50 μm.

Dependent variable	Genotype	Fixed effect	Normality of residuals	Homo-scedasticity	*F*-statistic	*p*-value
TUNEL	wt (35) $R^2_{adj.}$ = .80 n = 336	Concentration[1]	Yes	No	$F(3, 17.92) = 20.7656$	<0.0001
		Treatment			$F(1, 303.74) = 0.171$	0.6795
		Concentration x Treatment			$F(3, 22.8) = 29.6038$	<0.0001
	rd1 (36) $R^2_{adj.}$ = .88 n = 331	Concentration[1]	Yes	No	$F(3, 24.82) = 37.8570$	< 0.0001
		Treatment			$F(1, 306.63) = 0.0787$	0.7792
		Concentration x Treatment			$F(3, 27.75) = 31.0649$	<0.0001
	rd10 (10) $R^2_{adj.}$ = .84 n = 112	Concentration[4]	Yes	No	$F(1, 8.11) = 25.9134$	<0.0009
		Treatment			$F(1, 100.96) = 0.0026$	0.9598
		Concentration x Treatment			$F(1, 10.43) = 23.5461$	<0.0006
Calpain activity	wt (11) & *rd1* (11) $R^2_{adj.}$ = .86 n = 143	Concentration[4]	Yes	No	$F(1, 16.41) = 99.2752$	<0.0001
		Treatment			$F(2, 16.41) = 0.793$	0.4691
		Concentration x Treatment			$F(2, 16.41) = 2.055$	0.1598
Calpain- 2	wt (9) & *rd1* (9) $R^2_{adj.}$ = .83 n = 117	Genotype	Yes	No	$F(1, 12.14) = 9.0927$	0.0106
		Treatment			$F(2, 12.14) = 20.2775$	0.0001
		Genotype x Treatment			$F(2, 12.14) = 2.2535$	0.1471
Caspase-3	*rd1* (11) $R^2_{adj.}$ = .04 n = 58	Treatment	Yes	Yes	$F(2, 7.15) = 0.3799$	0.6970
ONL localisation TUNEL	*rd1* (9) $R^2_{adj.}$ = .72 n = 53	Treatment	Yes	No	$F(2, 10.11) = 49.4033$	<0.0001
Treatment: {D-cis-diltiazem, L-cis-diltiazem}, [1]{0, 25, 50, 100 µM}, [2]{0, 25 µM}, [3]{0, 50 µM}, [4]{0, 100 µM}						

Figure 3.15: **Data analysis using linear mixed-effects models:** Shown are the effects that explain the variability of the dependent variables TUNEL, calpain activity, calpain-2 positive cells, as well as localisation of TUNEL positive cells within the ONL. All models included the animal as a random effect to account for repeated measures. Numbers in brackets indicate the total number of animals used per genotype, n represents the number of observations used in the model. Normality of residuals was assessed visually; heterogeneity of residual variances (homoscedasticity) was tested with the Brown-Forsythe test. Linear mixed-effects models are shown to be robust against violations of model assumptions.

	Contrast LS means [95% confidence interval] (%)		LS means diff. ± SE (%)	F-statistic	*p*-value
ONL localisation TUNEL	*rd1* ctrl 59.98 [54.04, 65.92]	*rd1* D-25 µM 57.44 [52.05, 62.83]	2.54 ± 3.79	F(1, 16.33) = 0.4511	0.5112
		rd1 L-25 µM 85.03 [79.70, 90.36]	25.05 ± 3.40	F(1, 10.42) = 54.2025	< 0.0001
Calpain-2	*rd1* ctrl 1.82 [1.20, 2.44]	*rd1* D-50 µM 0.68 [0.07, 1.30]	1.13 ± 0.40	F(1, 12.52) = 7.9008	0.0152
		rd1 L-50 µM 2.73 [2.11, 3.35]	0.91 ± 0.40	F(1, 12.69) = 5.0979	0.0423
	wt ctrl 0.52 [0.09, 1.13]	wt L-50 µM 2.04 [1.43, 2.66]	1.52 ± 0.39	F(1, 11.87) = 14.7372	0.0024
TUNEL	*rd1* ctrl 98.10 [50.88, 145.32]	*rd1* D-100 µM 180.85 [111.06, 250.63]	82.75 ± 41.14	F(1, 28.11) = 4.0454	0.0540
	rd1 ctrl 101.96 [54.54, 149.38]	*rd1* L-100 µM 661.96 [593.66, 730.26]	560.00 ± 40.99	F(1, 26.68) = 191.1994	<0.0001
	rd10 ctrl 90.68 [201.44, 382.81]	*rd10* D-100 µM 401.33 [111.58, 691.07]	310.60 ± 178.75	F(1, 8.10) = 3.0200	0.1200
	rd10 ctrl 93.60 [198.61, 385.80]	*rd10* L-100 µM 1403.14 [1060.80, 1745.48]	1310.00 ± 199.71	F(1, 9.25) = 42.9966	<0.0001
	wt ctrl 105.35 [58.38, 152.32]	wt D-100 µM 112.44 [43.49, 181.39]	7.10 ± 39.87	F(1, 19.17) = 0.0316	0.8607
	wt ctrl 98.28 [51.36, 145.21]	wt L-50 µM 458.14 [406.36, 509.93]	359.90 ± 33.31	F(1, 18.59) = 116.6931	<0.0001
		wt L-100 µM 420.42 [366.06, 474.78]	322.10 ± 34.59	F(1, 21.63) = 86.7207	<0.0001

Figure 3.16: **Post hoc analysis of the linear mixed-effects models:** Results of contrast tests comparing the least-square means, which resulted from the linear mixed-effects models shown in Figure 3.15.

Linear mixed-effects models were used to analyse the effect of D- and L-cis-diltiazem treatment on TUNEL positive cells, shown in Figures 3.15, 3.16. Surprisingly, when the *rd1* retinal cultures are treated with L-cis-diltiazem (100 μM) a significant increase in cell death was found (F (1, 26.68) = 191.1994, p < 0.0001; see Figure 3.14 h). The effect was milder but not significant with 25 μM and 50 μM as compared to 100 μM. The results were cross-checked in another animal model *rd10*. Similar effect, that is, with a signif-

icant increase in TUNEL positive cells were found in L-cis-diltiazem treated retina (F (1, 9.25) = 42.9966, p < 0.0001; see Figure 3.14 j). The treatment with D-cis-diltiazem also showed much an average increase in cell death percentage but was not a statistically significant effect. The effect of treatments on the cell death was much stronger in *rd1* than in *rd10*. Both *rd1* and *rd10* are mutant animal models having a high concentration of cGMP which is believed to be driving the degeneration.

The effects of the compounds were further evaluated on the wt retinal explant cultures. Interestingly the treatment of L-cis-diltiazem (100 μM) on the wt retina showed a significantly high percentage of cell death (F (1, 21.63) = 86.7207, p < 0.0001). With concentration such as 50 μM the increase was also found to be significant. On the other hand, the treatment with D-cis-diltiazem showed no significant increase or decrease in cell death that implies no effect on the photoreceptor degeneration.

The distribution of degenerating photoreceptors in ONL was found to follow a pattern in our L-cis-diltiazem treatment conditions with respect to the untreated and with D-cis-diltiazem treated retina. The distribution of TUNEL positive cells in the untreated explants seemed to be evenly distributed across ONL which also seems to be the case for cultures treated with D-cis-diltiazem. But the distribution of degenerating photoreceptors seemed more closely localised with the OPL in the case of cultures treated with L-cis-diltiazem. Upon quantification, the distribution difference was found to be highly significant and about of TUNEL positive cells are localised closer to OPL in the retina treated with L-cis-diltiazem 85 ± 3% (F (1, 10.42) = 54.2025, p < 0.0001; see Figures 3.15, 3.16) while only about of dying cells were localised to the same space in the retina which is untreated or treated with D-cis-diltiazem (57 ± 4%), as compared to the untreated (60 ± 3%).

3.8 Effect of cGMP analogue on photoreceptor degeneration

The observed effect of diltiazem on the cell death was surprising in the context of the existing high Ca^{2+} hypothesis. To obtain further confirmation over our observations, the degeneration of photoreceptors was analysed using the cGMP analogues. The analogues are designed to bind the Cyclic Nucleotide Binding Domain (CNBD) of CNGC by the mechanism of competitive inhibition with intracellular cGMP. The cGMP analogues that specifically inhibit CNGC were generated in a European Union (EU) consortium called drugsford RD (a previous project network of our laboratory) in collaboration with an industrial partner called Biolog. The analogues chosen for these experiments have been characterised in cell cultures into CNGC and reduce the Ca^{2+} influx.

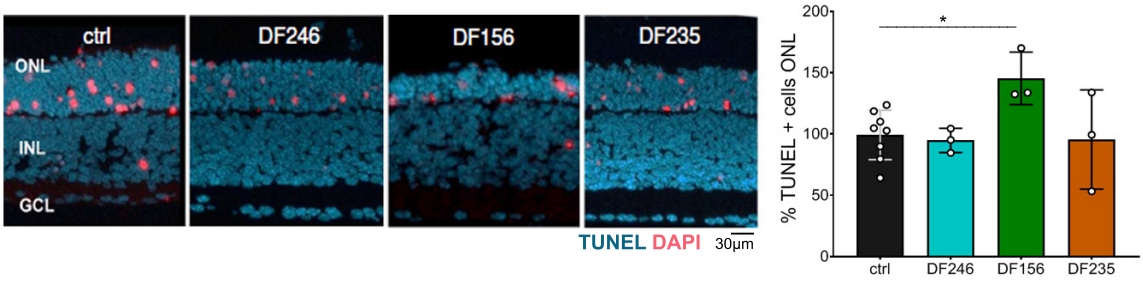

Figure 3.17: **Effect of CNGC inhibiting cGMP analogue on cell death:** Shows from the left to right exemplary *rd1* retinal sections untreated, treated with cGMP analogue DF246, DF156 and DF235. On the right shows the cell death quantification graph on treatment with cGMP analogues. These show no significant difference in the percent of dying cells on the retina treated with cGMP analogues as compared to untreated in *rd1*. Scale bar = 30 μm.

cGMP analogues RP-(2-N)ET-cGMPS (DF246), RP-8-Br(2-N)ET-cGMPS (DF156), and RP-β-1 N2-Ac-8-Br-cGMPs (DF235) were used for the experiment. The analogues DF246 and DF235 were found not to have any protective effect on the retina. The analogue DF156 however, showed a negative effect on the photoreceptor survival with a significantly high percent of cell death ($p = 0.02$, $n = 3$) (see Figure 3.17). For cGMP analogues no specific pattern in the localisation of dying cells were observed. These cGMP analogues bind to CNBD of CNGC and deactivate the channels. This is a mechanism of inhibition that is different than diltiazem enantiomers. The inhibition showed the blockage of Ca^{2+} influx could not prevent or slow the course of photoreceptor degeneration.

3.9 Relationship between calpain and photoreceptor degeneration

Calpain is believed to be the key mediator of photoreceptor degeneration in *rd1*. This belief is supported by the fact that the peak of calpain and cell death coincide with each other [Power *et al.* 2020]. Ca^{2+} being the activators of calpain, the blocking of Ca^{2+} channels are likely to prevent the activation of calpain and photoreceptor degeneration. When we inhibit the Ca^{2+} channels using the different enantiomers of diltiazem two different phenomena were found. In *rd1* lowering the intracellular Ca^{2+} influx (see Figure 3.18), surprisingly showed no significant change in the calpain activity or cleaved calpain but a significant increase in cell death percentage at 100 μM of L-cis-diltiazem. However,

this difference was not apparent at the lower concentration (50 μM) of L-cis-diltiazem, cGMP analogues DF246 and DF235. On the other hand, calpain and cell death showed a correlation to each other at all concentrations (50 and 100 μM) in wt. This may suggest that the photoreceptor degeneration in *rd1* is not directly influenced by the Ca^{2+} influx via CNGC and correlated to calpain. Also, the calpain activity might be a secondary phenomenon in *rd1* which coincides with the peak of cell death.

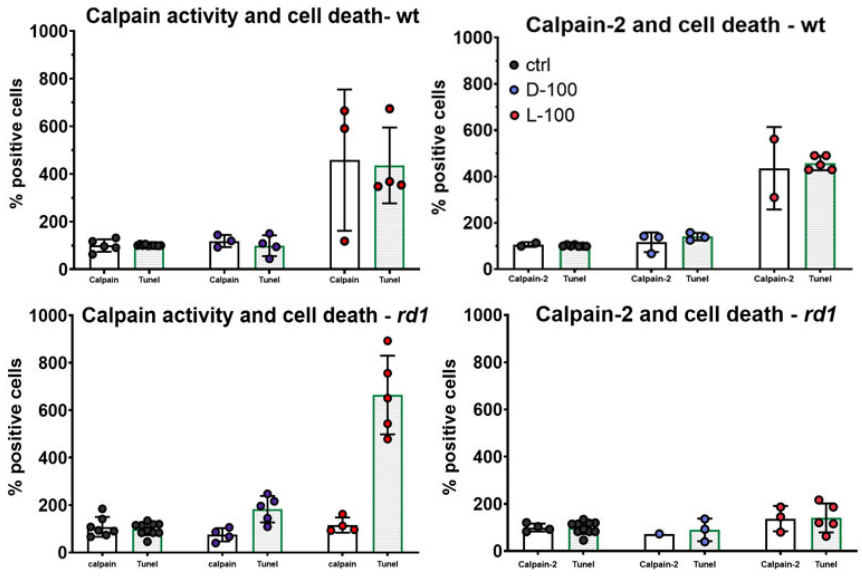

Figure 3.18: **Relative comparison calpain activity and cell death:** Shows a relative comparison between cell death, denoted by TUNEL assay (white) and calpain (green pattern), denoted by the calpain activity assay (wt, top left and *rd1*, bottom left) and calpain-2 staining (wt, top right and *rd1*, bottom right). All the data for the treatment with D-cis-diltiazem (blue) and L-cis-diltiazem (red) are normalised to 100% with respect to control (black).

3.10 Relationship between photoreceptor degeneration and apoptosis

Another type of proteolytic activity, commonly associated with apoptotic cell death, is the activity of caspase-type proteases as a key apoptotic marker. Degeneration in *rd1* has been reported to follow apoptosis independent pathway [Arango-Gonzalez *et al.* 2014].

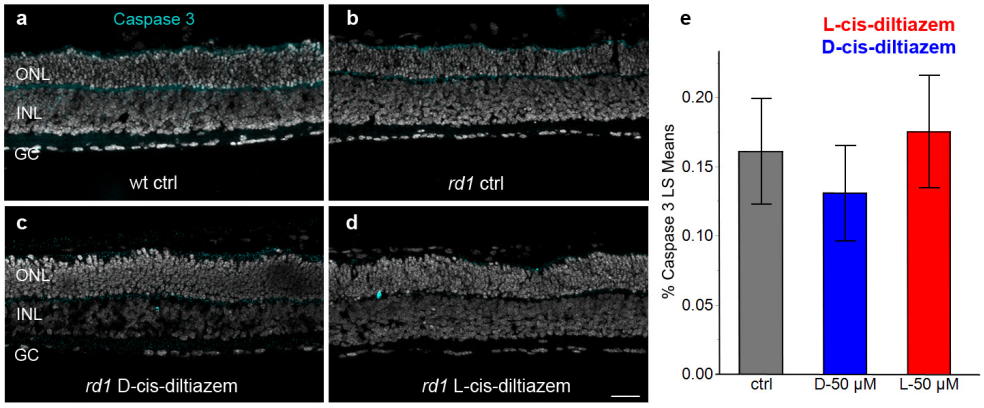

Figure 3.19: **Prevalence of cleaved caspase3:** Immunostaining for cleaved, activated caspase-3 (turquoise) was performed on *rd1* retinal sections treated with D- and L-cis-diltiazem (50 μM). While caspase-3 immunoreactivity was occasionally found in both ONL and INL the percentage of caspase-3 positive cells was far lower than the numbers of dying cells. Scale bar = 50 μm.

However, the observed elevation of cell death could result due to the activation of apoptosis. To investigate whether activation of caspase-3 could result from CNGC inhibition, the activation of caspase-3 was assessed using immunostaining with an antibody specifically directed against the active protease. The *rd1* retinal cultures treated with D- and L-cis-diltiazem were compared with the untreated retinal. The caspase-3 activity was not found in any of the conditions (see Figures 3.15, 3.19), which suggest that the degeneration of photoreceptors are independent of caspase activity. Thus, inhibition of CNGC or VGCC with diltiazem enantiomers does not seem to activate the apoptotic pathway.

3.11 Key findings

Our data show that L-cis-diltiazem efficiently blocks CNGC preventing hyperpolarisation of the photoreceptors thereby reduces the light-induced Ca^{2+} response to a large extent. L-cis-diltiazem was found strongly selective for heterotetrameric rod channels which is highlighted by its stronger effect on rod CNGCs than on cone CNGCs. Under physiological conditions (at -35 mV and $\sim$ 5 μM cGMP) both D- and L-cis-diltiazem did not show any influence on the CNGC activity at any concentration (25-100 μM). But under pathological cGMP concentration the inhibitory effect of both D- and L-cis-diltiazem were differential for rods and cones CNGC. L-cis-diltiazem showed a stronger block on rod CNGC than cone and D-cis-diltiazem also showed a partial block rod on CNGC at

higher concentrations which is nearly insignificant for cone CNGC. Deactivation kinetics of CNGC indicated a pore-blocking mechanism of diltiazem.

We found that the inhibition of the Ca^{2+} influx via CNGC elevated calpain activity in wt to the level of *rd1* retina but did not change the calpain activity in *rd1*. The inhibition of Ca^{2+} influx via VGCC into the photoreceptors did not show any change in the calpain activity. The photoreceptor degeneration was found to be elevated on CNGC inhibition using L-cis-diltiazem and cGMP analogue 2 with no elevation in the calpain activity. Thus we show that the CNGC deactivation and inhibition of Ca^{2+} influx via CNGC did not prevent or slow the course of photoreceptor degeneration with cGMP analogues. This suggests that the photoreceptor degeneration in *rd1* may not be directly influenced by the Ca^{2+} influx via CNGC and correlated to calpain. Also, the activity of calpain might be a secondary phenomenon in *rd1* which coincides with the peak of cell death.

Note: *Redefining the role of Ca^{2+}-permeable channels in hereditary photoreceptor degeneration using the D- and L-cis enantiomers of diltiazem*, **S. Das**, M. Power, V. Pop, K. Groeneveld, C. Melle, L. Rogerson, T. Euler, F. Schwede, F. Paquet-Durand, V. Nache (*manuscript submitted*).

4

Diltiazem: Effect on Poly (ADP-ribose) Polymerase Activity

Poly (ADP-ribose) Polymerase(PARP) is an abundant nuclear protein ubiquitously expressed. There are about 17 members in PARP protein family but all of the members are not enzymatically active [Vyas *et al.* 2013]. The activity of PARP-1 mediates DNA repair by functioning as DNA damage sensor responding to both single and double DNA breaks [D'Amours *et al.* 1999]. The PARP activity is reported to be elevated in *rd1* during the photoreceptor degeneration [Paquet-Durand *et al.* 2007]. Among all the 17 isoforms of PARP, only PARP-1,2,5 and 6 are known to PARylate long-chain polymer consistent to PAR synthesis [Vyas *et al.* 2014, Tan *et al.* 2012]. PARP-1 has three structural domains: (1) DNA binding domain, (2) automodification domain and (3) catalytic domain. The automodification domain is responsible for ADP-ribosylation. It is also called PARylation, that is a special post-translational modification in which (ADP-ribosyl) transferases catalyses the synthesis of ADP-ribose chain as a polymer (PAR) onto Glutamic acid substrate residue of PARP-1 from NAD^+ [Alemasova *et al.* 2019]. The signature motif predicted to be PAR generating, of the PARP substrate for PARylation, is a conserved His-Tyr-Glu (H-Y-E) triad (ART signature) in their catalytic domains [Hassa *et al.* 2008]. PARylation is structurally favoured by PARP-1 among others and is known to take place during several situations of stress such as DNA damage, apoptosis, heat shock, cytoplasmic stress and the unfolded protein response [Malanga *et al.* 2005, Koh *et al.* 2005, Petesch *et al.* 2008, Leung *et al.* 2011, Jwa *et al.* 2012]. PARylation can occur either by activation of PARP due to the cellular response or transPARylation of itself with automodification domain.

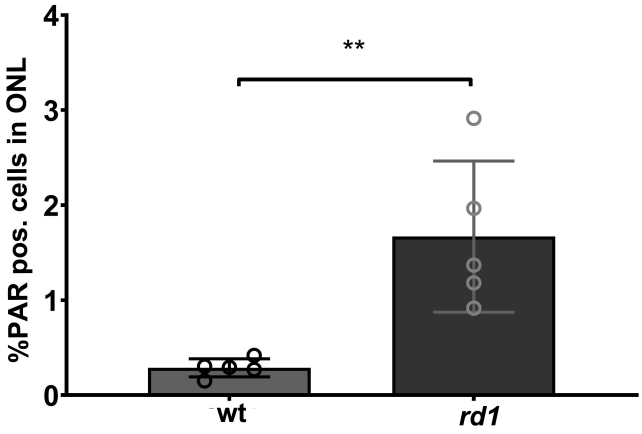

Figure 4.1: **PAR in wt and *rd1*:** Shows increased PAR level in the *rd1* ONL, depicting elevation in the PARP activity in *rd1* as compared to wt at P11.

4.1 Involvement of PARP-1 in cell death pathway

Increased PARP-1 activation has been known to be associated with stress response including elevated activation of PARP in photoreceptor degeneration, shown in Figure 4.1 [Koh *et al.* 2005, Paquet-Durand *et al.* 2007]. The increased activation of PARP leading to the generation of PAR is associated to Parthanathos. Yet excessive activation of PARP leading to depletion of NAD^+ and ATP are associated with MTP-driven necrosis [Galluzzi *et al.* 2018]. Activation of PARP releases PAR polymer which binds to AIF. PAR binds to AIF can release AIF to the cytoplasm [Virág *et al.* 2013]. AIF triggers the release of cytochrome c from the mitochondria and the activation of caspases associated with apoptosis. Advanced lines of evidence suggest that photoreceptor degeneration in *rd1* follow a cell death pathway which is caspase-independent, thus non-apoptotic in nature [Arango-Gonzalez *et al.* 2014]. PAR availability for binding to AIF is regulated by (1) PAR binding protein ring finger 146 (RNF146), which if bound to PAR cannot bind to AIF and (2) polyADP-ribosyl hydrolase like (ARH), which degrades free PAR. Cytoplasmic AIF further mediates (1) its translocation to the nucleus for DNA fragmentation and (2) promote nuclear translocation of Macrophage migration Inhibitory Factor (MIF) that in-turn catalyse the DNA fragmentation. Hexokinase-I is also believed to have a contribution in parthanathos [Galluzzi *et al.* 2018]. The formation of PAR and the depletion of NAD^+ leads to the activation of a cascade of events resulting in degeneration.

4.2 Effect of Ca^{2+} channel inhibition on PARP

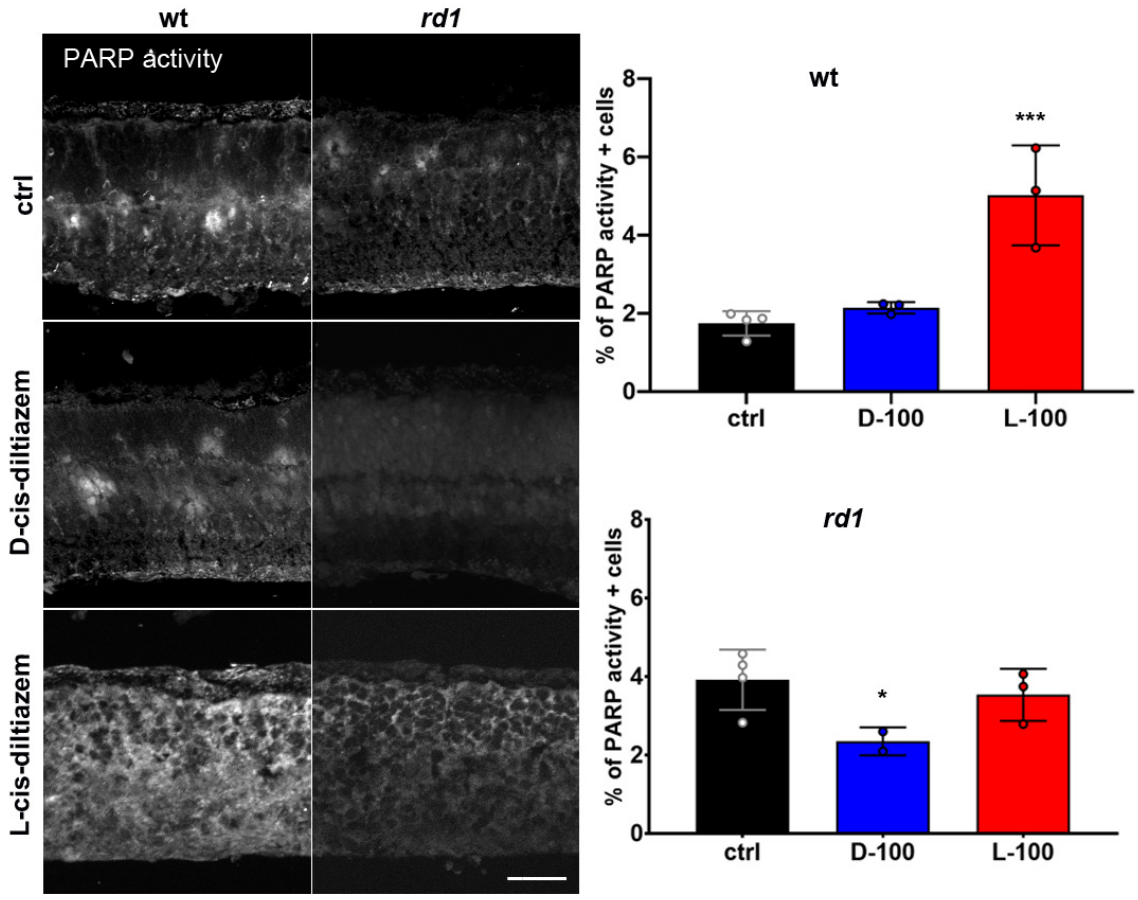

Figure 4.2: **PARP activity on *rd1* and wt retina with D- and L-cis-diltiazem:** Show the exemplary unfixed retinal sections of wt and *rd1* (left) untreated, (centre) treated with D- and (right) L-cis-diltiazem having performed with PARP activity assay. The retinal layers are denoted with DAPI (grey) having marked with ONL, INL and GC. The PARP activity positive cells are denoted with colour. The lower panel shows the quantification analysis of PARP activity positive cells in (C) wt and (D) *rd1* for untreated (black), treatment with D-cis-diltiazem (blue) and L-cis-diltiazem (red). The concentration used for the treatment is 100 μM. Scale bar = 50 μm.

The cell death pathway mediated by the pathological accumulation of cGMP in *rd1* [Farber *et al.* 1974, Paquet-Durand *et al.* 2006] proposed to have two possible independent pathways leading to the photoreceptor degeneration activated by cGMP, (1) via

the activation of CNGC and (2) via PKG activation. PARP has been earlier shown to be present downstream PKG [Arango-Gonzalez *et al.* 2014]. Ca^{2+}-dependent PARP-1 hyperactivation has been reported in cancer [Bentle *et al.* 2006]. In photoreceptors, the effect of Ca^{2+} modulation on the PARP activity was evaluated after the treatment of D- and L-cis-diltiazem. The *rd1* retinal explants were treated with D-cis-diltiazem and L-cis-diltiazem (100 μM). The PARP activity was analysed at P11 on unfixed sections. PARP activity was found to be significantly decreased in *rd1* ONL when treated with D-cis-diltiazem. The treatment with L-cis-diltiazem on the other hand, did not show any difference in the PARP activity compared to the untreated (see Figure 4.2). The wt retinal explants treated with L-cis-diltiazem showed a significant increase in the PARP activity in the ONL. D-cis-diltiazem treatment showed no change in the PARP activity in comparison to the untreated in wt ONL.

The results obtained from the PARP activity assay were validated with DAB immunostaining for the PAR polymer. This was done as an independent experiment. Fixed tissue sections were obtained after the treatment with D-cis- and L-cis-diltiazem (50 μM) and the DAB staining was performed. These results supported the observations from the PARP activity assay. The treatment with D-cis-diltiazem showed a significantly lowered PAR positive cells in the ONL of *rd1* retina. Whereas, the L-cis-diltiazem treatment showed no difference in PAR positive cells as compared to the untreated. In wt ONL, a significant increase in PAR positive cells was found on treatment with L-cis-diltiazem while D-cis-diltiazem did not show any significant difference as compared to the untreated (see Figure 4.3). Also, PAR positive cells in the ONL were found to localise themselves in line with the OPL when treated with L-cis-diltiazem. This pattern of localisation was found in both wt and *rd1*. The observed pattern was similar to the cell death pattern obtained with TUNEL assay discussed in Chapter 3, shown in Figure 3.14. The treatment with D-cis-diltiazem did not show any specific pattern of positive cells in the ONL. In the case of untreated and D-cis-diltiazem, no specific distribution pattern was observed.

In our results, the cGMP-dependent degeneration indicates a possible cross-talk between the two independent pathways via CNGC and PKG [Arango-Gonzalez *et al.* 2014]. In photoreceptors, the relationship between the intracellular Ca^{2+} concentration and PARP activity is indicated by: (1) the increase in PARP activity with L-cis-diltiazem treatment in wt and (2) the localisation of PAR positive cells close to OPL similar to the pattern of dying (TUNEL positive) cells. The similar indicative results between the PARP activity assay and DAB PAR immunostaining suggest that these are directly in correlation with each other. The absolute percentage of the PARP activity is always significantly higher than that of PAR. Figure 4.4 highlights the comparative quantification of PAR polymers and PARP activity assay. This suggests that either the PARP activity of the degenerating photoreceptor are involved in generating only a fraction of PAR, or

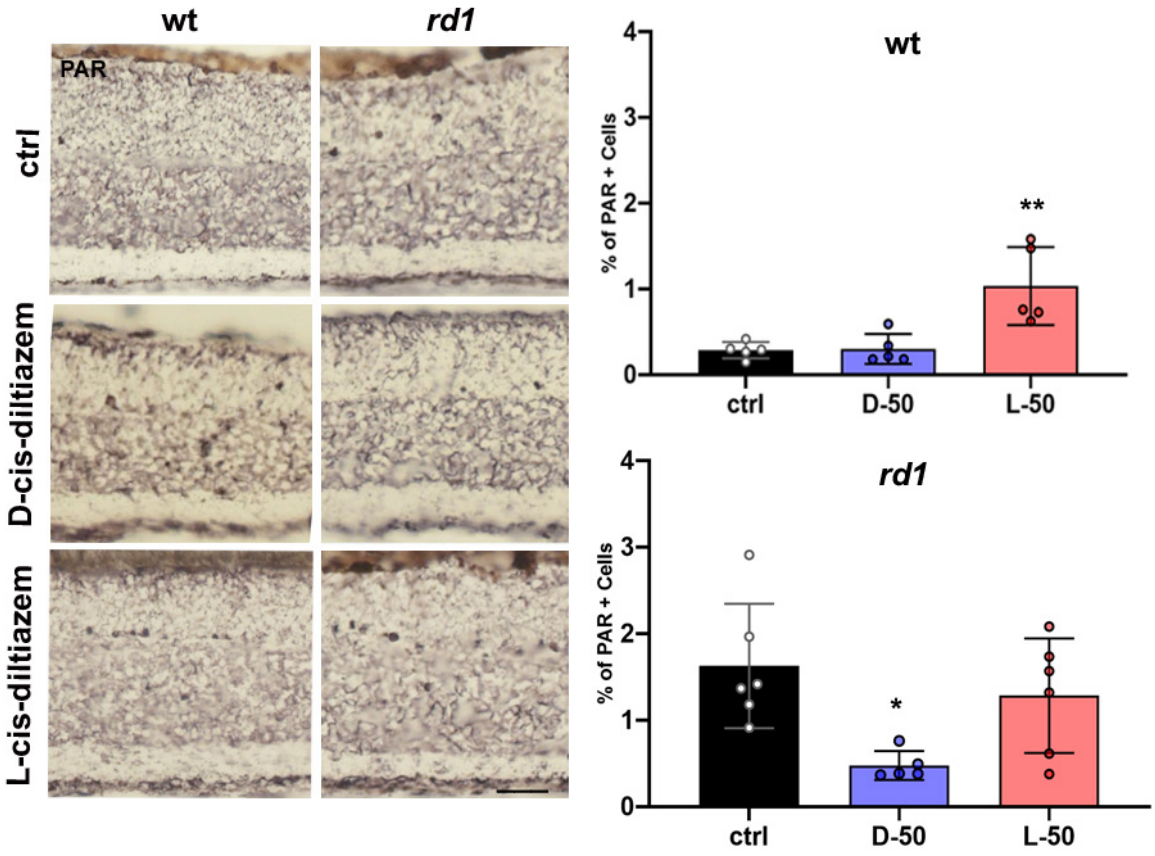

Figure 4.3: **PAR on *rd1* and wt retina with D- and L-cis-diltiazem:** Show the exemplary retinal sections of (A) wt and (B) *rd1* having performed with PAR DAB staining. The retinal layers of untreated (left), treated with D-cis-diltiazem (centre) and L-cis-diltiazem (right) retinal samples are marked with ONL, INL and GC. PAR positive cells are denoted with DAB staining (black). The lower panel shows the quantification analysis of PAR positive cells in (C) wt and (D) *rd1* for untreated (black), treatment with D-cis-diltiazem (blue) and L-cis-diltiazem (red). The concentration used for the treatment was 50 μM. Scale bar = 50 μm.

the degenerating photoreceptor is longer PAR positive than the PARP activity showing a peak at a later stage. The DNA damage, that activates PARP-1, is towards the end stage of photoreceptor degeneration [Gavrieli *et al.* 1992]. The increase in PARP-1 activation in a Ca^{2+}-dependent manner has been shown in cancer [Bentle *et al.* 2006]. Also, it has been shown in the literature, that PARP-1 has calpain cleavage sites [Chaitanya *et al.* 2010]. Taken together our results indicate that, in photoreceptors, the modulation of

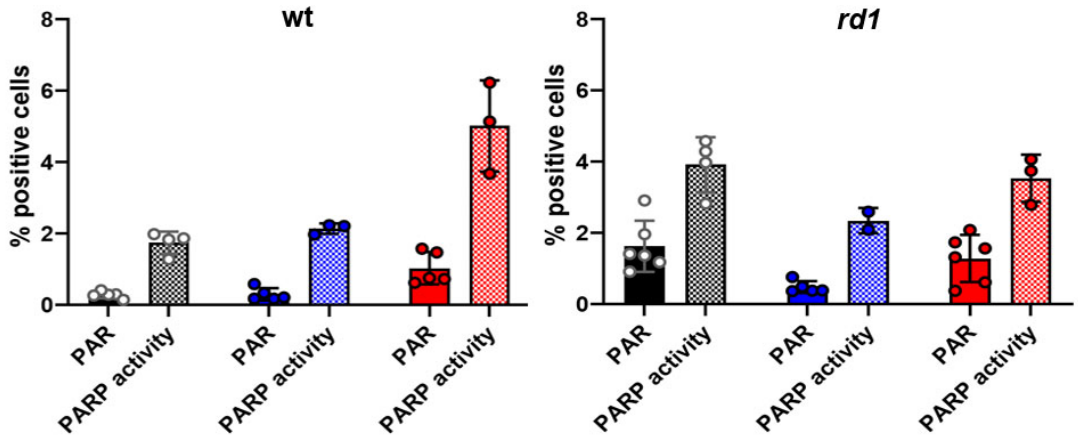

Figure 4.4: **PARP activity and PAR compared:** Shows a comparative quantification of PARP activity assay (square box pattern) and PAR (solid) between untreated (black), treatment with D-cis-diltiazem (blue) and L-cis-diltiazem (red) in wt and *rd1*. The concentration used for the treatment is 50 μM for PAR immuno assay and 100 μM for PARP activity assay.

intracellular Ca^{2+} imposes an effect on PARP activity and the activated calpain is likely to interact with PARP-1.

4.3 Key findings

The level of PARP activity in the cell is directly correlated to the formation of PAR polymer but the enzymatic activity was significantly higher than PAR accumulation. The PAR positive cells in L-cis-diltiazem treated ONL were found to follow a localisation pattern close to OPL, which is similar to the cell death pattern. The blocking of VGCC with D-cis-diltiazem in *rd1* reduced PARP activity and blocking of CNGC with L-cis-diltiazem increased PARP activity in photoreceptors. These indicate for the first time, that the level of intracellular Ca^{2+} could modulate the PARP activity in photoreceptors.

5 Expression of Glucose Transporter 3

The degeneration of photoreceptors shows increased activation of PARP-1 as a hallmark of cell death in *rd1* [Paquet-Durand *et al.* 2007], discussed in Chapter 4. The activity of PARP uses NAD^+ as a substrate. The increased activation of PARP-I is believed to cause cell death by the depletion of energy (NAD^+ and ATP) [Oka *et al.* 2012]. In physiological condition, photoreceptors are one of the most energy demanding cells of the human body and retina. The metabolism of healthy photoreceptors depicts that these are active in the dark and release a high amount of glutamate. During the light, these are metabolically less active as compared to the dark and the glutamate release is lowered [Okawa *et al.* 2008]. Glucose transporters are one of the important channels that are believed to help them cope with their energy requirement. GLUT 3 is regarded as the primary neuronal glucose transporter with a high affinity for glucose. The expression also changes with the course of development [Mantych *et al.* 1993]. All together GLUT 3 might be important for degenerating retina when the cells face an energy crisis. This chapter discusses the investigation and localisation of GLUT 3 to deduce its possible role in the degeneration.

5.1 Glucose transporter 3 and retina

GLUT 3 is recognised as the neuronal glucose transporter [Haber *et al.* 1993]. It has high affinity for glucose and greater transport capacity as compared to other classical transporters, responsible for uptake during the low glucose availability [Simpson *et al.* 2008]. Due to the high energy demanding nature, photoreceptors require energy even during the lower availability of glucose. In the literature, GLUT 3 is shown to be associated with neurodegeneration in the brain but it is less studied in the retina. GLUT 3 is shown to get up-regulated with increase in the concentration of glucose [Knott *et*

al. 1996] and located in the inner synapse of rat retina [Watanabe *et al.* 1996]. GLUT 3 is also suggested to be present in the axonal bundles of the optic nerve in the pig retina [Carreras *et al.* 2015]. To understand the function of GLUT 3 in metabolism, it is important to understand the correct localisation of this channel. Therefore, the localisation of GLUT 3 in the photoreceptors has been investigated in the adult mouse retina to shed any possible light on their involvement in the metabolism and/ or degeneration process.

5.2 Localisation of glucose transporter 3

To locate GLUT 3 in the wt adult mouse retina, GLUT 3 antibody was used in combination with retina specific markers such as, rhodopsin for rods, PNA for cones, Gt335 for primary cilium and DAPI for nuclear staining.

GLUT 3 was co-labelled with both the rods and the cones show that it is located between the OS and IS. It looked more likely to be associated with rod photoreceptors (see Figure 5.1). To understand whether or not GLUT 3 is rod specific, it was co-labelled with Peanut Agglutinin (PNA) that labels cone OS and IS (see Figure 5.1). GLUT 3 was not found to be cone specific. The co-labelling showed that GLUT 3 are densely localised like in the case of rhodopsin but not regularly interspaced like PNA. At lower magnification, it seems to co-localise with rhodopsin but with the 63× magnification the co-localisation of GLUT 3 and rhodopsin were difficult to distinguish. It might suggest two possibilities: (1) either GLUT 3 is associated with both rods and cones or (2) it is situated physically separated from either of them. Further to get a clearer understanding of this, a 3D reconstruction of the immunofluorescent signals were done with the help of ZEN software (ZEN, blue edition, 2.3). The 3D reconstruction of the immunostaining signal for both rods and cones (see Figure 5.2) showed that the fluorescent signal of GLUT 3 was distinctly separate from the rhodopsin as well as PNA signal. This suggests the expression of GLUT 3 is likely independent of rod OS disk and is also independent of the OS and IS of cone photoreceptors. This further suggests that GLUT 3 might be expressed only in rods and not cones in the adult mouse retina. Apart from the photoreceptors, GLUT 3 was also found to be expressed in the two synaptic connection layers in the IPL, demonstrated earlier in the literature [Watanabe *et al.* 1996].

5.2.1 GLUT 3 and outer segment

To check further its association with the OS, the expression of GLUT 3 were evaluated in the developing wt retina. In Chapter 3, Figure 3.1 showed that OS in wt develops from P11 (4.67 μm, $\pm$0.4 SD, n = 3) to P13 (9.2 μm, $\pm$0.8 SD, n = 3). Therefore, to

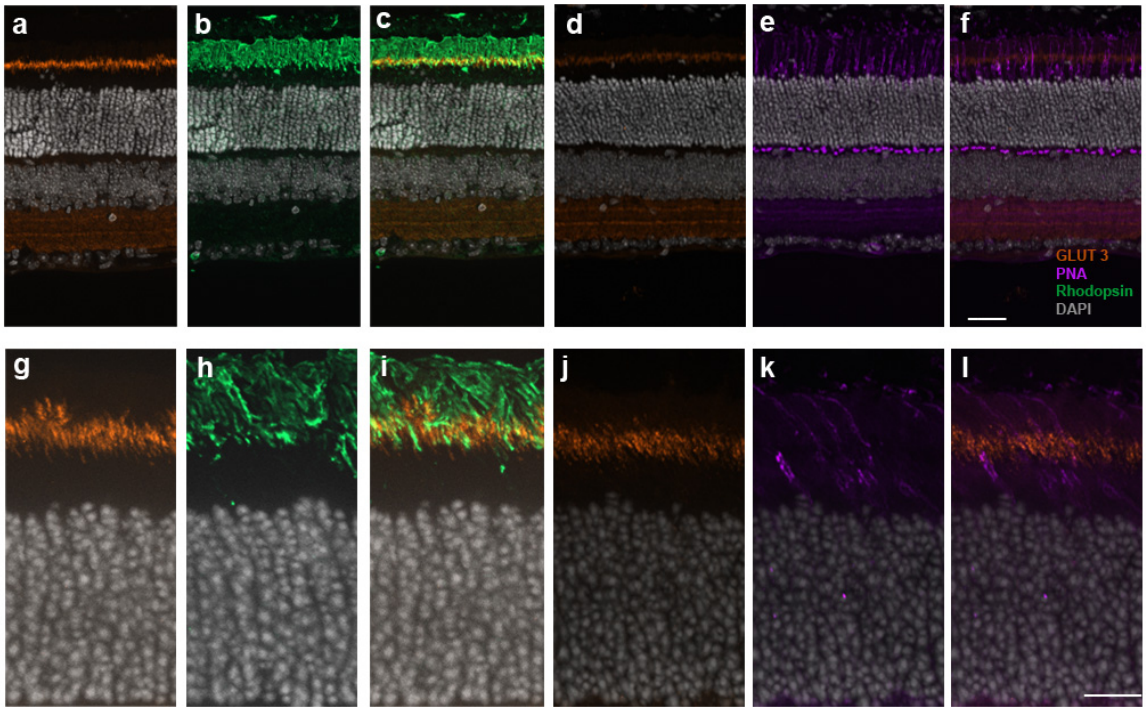

Figure 5.1: **Immunostaining GLUT 3 co-labelled with rhodopsin:** (a-f) show wt retina P30 in 20× magnification and (g-l) with 63× magnification. Sections immunolabelled with (a, g) GLUT 3 (orange) and (b, h) rhodopsin (green) as a marker for rod OS. (c,i) show the co-labelling with a merge. Similarly, (d, j) shows GLUT 3 immunostaining and (e, k) show PNA (purple). (f, l) show a merge of GLUT 3 and PNA co-labelling. The figure highlights the presence of GLUT 3 at the interphase of OS and IS. Scale bar; f = 30 μm, l = 15 μm.

understand any existing correlation between the OS and GLUT 3, immunostaining for GLUT 3 in P11 and P13 were performed. Figure 5.1 together with Figure 5.3 indicated GLUT 3 co-localisation with rhodopsin on wt retina with 20× and 63× magnification. The expression intensity found likely to increase from P11 to P13. This becomes more apparent visually at higher magnification. This could mean that the GLUT 3 is likely to increase with the maturation may not be a part of OS.

Further results from the electron microscopy were analysed to confirm the correlation between the expression of GLUT 3 and the OS development in the mouse retina. We used 15 nm gold secondary antibody (see Figure 5.4) to label the primary GLUT 3 antibody.

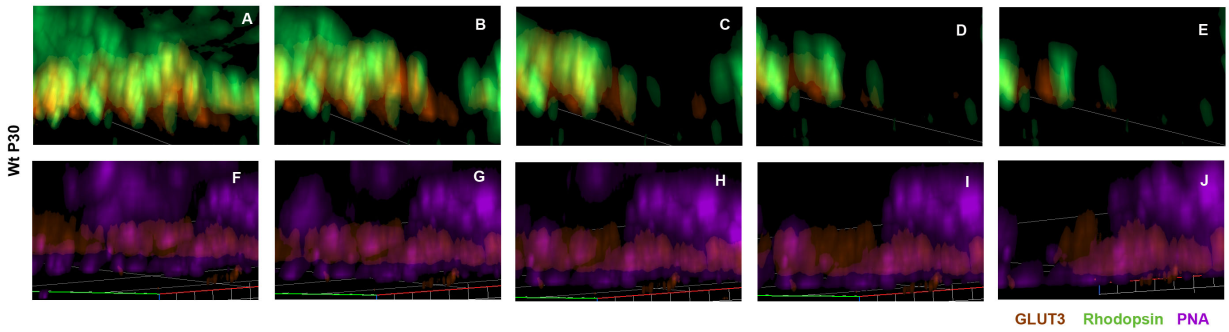

Figure 5.2: **3D reconstruction of immunostaining GLUT 3 co-labelled with rhodopsin and PNA:** (A-E) show GLUT 3 (orange) co-labelled with rhodopsin (green) and PNA (purple). Zoomed-in views (A-E and F-J) of the immunostaining signals in the OS reveal no existing co-localisation as these exist as distinct individual signals.

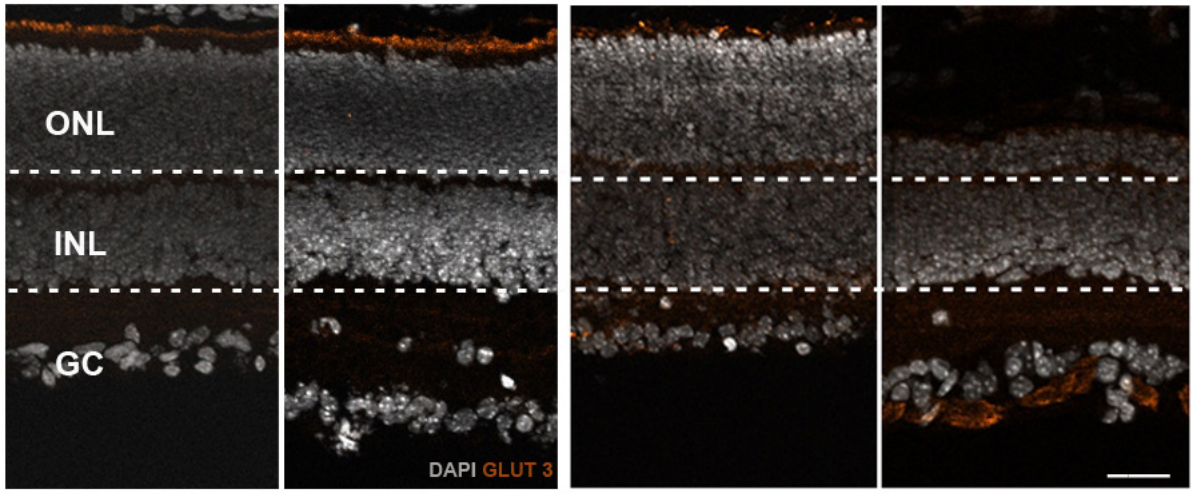

Figure 5.3: **GLUT 3 immunolabelling in wt and *rd1* retina:** (a-b) show maturation of wt retina from P11 to P13 and (c-d) show the degeneration of *rd1* mouse retina from P11 to P13 immunolabelled with GLUT 3. When compared the images of wt and *rd1* P11, wt P11 showed stronger expression of GLUT 3. Also, a strong signal of GLUT 3 expression near GCL was observed quite consistently. The expression could be at the end-feet of Müller cells in the degenerating retina at P13 that was not evident in P11. Scale bar = 50 μm

With the localisation of immunogold labelling GLUT 3 was found to be present at the base of OS but they are independent of the OS, *i.e.*, these are not present inside the OS

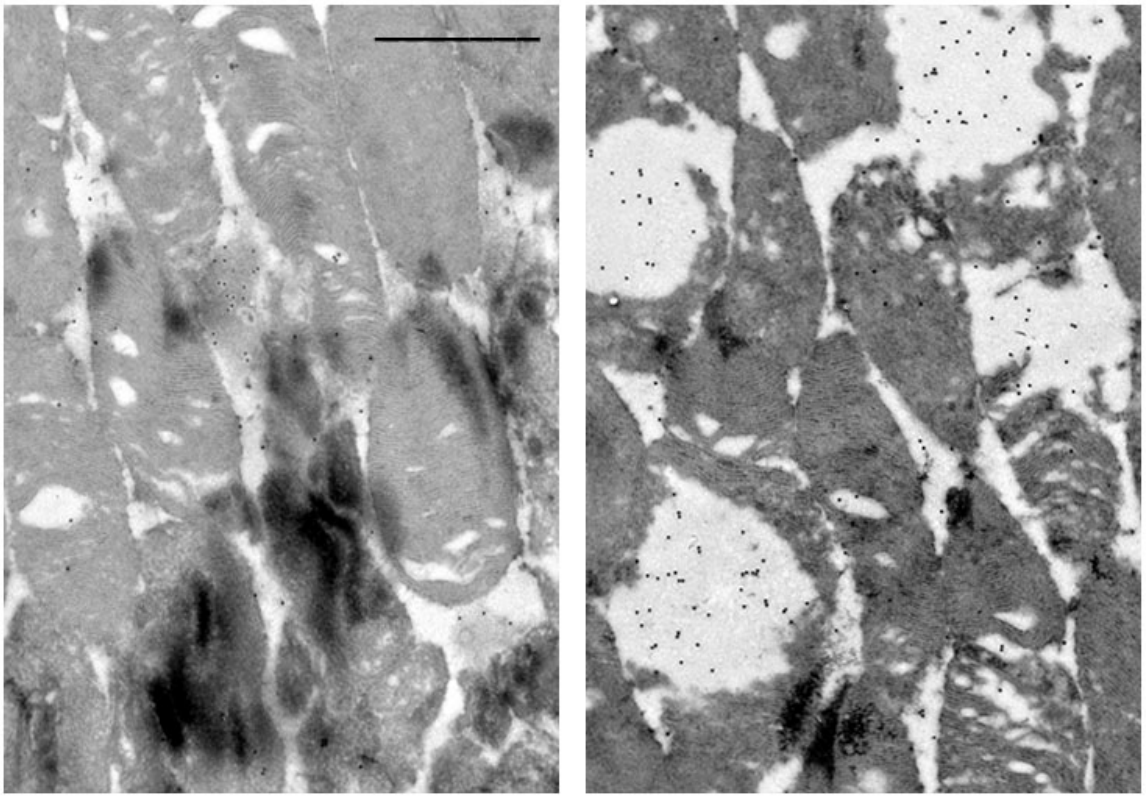

Figure 5.4: **Electron micrograph of OS with GLUT 3 immunogold labelling:** (left) shows the disk-like OS structure of the retina. Immunogold labelling (black dots) is found to be less dense in the disk of OS depicting GLUT 3 is not present in the OS but very closely associated with the OS structure. The micrograph of the OS base (right) further highlights a high density of immunogold particles in between the base of OS structures. Scale bar = 800 nm

structure.

5.2.2 GLUT 3 and connecting cilium

The indication from the above results shows that GLUT 3 is a physically independent structure and it was present approximately in between the OS and IS. Therefore, the possibility remains that it might be associated with other structures close to the interface of OS and IS. We investigated the association of GLUT 3 with the connecting cilium, which is a modified primary cilium connecting the IS and OS of photoreceptors (see Figure 1.1). Immuno-co-labelling of the connecting cilium with GT335 antibody was

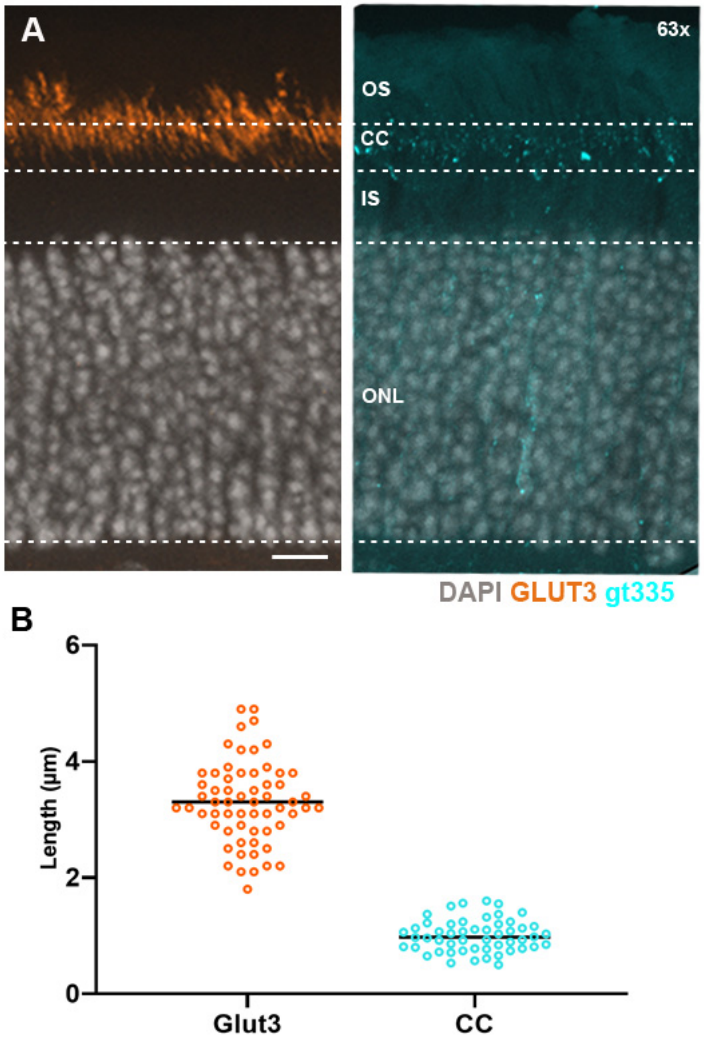

Figure 5.5: **Immunostaining of GLUT 3 and connecting cilium:** (A) shows 63× magnification image of wt mouse retina P30 with immunolabelling of GLUT 3 (orange) on the left and primary connecting cilium labelled by gt335 (turquoise); (B) gives quantification of expression (length in μm) of GLUT 3 as compared to the length of primary connecting cilium (denoted as cc) at P30. It shows that the length of primary connecting cilium is very small, an average of about 0.96 μm ($\pm$0.3 SD). On the other hand, the length of GLUT 3 is significantly longer ($p < 0.0001$) with an average of about 3.3 μm ($\pm$0.4 SD). Scale bar = 15 μm.

investigated under the high magnification (63×). The length of the primary connecting cilium was quantified with respect to the span of GLUT 3 expression (length measured in μm). The quantification showed that the expression length of GLUT 3 is variable and significantly much longer (3.3 μm, ±0.4 SD) as compared to the primary connecting cilium (0.96 μm, ±0.3 SD), labelled by gt335 [see Figure 5.5, ($p < 0.0001$)]. Moreover, the image showed that the expression of GLUT 3 is more shifted towards the end span of the OS than in the region of connecting cilium. The epitope of gt335 antibody is located at the carboxy-terminal [Bré *et al.* 1994]. The association of GLUT 3 with the outer segment of rod photoreceptors needs to be further investigated.

5.3 Key findings

GLUT 3 gives a continuous expression profile in close association with the interface of OS and IS of the photoreceptors in the adult mouse retina. Further, the localisation studies with the developing wt retina, 3D reconstruction of immunolabelling and electron micrograph of the adult retina showed that these were structurally independent of both rod and cone OS or IS. These were also found to be independent of connecting cilium of the photoreceptors. These indicate that the expression of GLUT 3 could still be in the photoreceptors independent of IS, OS and connecting cilium. These could also be expressed in the villi of RPE or in Müller cells. The results of degenerating retina (*rd1* P13) suggest that these are likely to be expressed in the apical end of Müller cells which change the course of expression during the degeneration and are expressed at their end-feet.

6

RNA Editing on in-vitro Retinal Explants

Editing RNA is another approach executed for preventing the downstream effects of *Pde6b* mutation. This chapter discusses the restoration of functional PDE6A by editing the *Pde6a* V685M mutation using the site-directed RNA editing in mice. It is an advancing approach which involves enzyme-mediated modification of specific nucleotides on RNA sequence post transcription. RNA editing is a natural process in eukaryotes that effects different populations of RNA such as mRNA, tRNA, rRNA and 7SLRNA [Ben-Shlomo *et al.* 1999].

As the editing is on the primary transcript (mRNA), the effect of editing is transient and reversible in nature. The corresponding change in the protein level is not due to the result of the modification in the genome. This makes the modification temporary and relatively safe because the modified RNA can result in a modified protein only until it is degraded in contrast to the case of DNA. These advantages have made the RNA capable of regulating the expression of genetic information. In terms of research it is a very good model for understanding biological functions because modifications or editing on RNA level can be reversibly applied in a given cellular environment. Clinically or therapeutically RNA editing is relatively safe because of their temporary nature. There is a room for rework with respect to the environmental changes [Rosenthal 2015]. Additionally, the modification via the recruitment of endogenous enzymes makes it very flexible. At the same time, the transient and reversible nature of the change raises lower ethical concerns as compared to gene therapy. Editing via deamination is one type of RNA editing that is executed by Adenosine Deaminases that act on RNA (ADAR) facilitated by the removal of ammonia from the nucleoside base.

6.1 ADAR mediated RNA editing

Mammalian ADARs are enzymes that catalyse Adinosine (A) to Inosine (I) modification in dsRNA. ADAR binds to A of RNA and changes it to I by removing ammonia. I is biologically recognised as Guanosine (G) during translation [Bass *et al.* 1988]. The phenomenon of A to I RNA editing via ADAR was first discovered in *Xenopus laevis* oocytes and embryos [Bass *et al.* 1987]. The N-terminal of ADAR has a dsRNA binding domain which binds directly to the target RNA [Stefl *et al.* 2006]. The C-terminal is the catalytic domain performing the deaminase activity. ADAR1 is ubiquitously expressed [Kim *et al.* 1994]. ASO mediated recruitment of endogenous ADARs has been shown to perform the targeted RNA editing [Merkle *et al.* 2019]. ADAR shows a high sequence selectivity for deamination of the base [Macbeth *et al.* 2005]. In a fully base-paired dsRNA sequence of about 100 bp, more than half of its A bases can be edited by ADARs [Macbeth *et al.* 2005]. By contrast, only a few A of short length sequence and/or partially base-paired dsRNAs are selectively edited, indicating that the secondary structure of substrates dictates the editing-site selectivity [Nishikura *et al.* 1991]. ADAR1 and ADAR 2 are found to express in the retina [Lehmann *et al.* 1999]. In humans ADAR2 is shown to be very efficient for the specific RNA editing [Wettengel *et al.* 2017]. ASO mediated down-regulation of a *CNGb1* has already been discussed in Chapter 3. This chapter discusses the ASO mediated RNA editing for the first time in mouse retinal tissue culture.

6.2 Site specific RNA editing mechanism with ASO

ADAR selectively recognizes and edits the long dsRNA. The two important steps are: (1) recognition of the site of mRNA editing and (2) the recruitment of ADAR to perform the deaminase reaction. These are achieved by the binding of specifically designed ASO (in collaboration with Prof. Stafforst's lab, Tübingen). Typically the ASOs for RNA editing have two domains. A hairpin loop structure at its one end which recruits ADAR for the site-directed editing. The other domain is single-stranded which forms a double-stranded structure by base-pairing with the target RNA (see Figure 6.1) [Merkle *et al.* 2019]. The binding of ASO can make the mRNA double-stranded and recruit ADAR for editing. The site-specific editing of A is executed by the deamination (removal of ammonia group) that converts A into I. Biologically I is recognized as G, which base-pairs with C resulting into A to G editing. Because these ASOs guide the ADAR to execute editing, these are also called guide RNA (gRNA).

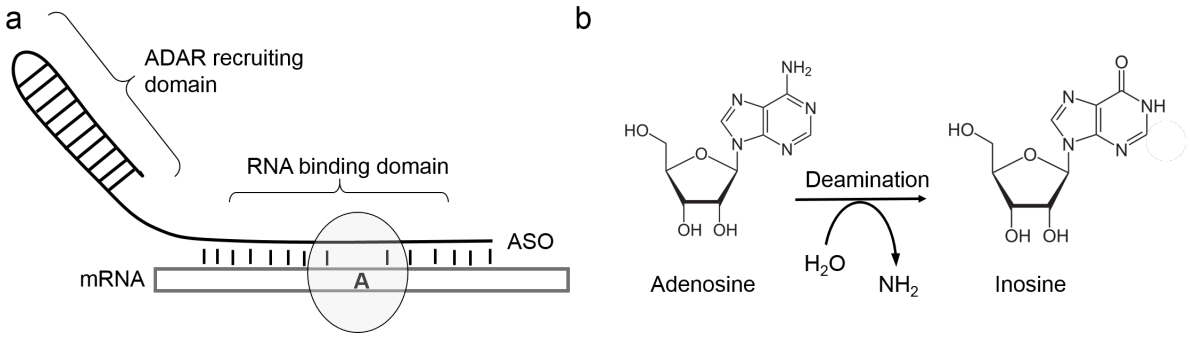

Figure 6.1: **Site-directed RNA editing – mechanism of action:** (a) shows the structure of site-directed RNA editing ASO. It has two domains, the ADAR recruiting domain that forms a hairpin loop structure and the RNA binding domain that is single stranded. The site of editing (encircled to highlight) undergoes deamination reaction (b) by the ADAR converting into I.

6.3 ASO efficacy and stability

The ASOs designed in this way were first tested in HeLa cells for their efficacy in terms of the percent of editing. Figure 6.2 shows the three most effective ASOs in the cell culture system. All the 3 ASOs or gRNA variants were found to have the average editing efficacy; TMR172 41.3% (±10.9 SD), TMR173 54% (±7.78 SD) and TMR188 20.67% (±1.88 SD). The editing for TMR 172 and 173 were found high but with a wider standard deviation.

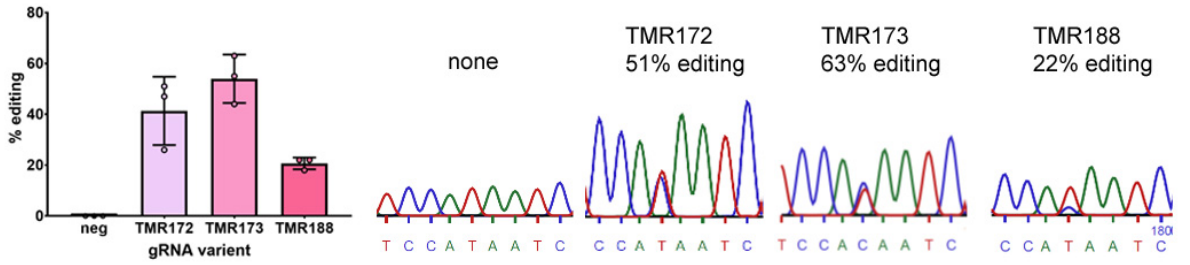

Figure 6.2: **Editing efficacy of gRNA variants on HeLa:** Left panel shows the average editing percent plotted for the three gRNA variants. The values are plotted with three replicates for each variant with SD. On the right, the sequencing histogram highlights the percent of editing. TMR173 shows the highest percent of editing followed by TMR172 and then TMR188.

Retinal explant cultures are performed in the serum free customised medium. The stability of the gRNA ASOs were checked with the complete medium used for the explants prior to the efficacy validation on tissues. The gRNA ASOs were tested across different time points (0, 5 minutes, 10 minutes, 1 hour, 3 hours, 6 hours, 24 hours, 48 hours, 72 hours, 96 hours and 7 days) moving from the left to the right as shown in the Figure 6.3.

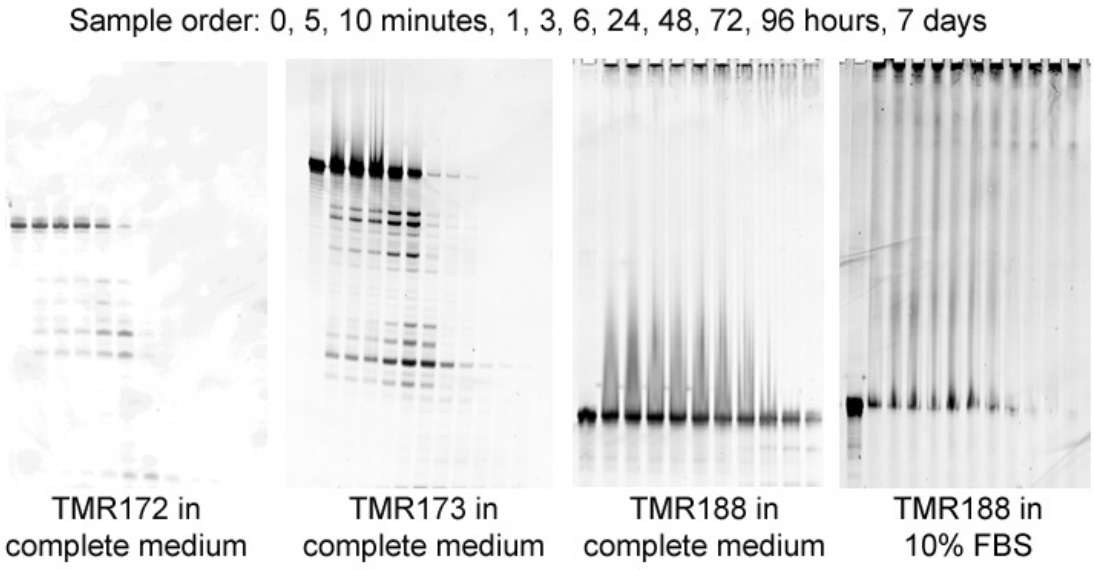

Figure 6.3: **Stability assay of ASOs:** Shows the gel with stability assay of gRNA variants. The stability was compared on the gel after assessing the stability for 0, 5 minutes, 10 minutes, 1 hour, 3 hours, 6 hours, 24 hours, 48 hours, 72 hours, 96 hours and 7 days respectively. TMR172 was found to be the least stable (about 3 hours) followed by TMR173 (about 24 hours) and TMR188 (about 7 days).

TMR172 was found to be stable for about 1 hour to a maximum of 3 hours, which was the least stable among the three ASOs. The stability of TMR173 was found to be for about 6 hours. The traces of the gRNA could be found also at 24 hours. However, most of the gRNA ASOs were supposedly degraded by 24 hours incubation and only a very faint band was found on our gel (see Figure 6.3). TMR 188 was found to be the most stable ASO which showed a very strong band until 96 hours. A fairly strong traces of TMR188 could be found on the gel even at 7 days. The stability of TMR188 was further cross-checked with 10% FBS and it showed stability up to 48 hours. The stability test is an important parameter before the validation of gRNA ASOs on long term tissue cultures. This is because the general medium change interval is 48 hours. To

move forward with the validation on the retinal explant culture system, TMR188 was selected, that showed good stability in the culture medium.

6.4 Restoration of functional Pde6a in retinal explants

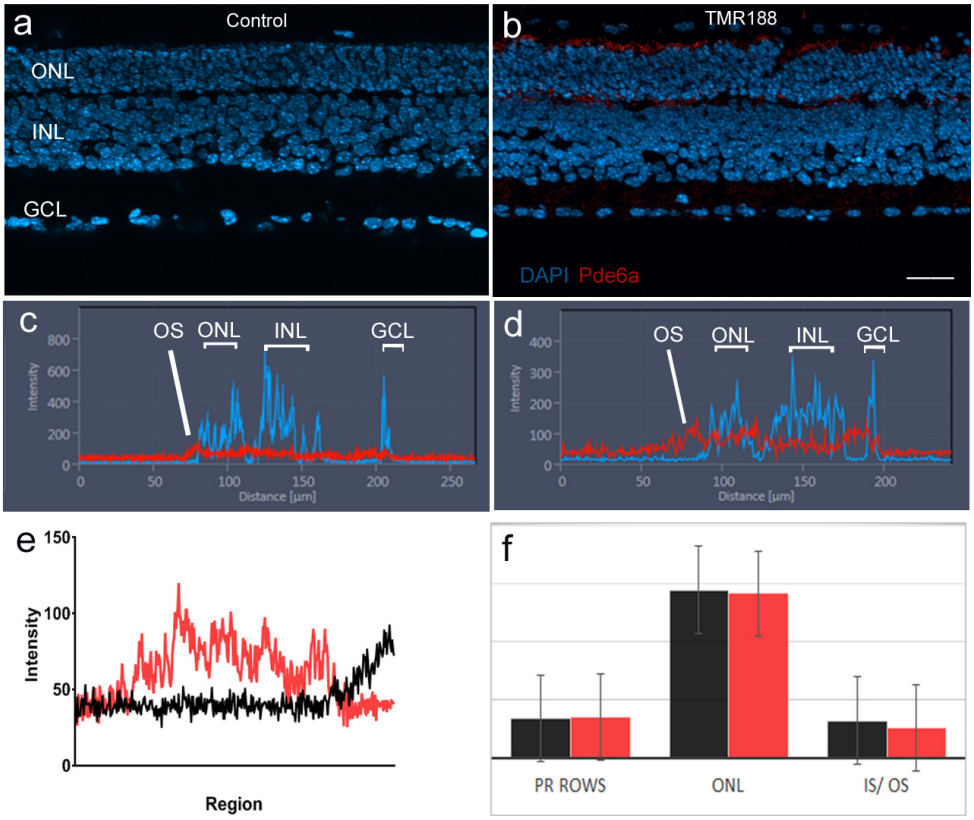

Figure 6.4: **Restoration of functional PDE6A on retinal explants:** (a,b) show the control retinal sections compared to the sections expressing functional Pde6A with TMR188 transfection that can also be seen in the intensity profile analysis (c, d, e). The ONL and IS/OS (f) quantification showed no toxic effect. Scale bar = 50 μm

Retinae were explanted from *Pde6a* V685M mouse models for the validation of site-directed RNA editing. This animal model, first described by Sakamoto [Sakamoto *et al.* 2009], has a c.2053G>A/p.Val685Met mutation which was found homologous with human causing autosomal recessive retinitis pigmentosa [Corton *et al.* 2010]. End of the

experiment using TMR188 was followed by sequencing *Pde6a* from the extracted total RNA and immunostaining of PDE6A on histological sections of explant cultures after experimentation.

The percentage of editing for TMR188 was compared with its respective negative control. The transfected retinal explants were analysed for the editing of *Pde6a* by sequencing. The sequencing histogram showed very low traces of editing which was about 3% editing (see Figure 6.4). The formation of functional PDE6A was analysed by the histological analysis of retinal cultures. The histological sections of the retinal cultures were immunolabelled with antibody against PDE6A and successful expression of PDE6A in the OS of the retinal sections were found (see Figure 6.4 a, b). The intensity of the expression was analysed by drawing the intensity profile across the retina from OS to GCL for PDE6A and DAPI. The intensity profile showed a peak for TMR188 treated cultures against the control sections, which upon plotting showed an increased intensity of PDE6A expression with TMR188. This likely indicates the restoration of Pde6A in the retinal cultures of *Pde6a* V685M animal models. Further, the thickness of ONL with a number of photoreceptor rows was quantified for both control and TMR188 transfected retinal sections. No significant difference was found in the thickness of ONL or photoreceptor rows indicating negligible toxicity on the tissue culture by ASOs.

6.5 Key findings

Successful restoration of functional PDE6A was shown on the retinal tissue culture for the first time using gRNA ASO for site-directed RNA editing. The stability of ASO plays an equal contributing factor with editing efficacy on retinal tissues. The toxicity of ASOs were found to be negligible.

7 Malarial Retinopathy

This chapter discusses the malarial retinopathy which is another form of retinal degeneration caused due to an external factor, *i.e.*, the invasion of malarial parasite. The retina is a part of central nervous system which is connected to the brain with a direct extended vasculature [Tata *et al.* 2015]. Unlike the brain, the retinal neuronal network is highly accessible which makes it easier to study. Therefore, retina has been suggested as a window to brain for understanding the functionality including neurodegenerative disorders [London *et al.* 2013]. It has several common features of brain among which the inner Blood Retinal Barrier (BRB) is considerably very close to the Blood Brain Barrier (BBB) [Trost *et al.* 2016]. Although the ease of study and high accessibility of retina promoted research on cerebral malaria [MacCormick *et al.* 2014], not much is known about its basic interaction nature during the retinopathy in malarial infection.

Most patients, especially children, who die of malaria in Africa have cerebral malaria manifest as profound coma [Marsh *et al.* 1995]. The common unique clinical manifestations displayed by the retina during severe malaria are retinal whitening, macular whitening, vessel changes, retinal haemorrhages and papilledema [Barrera *et al.* 2018, Beare *et al.* 2006, Lewallen *et al.* 2000, Schemann *et al.* 2002]. Rapid available diagnostic tests are based on the detection of *Plasmodium*-specific proteins which are subjected to variability and thus difficult to interpret [Hanscheid 2003]. Due to all these mentioned factors, it would be highly desirable to have an animal model that displays human clinical manifestations of cerebral malaria [Craig *et al.* 2012] and monitor retinopathy using non-invasive techniques such as Optic Coherence Tomography (OCT) and Scanning Laser Ophthalmoscopy (SLO) to gain an understanding of disease progression and early detection.

7.1 Malarial parasite and neuroretina

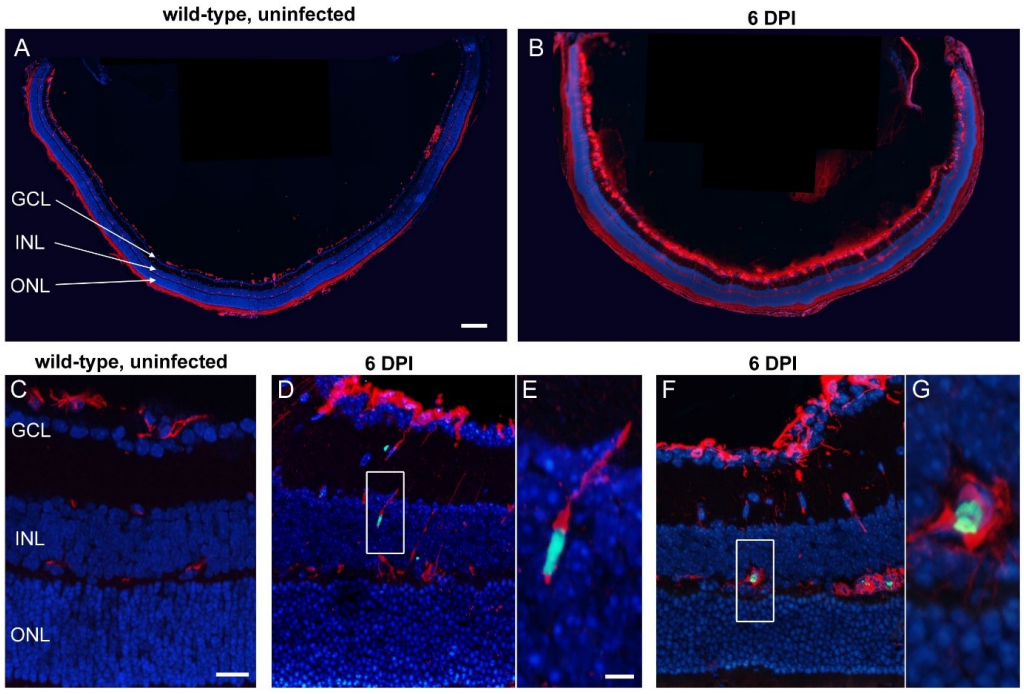

Figure 7.1: **Activation of GFAP in Müller cells during malarial retinopathy:** The upper panel shows a full cross-section of an uninfected wt retina (A) showing base level expression of GFAP and 6 DPI, (B) showing increased activation of Müller cells highlighted by the increased up-regulation of GFAP. The panel below shows the zoomed-in view of wt uninfected retina, (C) and retina 6 DPI, (D-E, F-G) showing the co-localisation of GFP-labelled parasite and GFAP of activated Müller cells. This highlights the interaction of malarial parasite in two possible ways. Either the parasites are internalised by Müller cells, clearing the debris of the infected retina, or the parasites sequestered in the retinal vasculature reaches in the neuroretina via Müller cells. Scale bar; A = 200 μm, C = 25 μm, E = 5 μm.

In this study, *in-vivo* retinal structure [Fischer *et al.* 2009] was assessed in the mice of C57BL/6J strain infected with the fluorescent *Plasmodium berghei* [Franke-Fayard *et al.* 2004]. Both uninfected animals measured as controls and animals infected with *Plasmodium berghei* were analysed at 6 Days Post Infection (DPI). The animals were subsequently treated with a standard anti-malarial drug Dihydroartemisinin (DHA) at 6 DPI and were monitored further for 12 days. The experiment was ended on 18 DPI. The animals were analysed for the retinal structure using non-invasive methods such as OCT, SLO and Electroretinogram (ERG) as well as histology. Histological analysis was performed at

6 DPI and 18 DPI. For the discussion in this thesis chapter the histological analysis is mainly focused, for the detailed outcome of the complete study refer to [Paquet-Durand *et al.* 2019].

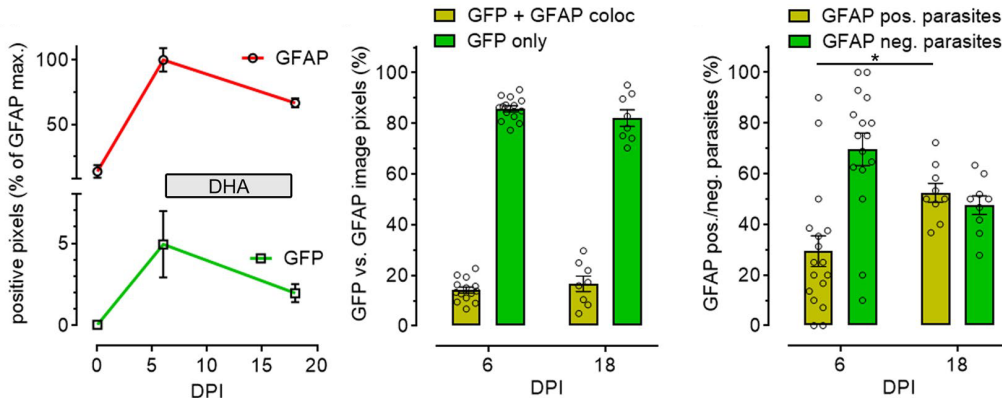

Figure 7.2: **Quantification of activated GFP and GFAP during retinal parasitemia:** The panel on the left shows the comparative expression level of GFAP in the infected retina as compared to the presence of parasite (GFP). The x-axis indicates DPI and the y-axis shows positive pixels percentage. A peak is observed at 6 DPI as it is the day of DHA administration. The central graph shows GFP and GFP-GFAP co-localisation with respect to free GFP in the retina (y-axis) at 6 DPI and 18 DPI (x-axis). The panel on the right shows GFAP positive and GFAP negative parasite percent (y-axis) at 6 DPI and 18 DPI (x-axis).

As immunoreactive Müller cells show profound up-regulation of GFAP during the infection or neurodegeneration, when compared to healthy retina. The GFAP expression was used as a readout for retinal reactivity in the presence of the parasite. In the histological sections of our experiment, free fluorescent labelled parasites could be traced in the retina. Also, both GFAP and GFP could be co-localised at 6 DPI highlighting the role of retinal Müller cells in the malarial retinopathy. This might suggest that the parasites actually cross the BRB. The crossing of BRB by malarial parasites are supported by the earlier studies showing an increased percentage of parasitised RBCs sequestration in retinal microvessels in patients having malarial retinopathy [Barrera *et al.* 2015]. The co-localisation of parasites with Müller cells might suggest the phagocytosis of parasites by the activated Müller cells. Müller cells lie at the interface of the inner and outer limiting membrane and have direct contact with the retinal vasculature. Increased sequestration of parasites at retinal microvessels makes it highly probable for them to come in contact with Müller cells. It might also suggest that parasites may cross the BRB indirectly by infecting the Müller cells. To further understand the overall effect of the parasitemia at 6

DPI and the effect of anti-malarial drug DHA at 18 DPI, the presence of parasite (GFP) within the activated Müller cells (GFAP) and their co-localisation percentage were quantified on our sections.

The parasitemia is found to increase linearly starting from the first DPI and was found to be highest at 6 DPI. It was indicated by the expression of GFAP by the Müller cells. After DHA administration at 6 DPI, GFP starts to decrease which forms a peak (see Figure 7.2). Therefore considering GFAP intensity of 100% at 6 DPI, the uninfected animals showed 13.5% (±6.9 SD) of GFAP-labelling intensity. Interestingly, some Müller glia cells were found to be co-localised with parasites, further confirming disruption of the BRB by the parasites and enter into the neuroretina. The animals undergoing DHA treatment for 12 days appeared normal and showed no symptoms of the disease at 18 DPI [Paquet-Durand *et al.* 2019]. Compared to 6 DPI, GFAP immunoreactivity in 18 DPI retinal tissue sections were reduced to 69.2% (±6.4 SD) but were elevated when compared to control. Relative to 6 DPI GFAP-positive labelling, 4.9% (±3.5) of pixels were positive for GFP at 6 DPI. This value was lowered by 2.6% (±1.6) at 18 DPI (see Figure 7.2). Co-localisation between GFP and GFAP was relatively low, with 14.2% (±4.5) and 16.5% (±8.6) of all GFP positive pixels, also positive for GFAP at 6 DPI and 18 DPI, respectively. Indeed, rather than co-localising, in many cases the GFP-positive parasites appeared to be displacing the GFAP label inside the Müller glial cells. To assess the precise number of parasites inside the Müller glia cells, the intraretinal GFP-positive parasites associated with the Müller cells and single GFP-positive signals indicating parasites were quantified together. The quantification showed a significant increase of parasites in the Müller cells from 6 DPI (29.4% ±6.1) to 18 DPI (52.5 ±3.7; $p \leq 0.05$), suggesting that the Müller cells may have prevented the effectiveness of DHA treatment on the parasites.

7.2 Key findings

A preclinical murine model for cerebral malaria was shown to reproduce the main hallmarks of human malarial retinopathy. The malarial parasites could cross BRB after the infection and were found in retina even after 12 days of antimalarial treatment. A prolonged interaction of parasites with the Müller cells was observed before and after the treatment indicating their important role during the parasitaemia.

Note: *A retinal model of cerebral malaria*, F. Paquet-Durand, S. C. Beck, **S. Das**, G. Huber, L. Chang, T. Schubert, N. Tanimoto, M. Garcia-Garrido, R. Mühlfriedel, S. Bolz, W. Hoffmann, U. Schraermeyer, B. Mordmüller, M. W. Seeliger, Sci. Rep. **9**, 3470 (2019) (*published*).

8

Discussion and Conclusion

High accumulation of cGMP is a major characteristic feature found in hereditary retinal degeneration [Farber *et al.* 1974, Arango-Gonzalez *et al.* 2014]. One hypothesis suggests that the high intracellular cGMP leads to increased influx of Ca^{2+} via CNGC in the OS of photoreceptors [Fesenko *et al.* 1985]. This in-turn may activate Ca^{2+}-dependent cysteine proteases (calpains) further downstream, thereby accelerating photoreceptor degeneration [Paquet-Durand *et al.* 2006]. In this study, diltiazem enantiomers were used on photoreceptors to block CNGC and VGCC. These blocks resulted in the modulation of Ca^{2+} influx in photoreceptors. Here, we discuss the downstream effect of modulated Ca^{2+} concentration on calpain and PARP activity and suggest their possible involvement in the cell death pathway.

Photoreceptors maintain their Ca^{2+} homeostasis with the extracellular environment using different Ca^{2+} permeable channels. Ca^{2+} enters via CNGC in the OS and VGCC around the synaptic terminal [Nachman-Clewner *et al.* 1999]. The intracellular Ca^{2+} is extruded by the Plasma Membrane Ca^{2+} ATPase (PMCA) from the cell body and IS of photoreceptors [Krizaj *et al.* 1998]. Na^{+}/Ca^{2+} K^{+} exchanger (NCKX) extrudes Ca^{2+} from the OS [Sharon *et al.* 2002]. Other channels contributing to the Ca^{2+} homeostasis are Na^{+}/K^{+}-ATPases (NKX) in the IS [Wetzel *et al.* 1999], Receptor-Operated Ca^{2+} Channels (ROC) and Store-Operated Ca^{2+} Channels (SOC) [Molnar *et al.* 2012].

CNGC and VGCC in the photoreceptors are arguably the two major sources of Ca^{2+} [Mansergh *et al.* 2005]. High Ca^{2+} has been hypothesised as the main component that drives the photoreceptor degeneration in *rd1* [Fox *et al.* 1999]. Frasson and colleagues [Frasson *et al.* 1999] tried to block the Ca^{2+} influx using D-cis-diltiazem and found significant improvement in the survival of photoreceptors *in-vivo*. This study further motivated other studies to use D-cis-diltiazem or the racemic mixture of D- and

L-cis-diltiazem to prevent the retinal degeneration. D-cis-diltiazem could not rescue the photoreceptor degeneration either in P23H rats [Bush *et al.* 2000] or in the rcd canine model [Pearce-Kelling *et al.* 2001]. In contrast to [Frasson *et al.* 1999], no protective effect of D-cis-diltiazem could be found on the retina with follow-up studies on the *rd* mouse model [Pawlyk *et al.* 2002]. However, one of the subsequent studies showed a delay in the retinal degeneration by using L-cis-diltiazem on *rd1* mice [Takano *et al.* 2004, Vallazza-Deschamps *et al.* 2005]. The outcome of these studies indicated that L-cis-diltiazem acting on CNGC might delay the photoreceptor degeneration. Moreover, mutations in CNGC subunits are known to cause RP in human patients [Bareil *et al.* 2001, Boycott *et al.* 2001, McLaughlin *et al.* 1993]. Knockout studies were performed later for the respective channels, *i.e.*, $Cngb1^{-/-}$ for CNGC and $Cacna1f^{-/-}$ for VGCC. In these studies, $Cacna1f^{-/-}\times rd1$ showed only a slight delay in the photoreceptor degeneration with no significant effect [Schön *et al.* 2016, Read *et al.* 2002]. However, $Cngb1^{-/-}\times rd1$ double mutant showed improved retinal function with a strong delay in the peak of cell death [Paquet-Durand *et al.* 2011]. Besides, $Cngb1^{-/-}\times rd10$ double mutants also showed a delayed peak of degeneration compared to both *rd10* and $Cngb1^{-/-}$ parent strains [Wang *et al.* 2018]. Clearly Ca^{2+} influx via both the channels has important but different roles in the cell death pathway.

Enantiomers of diltiazem were reported to differentially effect CNGC and VGCC [Haynes 1992, Cia *et al.* 2005]. Diltiazem was also reported to increase ionic permeability at very high concentrations on bovine or toad photoreceptors [Caretta *et al.* 1991], but this effect could not be reproduced in later studies. L-cis-diltiazem showed reduced cGMP-activated conductance on isolated rod photoreceptors from tiger salamander [Stern *et al.* 1986] and showed a block on cGMP-gated channels in photoreceptors isolated from catfish [Haynes 1992], indicating its specificity for CNGC. D-cis-diltiazem, on the other hand, showed an inhibition with lesser efficiency on CNGC in tiger salamander [Stern *et al.* 1986]. L-cis-diltiazem's blocking potential for rat olfactory CNGC seemed to be higher than bovine retinal CNGC, when their current conductance capacities were compared. L-cis-diltiazem was found to be the least effective for rat gustatory CNGC [Lee *et al.* 2001]. The patch-clamp recording showed about 70% inhibition of VGCC on using 100 μM D-cis-diltiazem on porcine photoreceptors [Cia *et al.* 2005] and tiger salamander photoreceptors [Hart *et al.* 2003]. Thus, increased inhibition of VGCC was found at higher concentrations of D-cis-diltiazem. These studies report the blocking efficacy of D-cis and L-cis-diltiazem enantiomers across different animal models. Our systematic analysis on mouse CNGC showed no considerable inhibitory effect of D-cis or L-cis-diltiazem at physiological cGMP level (5 μM) on heterologously expressed CNGC subunits (both rods and cones). However, at high cGMP concentrations L-cis-diltiazem showed a stronger inhibitory effect on rod CNGC than D-cis-diltiazem, indicating selectivity for rod CNGC. This finding strengthens the above argument that the inhibitory effect of L-cis-diltiazem

might have resulted in the rescue of photoreceptor cell death in the earlier studies. The selectivity of L-cis-diltiazem for rod CNGC and D-cis-diltiazem for VGCC, facilitated the modulation of Ca^{2+} influx selectively via CNGC or VGCC.

8.1 Modulation of intracellular Ca^{2+} concentration

Ca^{2+} is an important secondary messenger, which is regulated precisely in different functional compartments of photoreceptors [Krizaj *et al.* 1998]. In rods, about 18% of the dark current is carried by Ca^{2+} [Gray-Keller *et al.* 1994]. Light-dependent modulation of Ca^{2+} concentration was shown in rod OS [Sampath *et al.* 1999]. We show evidence that in pathological cGMP, cone CNGC was inhibited about 30-50% with L-cis-diltiazem (corresponds to 25-100 μM), while D-cis-diltiazem showed no inhibitory effect. On healthy wt retinal slices, L-cis-diltiazem showed a decrease in light-induced cone Ca^{2+} response in a concentration-dependent manner. This indicates the inhibitory effect of L-cis-diltiazem on cone CNGC at physiological cGMP. This is further supported by the trend towards a lower Ca^{2+} baseline and the absence of light-induced hyperpolarisation-depolarisation cycle of the cells with L-cis-diltiazem (see Figure 3.11).

The observed effect of L-cis-diltiazem on the wt retina suggests that there might exist an ongoing feedback loop during the L-cis-diltiazem treatment. Cones have been shown to have the higher GC activity than rods [Takemoto *et al.* 2009] and the inhibition mechanism of L-cis-diltiazem on CNGC is mainly due to its interaction with the channel pore [McLatchie *et al.* 1992, Haynes 1992]. Pore interaction was indicated in a study that compared the binding affinity of D-cis-diltiazem with its bulkier derivative benziazem, DMBODIPY-BAZ on CNGC. They showed decreased binding affinity with the heavier diltiazem derivative. Their results indicated that the interaction of D-cis-diltiazem with the channel pore could be dynamic in nature [Kraus *et al.* 1998]. The pore blocking phenomenon of L-cis-diltiazem has also been observed in the deactivation kinetics of the CNGC in the presence of L-cis-diltiazem (Chapter 3). In photoreceptors, the actual physiological concentration of cGMP is likely to vary between 5-10 μM, depending on the activity of GC in light and dark situation [Cote *et al.* 1993]. This concentration of cGMP was is denoted by white shade in the graph (see Figure 3.10) by L-cis-diltiazem on CNGC. The interaction at this stage is likely to be unstable, therefore L-cis-diltiazem might not bind to CNGC and influences a block. On the other hand, with increasing concentration of L-cis-diltiazem (from 25-100 μM) the likelihood of its interaction with the channel pore increases. Induced by such increased interaction, lower intracellular Ca^{2+} concentration might activate GC to produce more cGMP [Koch *et al.* 1988, Olshevskaya *et al.* 2002]. The presence of cGMP in turn, also influences the block by L-cis-diltiazem [Stern *et al.* 1986]. The increasing cGMP concentration could result in

a stronger block and the concentration-dependent reduction in the light-induced Ca^{2+} response. NCKX is sensitive to intracellular Ca^{2+} concentration [Yau *et al.* 1984] and gets inactivated at lower concentrations of intracellular Ca^{2+} [Sharon *et al.* 2002]. This would, in-turn, cease Na^{+} influx and also effect the concentration gradient of Na^{+} across the membrane. NKX extrudes Na^{+} in exchange with K^{+} with a very high energy demand [Wetzel *et al.* 1999]. The deactivation of NCKX would lead to the deactivation of NKX in the IS, thus influencing its activity. This would further prevent energy depletion in the photoreceptors. PMCA, in turn, has the highest affinity for Ca^{2+} [Schnetkamp 1995, Chambers *et al.* 1990]. This might continuously extrude Ca^{2+} from the IS [Morgans *et al.* 1988, Krizaj *et al.* 1998], thereby further lowering the Ca^{2+} baseline of the cell, as found in our experiment (see Figure 3.11 b).

The inhibition of VGCC by D-cis-diltiazem, on the other hand, should block Ca^{2+} influx in the photoreceptor cell body and synapse [Cia *et al.* 2005]. In cones however, hyperpolarisation was not affected by the Ca^{2+} influx via VGCC and the activity of CNGC was affected to a minor extent. This would not result both in lowering of the Ca^{2+} baseline and the light-induced Ca^{2+} response in cones. The induced block leads the photoreceptors to experience prolonged hyperpolarisation.

8.2 Correlation of calpain activity with *rd1* photoreceptor degeneration

Ca^{2+} is regulated precisely and quasi-independently in different functional compartments of the photoreceptors [Krizaj *et al.* 1998]. The increased concentration of intracellular Ca^{2+} and the subsequent activation of calpain on its downstream is one explanation surrounding the cause of cell death in *rd1* [Fesenko *et al.* 1985, Paquet-Durand *et al.* 2006, Power *et al.* 2020]. Our analysis of photoreceptor degeneration in mutant *rd1* and healthy wt, showed a relative relationship between Ca^{2+} concentration, calpain activity and cell death. It shows that the increased calpain activity in *rd1* degeneration might be actually independent of Ca^{2+} influx in the OS via CNGC caused due to high cGMP concentration. This phenomenon was indirectly observed earlier [Vallazza-Deschamps *et al.* 2005] while comparing between the cell death percent and the activation of GC. They suggested no significant contribution of Ca^{2+} channels in the degeneration. The hypothesis that the cell death pathway in *rd1* is independent of Ca^{2+} influx via OS, is supported by the following pieces of evidences: (1) We show that in *rd1* D-cis-diltiazem can exhibit a block up to 50% on rod CNGC and L-cis-diltiazem about 100% (see Figure 3.10 e, f). Thus, in the OS the Ca^{2+} concentration is likely to reduce largely with L-cis-diltiazem than with D-cis-diltiazem as compared to the untreated. The cells might be extremely and moderately hyperpolarised. (2) The calpain activity in *rd1* was found unchanged in

the case of both D-cis-diltiazem and L-cis-diltiazem treatment compared to the untreated group (see Figure 3.12), indicating no effect of hyperpolarisation on the calpain activity. These highlights the indirect correlation between the Ca^{2+} concentration in the OS and the calpain activity in the cytoplasm in *rd1*.

Our subsequent analysis showed increased cell death (6 times higher) with respect to the unchanged calpain activity in *rd1* L-cis-diltiazem (100 μM) treated condition (see Figures 3.12 and 3.18). This again indicates the indirect correlation between the calpain activity and the photoreceptor degeneration in *rd1*. These results strongly suggest that the resultant degeneration of photoreceptors are caused by additional factors that are independent of calpain. The physiological concentration of cGMP in a photoreceptor is not precisely quantified but is estimated based on the relative activation of GCAP and CG [Burns *et al.* 2002]. The reduction in the OS Ca^{2+} concentration (in the case of L-cis-diltiazem treatment) might lead to increase in the activation of GCAP and GC [Olshevskaya *et al.* 2002] for producing more cGMP. Lower Ca^{2+} concentration increases the affinity of CNGC for cGMP via CaM dissociation, making it more permeable [Hsu *et al.* 1993, Molday 1996]. However, the pharmacological block does not allow the influx of Ca^{2+}, which creates an imbalanced state. Low Ca^{2+} is also reported to be deleterious for photoreceptor survival [Fain *et al.* 1999, Li *et al.* 2003, Benedetto *et al.* 2019]. Continued activation of PMCA due to its high Ca^{2+} affinity [Carafoli 1991], is likely to maintain the cells hyperpolarised at low Ca^{2+} baseline. The activation of calpain is reported to deactivate PMCA [Brown *et al.* 2007, Guerini *et al.* 2003]. In the case of L-cis-diltiazem treatment in *rd1*, the unaltered calpain activity may not result in the deactivation of PMCA. This might lead to depletion of ATP and activation of the necrotic pathway [Bruce 2018]. Paradoxically, the Ca^{2+} overload and the ATP depletion is suggested to be associated with necrosis in muscular disorders [Wrogemann *et al.* 1976] and cancer [Charles *et al.* 2017].

Ca^{2+} channels are reported to be present in high density at the synaptic terminal of the photoreceptors [Nachman-Clewner *et al.* 1999, Krizaj *et al.* 1998], suggesting VGCC as the major source of cytoplasmic Ca^{2+}. The indirect correlation between the Ca^{2+} concentration in the OS and the cytoplasmic calpain activity, in our results, further strengthen the hypothesis that the calpain activity is contributed by the influx of Ca^{2+} via VGCC [Schön *et al.* 2016]. Earlier studies have suggested the calpain activity coincides with the event of degeneration [Power *et al.* 2020]. These results provide a strong indication that the calpain activity might be a parallel effect during the degeneration but most likely not the primary factor resulting in degeneration. As a consequence Ca^{2+}-dependent processes such as the activity of calpain, are likely to accelerate the degradation process, but could remarkably be less important for the photoreceptor degeneration than earlier thought. This may help to explain some of the controversial data

obtained with Ca^{2+} channel blockers in the past.

8.3 The possible role of Store-Operated Ca^{2+} Entry (SOCE)

In darkness, the Ca^{2+} influx via CNGC mediates Ca^{2+}-induced glutamate release via VGCC [Barnes *et al.* 2002, Choi *et al.* 2005]. D-cis-diltiazem on VGCC at higher concentration (100 μM) shows a pronounced block of about 70-71% as compared to L-cis-diltiazem of about 59% in physiological cGMP [Cia *et al.* 2005, Hart *et al.* 2003]. Interestingly, treatment with D-cis-diltiazem showed no significant effect on the calpain activity. L-cis-diltiazem showed a strong increase in calpain-2 but not the calpain activity in healthy wt. This could be the result of unaltered and increased cytoplasmic Ca^{2+} concentration respectively. Keeping in mind our hypothesis that the calpain activity is contributed by the Ca^{2+} influx via VGCC, the question might arise, how the inhibition of VGCC with D-cis-diltiazem leads to unchanged Ca^{2+} concentration in the cytoplasm and L-cis-diltiazem treatment increases the cytoplasmic Ca^{2+}. To explain this observation, we propose that the exposure of L-cis-diltiazem might lead to the depletion of intracellular Ca^{2+} concentration and the subsequent activation of SOCE.

In healthy wt retina, L-cis-diltiazem treatment would mimic the constant light situation. In bright light, the Ca^{2+} concentration drops at the synapse [Choi *et al.* 2008] to a very large extent. In many cell types, prolonged depletion of intracellular Ca^{2+} level is reported to induce SOCE, triggered by the reduction in Ca^{2+} concentration in the ER lumen (reviewed in [Parekh *et al.* 2005]). The intracellular Ca^{2+} stores such as Endoplasmic Reticulum (ER), mitochondria and OS disk act as Ca^{2+} reserve to maintain Ca^{2+} homeostasis [Krizaj 2012]. Diltiazem (20-50 μM) mediated block of VGCC has been shown to activate SOCE in vascular smooth muscle cells [Johnson *et al.* 2020], however, the enantiomeric isoform of diltiazem is not specified. This process is likely to selectively activate calpain-2 [Saraiva *et al.* 2013]. All these suggest that the inhibition of CNGC with L-cis-diltiazem may result in a complete block of Ca^{2+} influx. The combined effect of NCKX, NKX and PMCA activity, after CNGC blocking, might lead to a prolonged state of hyperpolarisation and the depletion of the intracellular Ca^{2+} concentration in the photoreceptors. Modulation of Ca^{2+} baseline has shown to trigger SOCE in light-adapted rods [Szikra *et al.* 2008]. The SOCE could get triggered in the hyperpolarised photoreceptors resulting in depletion of Ca^{2+} from intracellular stores and raising the concentration of cytoplasmic Ca^{2+}. This increased cytoplasmic Ca^{2+} could be responsible for the observed increase in calpain-2 activation in wt photoreceptor cell bodies treated with L-cis-diltiazem. Also, the increase in calpain activity in wt was comparable to that of *rd1*. The possible activation of SOCE with D-cis-diltiazem treatment could

be the reason why we did not find a decrease in calpain activity. The inhibition percent of VGCC with D-cis-diltiazem is however much lower than the effect of L-cis-diltiazem on CNGC. Therefore, a decrease in cleaved calpain-2 could still be found in *rd1* retina. These results again support our idea that the calpain activation in *rd1* is not directly downstream Ca^{2+} influx via CNGC. TRPC1, which is shown as an essential component of SOCE [Szikra *et al.* 2008] could also provide an additional, SOCE-independent but ROC mediated Ca^{2+} entry in the cell body as a regulatory mechanism to maintain the average cytosolic Ca^{2+} level [Molnar *et al.* 2012]. To affirm the SOCE hypothesis, assessing the effect of calpain activity on wt photoreceptors by hyperpolarising them (using L-cis-diltiazem) and simultaneously exposing them to the inhibitors of SOC could be of importance.

8.4 Modulation of PARP activity by intracellular Ca^{2+}

The increased activation of cGMP, in earlier studies, suggested two possible degeneration pathways mediated by its targets; the activation of CNGC and PKG. These pathways were believed to be active simultaneously but independent of each other [Arango-Gonzalez *et al.* 2014]. We show evidence for the first time in photoreceptors that PARP activity can be modulated by the intracellular Ca^{2+} concentration. The increase in PARP activity after the treatment with L-cis-diltiazem in healthy wt photoreceptors is indicative of a existing relationship between the intracellular Ca^{2+} concentration and PARP activity. Although it is not reported in photoreceptors, epithelial cells have been reported to show the SOCE coupled PARP-1 activation which is likely to contribute to a PARP-dependent necrotic cell death [Munoz *et al.* 2017]. The possible activation of SOCE in wt photoreceptors upon treated with L-cis-diltiazem (discussed above) might also increase the observed PARP activity and PARlylation. The nature and the strength of the SOCE coupled PARP activation are not reported. Although the VGCC block with diltiazem showed the activation of SOCE [Johnson *et al.* 2020], it is possible that their interaction is either indirect or not strong enough to increase the PARP activity in *rd1* (treated with D-cis-diltiazem) as compared to L-cis-diltiazem treatment. In line with the SOCE hypothesis, this might explain the increased PARP activity in L-cis-diltiazem treated wt photoreceptors.

The increase in PARP-1 activation in a Ca^{2+}-dependent manner has been shown in cancer [Bentle *et al.* 2006]. DNA damage could activates PARP-1 towards the end stage of photoreceptor degeneration [Gavrieli *et al.* 1992]. Thus, the activation of PARP in *rd1* could be contributed by PARP-1. SOCE coupled PARP-1 activation demands to have Ca^{2+} interacting sites. PARP-1 is not reported to have sites that interact with

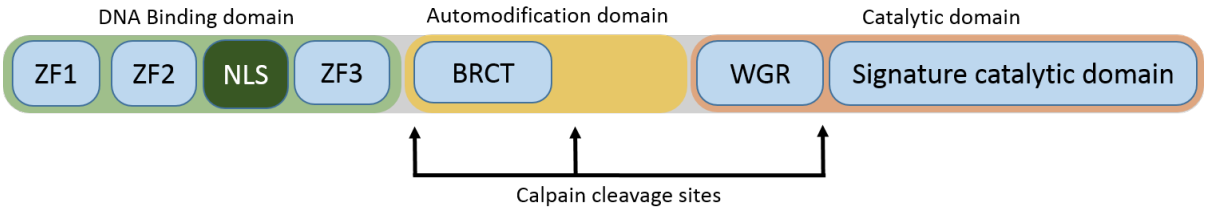

Figure 8.1: **Structure of PARP-1 with calpain cleavage sites**: PARP-1 is divided into three main functional domains: DNA Binding Domain (DBD), automodification domain and catalytic domain. Zinc Finger (ZF) I, II and III are the part of DBD with Nuclear Localisation Sequence (NLS). Automodification domain mediates PARylation in which BRCT is mostly uncharacterised. C-terminal is the catalytic domain having WGR. PARP-1 possess 3 calpain cleavage sites.

Ca^{2+}, however it has calpain cleavage sites which in turn is activated by Ca^{2+} [Goll *et al.* 1992](see Figure 8.1). Therefore, the possibility remains that the interaction with SOCE mediated calpain activation could be related to the PARP-1 activation. Ca^{2+} is known to promote the PARP-1 activation via the production of ROS [Virág *et al.* 2013] and Ca^{2+} chelation has shown to reduce the activity of PARP-1 in cancer [Bentle *et al.* 2006]. In photoreceptors, the relationship between calpain and PARP-1 is not well understood. PARP-1 is a 113 KDa protein cleaved by calpain at 4 sites. The calpain cleavage sites on PARP-1 could indicate 3 different possibilities: (1) calpain and PARP-1 activity could be inversely proportional to each other. The increased activity of calpain could cleave PARP-1 in the specific cleavage sites resulting in decreased PARP activity. This could lead to a calpain-mediated photoreceptor degeneration. (2) Calpain and PARP-1 could be directly proportional to each other. The interaction between the calpain cleavage sites of PARP-1 and activated calpain could lead to increased activation of PARP-1 in *rd1*. This might lead to the degeneration via two parallel independent pathways, calpain and PARP-1, influenced by each other. Activation of both calpain and PARP-1 is strongly elevated during the photoreceptor degeneration [Kaur *et al.* 2011, Paquet-Durand *et al.* 2006, Paquet-Durand *et al.* 2007], which favours this possibility. Moreover, the cleavage sites of calpain indicate that proteolysis of PARP-1 separates the DNA binding domain from the catalytic domain [Chaitanya *et al.* 2010], as shown in Figure 8.1. The proteolysis might also result in the activation of the catalytic domain, captured as increased PARP-1 activity in *rd1*. However, the resulting PARP-1 activity might deplete NAD^+, it would likely to be least helpful for repairing the DNA damage. (3) Calpain and PARP-1 could interact with each other but function in an independent manner. The DNA breaks repair during the *rd1* degeneration might result in increased PARP activity [Paquet-Durand *et al.* 2007]. The activation of calpain in parallel during degeneration might eventually cleave PARP-1. The proteolysis of PARP-1 might either lose its activity

eventually or remain active upon cleavage and deplete NAD^+. The calpain and PARP-1 activity would show different peak during the degeneration. The energy depletion due to the consumption of NAD^+ might result in the formation of Reactive Oxygen Species (ROS) or regulated necrotic pathway [Berghe *et al.* 2014] resulting in the photoreceptor degeneration.

The modulation of intracellular Ca^{2+} can also influence the regulation of gene expression. This could also affect the photoreceptor viability, independent of calpain or PARP-1 activity. Ca^{2+} can interact with the DNA directly and modify the 3D structure, depending on the percentage of GC content in DNA [Braunlin *et al.* 1992]. Increase in the intracellular Ca^{2+} concentration has shown to reactivate gene expression via the activation of Ca^{2+}-calmodulin kinase in cancer [Raynal *et al.* 2015]. High Ca^{2+} is reported to activate of MEF2-dependent genes in the heart. The activation is caused by the phosphorylation of HDAC5 via phosphorylated PKC isoforms [Zhang *et al.* 2011]. Calmodulin is a highly conserved Ca^{2+} sensor protein. Binding with Ca mediates conformational changes in calmodulin and the protein interaction sites are released [Strynadka *et al.* 1989]. It further activates Ca^{2+}-sensitive enzymes such as Ca^{2+}/calmodulin-dependent protein Kinase-II (CaMKII) and calcineurin. The activation modulates the gene expression via Calmodulin-binding Transcriptional Activator (CAMTA) [Finkler *et al.* 2007].

8.5 Ca^{2+} channels as a therapeutic target

Precise regulation of Ca^{2+} in photoreceptors is of high importance for its viability. Mutation in CNGC subunits resulting in loss of its function are reported to cause RP in human patients [Bareil *et al.* 2001, **?**]. As discussed earlier, degeneration in *rd1* was suggested to be rescued by blocking Ca^{2+} channels [Frasson *et al.* 1999, Takano *et al.* 2004, Vallazza-Deschamps *et al.* 2005]. Knockout studies on the $Cngb1^{-/-} \times rd1$ [Paquet-Durand *et al.* 2011] and $Cngb1^{-/-} \times rd10$ [Wang *et al.* 2018] double-mutants further suggested improved retinal function by lacking functional CNGC. This suggested CNGC as a target for therapeutic interventions. Our study with inhibition of CNGC and investigation of its downstream effects showed contrasting results. Our results strongly suggest that the inhibition of Ca^{2+} channels like CNGC in *rd1* is not able to delay the photoreceptor degeneration. The possible reason behind improved retinal function in double mutants as compared to L-cis-diltiazem treated explants could be the formation of homotetrameric CNGC constituting CNGA1 subunits in those animals [Chen *et al.* 1993]. *Cnga1* is reported to be capable of assembling into a homotetrameric channel which is not influenced by the cGMP binding and is also inefficient in conducting Ca^{2+} as compared to heterotetramers [Nache *et al.* 2006]. The formation of homotetrameric channels could reduce the intracellular Ca^{2+} as compared to *rd1*. This might have resulted a shift in the

peak of cell death but not rescue degeneration altogether.

Loss of function mutations in *Cacna1f* (a VGCC subunit) is reported to disrupt Ca^{2+} homeostasis and cause congenital stationary night blindness [Boycott *et al.* 2001, Mansergh *et al.* 2005]. The reduced release of glutamate is suggested as a cause of compromised dark adaptation capability of the photoreceptors, caused by a lowered influx of Ca^{2+} [Wutz *et al.* 2002]. The protective effect of D-cis-diltiazem was suggested on photoreceptors by [Frasson *et al.* 1999], but knockout studies showed $rd1 \times Cacna1f^{-/-}$ double-mutants did not have any significant protective effect on the photoreceptor degeneration [Schön *et al.* 2016, Read *et al.* 2002]. Our results with D-cis-diltiazem support the knockout study along with others [Bush *et al.* 2000, Pearce-Kelling *et al.* 2001, Pawlyk *et al.* 2002] showing that the inhibition of VGCC has no significant protective effect on the photoreceptor degeneration. The observed effect could be due to the fact that, the VGCC block can mediate the reduction in synaptic glutamate release but it is not involved in regulating the depolarised and hyperpolarised state of photoreceptors.

Both low Ca^{2+} as well as high Ca^{2+} have been proposed to be deleterious for photoreceptor survival [Paquet-Durand *et al.* 2006, Fain *et al.* 1999, Li *et al.* 2003]. L-cis-diltiazem, that imposes a strong block on CNGC, increased the photoreceptor degeneration with increasing concentration (25-50-100 μM). Pharmacological compounds at extremely high concentrations have been found to show toxicity on cells. However, the non-protective effect, in our case, was also found with lower concentrations of L-cis-diltiazem and cGMP analogues [RP-(2-N)ET-cGMPS (DF246), RP-8-Br(2-N)ET-cGMPS (DF156), RP-β-1 N2-Ac-8-Br-cGMPs (DF235)]. Moreover, one of the cGMP analogue specific for CNGC inhibition (DF156) showed significant toxic effect at 10 times lower concentration. These clearly indicate that the CNGC inhibition is not protective favouring the photoreceptor survival. It can be therefore concluded that neither the inhibition of CNGC nor VGCC will be able to delay the degeneration in photoreceptors.

The increased photoreceptor degeneration observed on inhibiting CNGC might be contributed by other factors, such as (1) elevated synthesis of cGMP: this may lead to the activation of other targets of cGMP, such as PKG [Paquet-Durand *et al.* 2009], (2) increased intracellular Ca^{2+} via SOCE: this may result in cell death by activating Ca^{2+}-dependent proteases like calpain [Paquet-Durand *et al.* 2006], (3) PARP-1 activation: might lead to parthanathos and (4) depletion of ATP: as a result of PMCA and PARP-1 activity leading to necrosis [Galluzzi *et al.* 2018]. The resultant pathway of degeneration in *rd1* is likely the amplification of the degeneration cascade once initiated by high cGMP.

8.6 New insights into cell death mechanisms

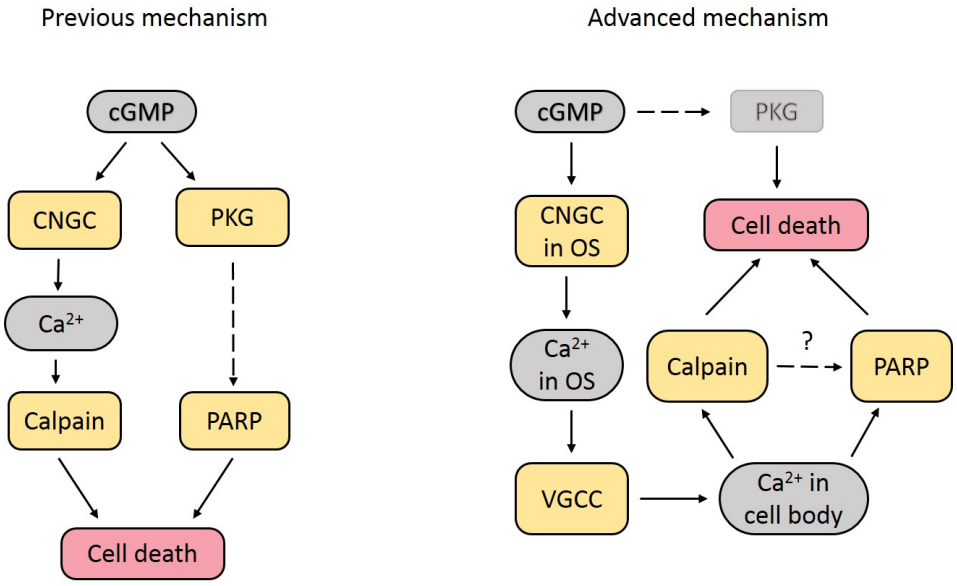

Figure 8.2: **Insight into photoreceptor degeneration mechanism in *rd1***: Two cell death pathways are shown. The photoreceptors in *rd1* have previously been suggested to follow the pathway shown on the left during their degeneration [Arango-Gonzalez *et al.* 2014]. The pathway on the right suggests new understanding on the cell death pathway incorporating all the data discussed in this thesis. The Ca^{2+} influx via VGCC, but not CNGC, was found to be correlated to calpain activation. Thus, the modulation of Ca^{2+} concentration in the cell body is likely to be governed by VGCC. Earlier, PARP-1 was suggested to be downstream of PKG. We show that PARP activity was modulated by the intracellular Ca^{2+} concentration indicating a cross-talk. PKG, the second target of cGMP, is likely unrelated to PARP activity. The dashed lines and the interrogation mark indicate unclear understanding of those pathways or interactions.

In the cGMP-dependent degeneration in *rd1* photoreceptor, cGMP is known to cause cell death by acting upon two targets, activation of CNGC and PKG. Calcium and calpain are known to be downstream CNGC and PARP has been suggested to be downstream of PKG activation, as two separate pathways [Arango-Gonzalez *et al.* 2014]. The degeneration via cGMP is believed to result from the overactivation of CNGC [Fesenko *et al.* 1985] and subsequently high influx of Ca^{2+} leading to calpain activation and cell death [Paquet-Durand *et al.* 2006]. The PARP activity has also been shown to be elevated during the *rd1* degeneration [Paquet-Durand *et al.* 2007]. Here, we show for the first time a cross-talk between the two pathways downstream cGMP, earlier believed to

be independent of each other. The modulation of PARP activity by the intracellular Ca^{2+} concentration in photoreceptors indicated a possible interaction between the two parallel pathways. We also show that, although the OS Ca^{2+} concentration is primarily governed by CNGC, the Ca^{2+} influx via CNGC is unlikely to be directly involved in calpain activation. Instead, the calpain activation is more likely to be mediated by VGCC (see Figure 8.2). Also, the observed calpain activity may not solely responsible for photoreceptor degeneration. Therefore, the degeneration in *rd1* could be the result of the combined effect of calpain and PARP activity after being initiated by high cGMP or Ca^{2+}.

Outlook and Future Directions

Retinitis pigmentosa is extremely genetically heterogeneous in nature. RP is a rare disease in which the degeneration is contributed by many different genes, increasing its level of complexity. Therefore the establishment of therapeutic strategy is extremely challenging. We have addressed the effect of mutations in PDE6 using genetically defined mouse models for hereditary retinal degeneration.

ASO mediated RNA editing

ASO mediated therapeutic strategies are emerging as a successful treatment option for several diseases. For ocular dystrophies these seem promising as the eye is very accessible and immunoprivileged organ. In our results with ASO mediated approaches, we found some positive indications of restoring the functional PDE6A with the site-directed RNA editing. ASO mediated restoration of functional protein on mouse tissue could be a promising therapeutic strategy for patients in the future. However, one of the biggest challenges is the unavailability of stable cell lines showing basic characteristics of rod and cone photoreceptors. Rod and cone photoreceptors are metabolically very different from each other having a wide difference in their gene expression and protein isoforms. For example, CNGC is a heterotetrameric protein composed of CNGa1 and CNGb1 in rods and CNGa3 and CNGb3 in cones (see Figure 1.4 in Chapter 1). The cell line 661W, which is widely available as photoreceptor like cell line, expresses subunits of cone CNGC but not rods. This makes the analysis of rod photoreceptor specific proteins or genes difficult. In this regard primary cell cultures of rod photoreceptors could serve as a better system for accessing the functional efficacy of the ASOs however, the viability

of primary photoreceptors in culture conditions are very short. The development of cell lines that express rod specific genes, for example by using Neural Retina Leucine zipper *nrl* gene, could help to study the effect of modulating rod specific genes. Another major challenge was the untargeted delivery of the ASO to a specific target cell population, which compromised the efficacy of ASOs. The lack of a delivery vehicle makes it very difficult to improve the uptake efficiency of the ASOs by the cells. Therefore, the detection of the amount of ASOs practically reaching the rods for performing the editing or down-regulation, becomes extremely variable and difficult. Nonetheless, the positive effects on cell lines and indications of positive effect on retinal tissues highlight that the RNA editing ASO has potential to emerge as a successful treatment.

Targeting Ca^{2+} homeostasis

Our data indicates that the Ca^{2+} influx via CNGC is very likely not the primary factor for degeneration in *rd1*. Therefore, it would be interesting to investigate other factors that could be induced by increased cGMP such as activation of PKG for understanding the primary degeneration pathway. PKG is another target of cGMP, which could lead the degeneration in *rd1*. Our results highlighted the altered behaviour of wt retina with respect to the *rd1* in the case of CNGC inhibition. Although Ca^{2+} influx via CNGC is not the primary degenerating factor, degeneration of photoreceptors might be linked to intracellular Ca^{2+} modulation. Calpain is activated by Ca^{2+} and found elevated in the *rd1* situation. In addition, PARP (likely PARP-1) is found to be highly activated in the *rd1* situation. Interestingly, PARP-1 has calpain cleavage sites. For a more clear understanding, the relationship between calpain and PARP-1 could be studied in different models of retinal degeneration. Mutant animal models such as *Cngb1*$^{-/-}$ and *Cngb1*$^{-/-}$ * *rd1* double mutants could be studied independently for the observed factors. Fragmentation of PARP-1 during inhibition of Ca^{2+} influx and enzymes associated with the fragmentation could be studied using western blot and mass spectrometric analysis.

Bibliography

[Aartsma-Rus *et al.* 2009] A. Aartsma-Rus, L. van Vliet, M. Hirschi, A. A. Janson, H. Heemskerk, C. L de Winter, S. de Kimpe, J. CT van Deutekom, P. A. Hoen, G. B. van Ommen, Mol. Ther. **17**, 548-553 (2009).

[Arango-Gonzalez *et al.* 2014] B. Arango-Gonzalez, D. Trifunovic, A. Sahaboglu, K. Kranz, S. Michalakis, P. Farinelli, S. Koch, F. Koch, S. Cottet, U. Janssen-Bienhold, K. Dedek, M. Biel, E. Zrenner, T. Euler, P. Ekström, M. Ueffing, F. Paquet-Durand, PLoS One **9**, e112142 (2014).

[Ardell *et al.* 2000] M. D. Ardell, D. L. Bedsole, R. V. Schoborg, S. J. Pittler, Gene **245**, 311-318 (2000).

[Alemasova *et al.* 2019] E. E. Alemasova, O. I. Lavarik, Nucleic Acids Res. **47**, 3811-3827 (2019).

[Andrabi *et al.* 2014] S. A. Andrabi, G. K. E. Umanah, C. Chang, D. A. Stevens, S. S. Karuppagounder, J. Gagné, G. G. Poirier, V. L. Dawson, T. M. Dawson, Proc. Natl. Acad. Sci. U.S.A. **111**, 10209-10214 (2014).

[Barrera *et al.* 2015] V. Barrera, P. S. Hiscott, A. G. Craig, V. A. White, D. A. Milner, N. A. V. Beare, I. J. C. MacCormick, S. Kamiza, T. E. Taylor, M. E. Molyneux, S. P. Harding, J. Infect. Dis. **211**, 1977–1986 (2015).

[Bakondi *et al.* 2002] E. Bakondi, P. Bai, É. Szabfó, J. Hunyadi, P. Gergely, C. Szabfó, L. Virfág, J. Histochem. Cytochem. **50**, 91-98 (2002).

[Barabas *et al.* 2010] P. Barabas, P. C. Cutler, D. Krizaj, Adv. Exp. Med. Biol. **664**, 491-499 (2010).

[Bareil *et al.* 2001] C. Bareil, C. P. Hamel, V. Delague, B. Arnaud, J. Demaille, M. Claustres, Hum. Genet. **108**, 328-334 (2001).

[Barnes *et al.* 2002] S. Barnes, M. E. M. Kelly, Calcium channels at the photoreceptor synapse. In: W. Baehr, K. Palczewski (eds) Photoreceptors and calcium, Adv. Exp. Med. Biol. **514**, 465-476 (2002).

[Bauman *et al.* 2009] J. Bauman, N. Jearawiriyapaisarn, R. Kole, Oligonucleotides. **19**, 1-13 (2009).

[Bastian *et al.* 2020] F. B. Bastian, J. Roux, A. Niknejad, A. Comte, S. S. F. Costa, T. M. de Farias, S. Moretti, G. Parmentier, V. R. de Laval, M. Rosikiewicz, J. Wollbrett, A. Echchiki, A. Escoriza, W. Gharib, M. Gonzales-Porta, Y. Jarosz, B. Laurenczy, P. Moret, E. Person, P. Roelli, K. Sanjeev, M. Seppey, M. Robinson-Rechavi, bioRxiv 2020.05.28.119560.

[Barrera *et al.* 2018] V. Barrera, I. J. MacCormick, G. Czanner, P. S. Hiscott, V. A. White, A. G. Craig, N. A. V. Beare, L. H. Culshaw, Y. Zheng, S. C. Biddolph, D. A. Milner, S. Kamiza, M. E. Molyneux, T. E. Taylor, S. P. Harding, eLife **7**, e32208 (2018).

[Bass *et al.* 1987] B. L. Bass, H. Weintraub, Cell **48**, 607-613 (1987).

[Bass *et al.* 1988] B. L. Bass, H. Weintraub, Cell **55**, 1089-1098 (1988).

[Beare *et al.* 2006] N. A. Beare, T. E. Taylor, S. P. Harding, S. Lewallen, M. E. Molyneux, Am. J. Trop. Med. Hyg. **75**, 790-797 (2006).

[Bech-Hansen *et al.* 1998] N. T. Bech-Hansen, M. J. Naylor, T. A. Maybaum, W. G. Pearce, B. Koop, G. A. Fishman, M. Mets, M. A. Musarella, K. M. Boycott, Nat. Genet. **19**, 264-267 (1998).

[Benedetto *et al.* 2019] M. M. Benedetto, M. A. Contin, Front. Cell Neurosci. **13**, 139 (2019).

[Bennett 2019] C. F. Bennett, Annu. Rev. Med. **70**, 307-321 (2019).

[Bentle *et al.* 2006] M. S. Bentle, K. E. Reinicke, E. A. Bay, D. R. Spitz, D. A. Boothman, J. Biol. **281**, 33684-33696 (2006).

[Berghe *et al.* 2014] T. V. Berghe, A. Linkermann, S. Jouan-Lanhouet, H. Walczak, P. Vandenabeele, Nat. Rev. Mol. Cell. Biol. **15**, 135-147 (2014).

[Ben-Shlomo *et al.* 1999] H. Ben-Shlomo, A. Levitan, N. E. Shay, I. Goncharov, S. Michaeli, J. Biol. Chem. **274**, 25642-25650 (1999).

[Belhadj, Tolone, Christensen, Das *et al.* 2020] S. Belhadj, A. Tolone, G. Christensen, S. Das, Y. Chen, F. Paquet-Durand, J Vis. Exp. **165** (2020).

[Berger *et al.* 2010] W. Berger, B. Kloeckener-Gruissem, J. Neidhardt, Prog. Retin. Eye Res. **57**, 335-375 (2010).

[Bin-Guang *et al.* 2008] M. Bin-Guang, C. Lei, J. Hong-Fang, C. Zhong-Hua, Y. Fu-Rong, W. Ling, Q. Ge, J. Ying-Ying, J. Cong, Z. Hong-Yu, Biochem. Biophys. Res. Commun. **366**, 607-611 (2008).

[Bowes *et al.* 1990] C. Bowes, T. Li, M. Danciger, L. C. Baxter, M. L. Applebury, D. B. Farber, Nature **347**, 677-680 (1990).

[Bowes *et al.* 1993] C. Bowes, T. Li, W. N. Frankel, M. Danciger, J. M. Coffin, M. L. Applebury, D. B. Farber, Proc. Natl. Acad. Sci. U.S.A. **90**, 2955-2959 (1993).

[Boycott *et al.* 2001] K. M. Boycott, T. A. Maybaum, M. J. Naylor, R. G. Weleber, J. Robitaille, Y. Miyake, A. A. B. Bergen, M. E. Pierpont, W. G. Pearce, N. T. Bech-Hansen, Hum. Genet. **108**, 91-97 (2001).

[Braunlin *et al.* 1992] W. H. Braunlin, T. Drakenberg, L. Nordenskiöld, J. Biomol. Struct. Dyn. **10**, 333-343 (1992).

[Bré *et al.* 1994] M. H. Bré, B. de Néchaud, A. Wolff, A. Fleury, Cell Motil. Cytoskeleton. **27**, 337-349 (1994).

[Brown *et al.* 2007] C. S. Brown, W. L. Dean, Platelets. **18**, 207-211 (2007).

[Bruce 2018] J. I. E. Bruce, Cell Calcium **69**, 28-36 (2018).

[Brückner 1951] R. Brückner, Doc. Ophthalmol. **5**, 452-554 (1951).

[Burns *et al.* 2002] M. E. Burns, A. Mendez, J. Chen, D. A. Baylor, Neuron **36**, 81-91 (2002).

[Burns *et al.* 2014] M. E. Burns, E. N. Pugh (2014), Visual transduction by rod and cone photoreceptors, in The New Visual Neurosciences, eds J. S. Werner and L. M. Chalupa (Cambridge, MA:TheMITPress), 7-18.

[Bush *et al.* 2000] R. A. Bush, L. Kononen, S. Machida, P. A. Sieving, Invest. Ophthalmol. Vis. Sci. **41**, 2697-2701 (2000).

[Caffé *et al.* 1989] A. R. Caffé, H. Visser, H. G. Jansen, S. Sanyal, Curr. Eye Res. **8**, 1083-1092 (1989).

[Caffé *et al.* 2002] A. R. Caffé, P. Ahuja, B. Holmqvist, S. Azadi, J. Forsell, I. Holmqvist, A. K. Söderpalm, T. van Veen, J. Chem. Neuroana. **22**, 263-273 (2002).

[Carafoli 1991] E. Carafoli, Physiol. Rev. **71**, 129-153 (1991).

[Caretta *et al.* 1991] A. Caretta, R. T. Sorbi, P. J. Stein, R. Tirindelli, J. Membrane Biol. **122**, 203-213 (1991).

[Carreras *et al.* 2015] F. J. Carreras, C. J. Aranda, D. Porcel, F. Rodriguez-Hurtado, O. Martínez-Agustin, A. Zarzuelo, PLoS One **10**, e0128516 (2015).

[Cartegni *et al.* 2003] L. Cartegni, J. Wang, Z. Zhu, M. Q. Zhang, A. R. Krainer, Nucleic Acids Res. **31**, 3568-3571 (2003).

[Chaitanya *et al.* 2010] G. V. Chaitanya, J. S. Alexander, P. P. Babu, Cell Commun. Signal **8**, 31 (2010).

[Charles *et al.* 2017] E. Charles, M. Hammadi, P. Kischel, V. Delcroix, N. Demaurex, C. Castelbou, A. M. Vacher, A. Devin, T. Ducret, P. Nunes, P. Vacher, Oncotarget. **8**, 3181-3196 (2017).

[Chambers *et al.* 1990] J. P. Chambers, P. Kumar, A. T. C. Tsin, J. J. Valdes, Exp. Eye Res. **50**, 127-134 (1990).

[Chang *et al.* 2000] B. Chang, N. L. Hawes, R. E. Hurd, M. T. Davisson, S. Nusinowitz, J. R. Heckenlively, Investig. Ophthalmol. Vis. Sci. **41**, S533 (2000).

[Chen *et al.* 1993] T. Y. Chen, Y. W. Peng, R. S. Dhallan, B. Ahamed, R. R. Reed, K. W. Yau, Nature **362**, 764-767 (1993).

[Choi *et al.* 2005] S. Y. Choi, B. G. Borghuis, R. Rea, E. S. Levitan, P. Sterling, R. H. Kramer, Neuron **48**, 555-562 (2005).

[Choi *et al.* 2008] S. Choi, S. Jackman, W. B. Thoreson, R. H. Kramer, Vis. Neurosci. **25**, 693-700 (2008).

[Cideciyan *et al.* 2019] A. V. Cideciyan, S. G. Jacobson, A. V. Drack, A. C. Ho, J. Charng, A. V. Garafalo, A. J. Roman, A. Sumaroka, I. C. Han, M. D. Hochstedler, W. L. Pfeifer, E. H. Sohn, M. Taiel, M. R. Schwartz, P. Biasutto, W. de Wit, M. E. Cheetham, P. Adamson, D. M. Rodman, G. Platenburg, M. D. Tome, I. Balikova, F. Nerinckx, J. De Zaeytijd, C. Van Cauwenbergh, B. P. Leroy, S. R. Russell, Nat. Med. **25**, 225-228 (2019).

[Cia *et al.* 2005] D. Cia, A. Bordais, C. Varela, V. Forster, J. A. Sahel, A. Rendon, S. Picaud, J. Neurophysiol. **93**, 1468-1475 (2005).

[Corton *et al.* 2010] M. Corton, M. J. Blanco, M. Torres, M. Sanchez-Salorio, A. Carracedo, M. Brion, Clin. Genet. **78**, 495-498 (2010).

[Cote *et al.* 1993] R. H. Cote, M. A. Brunnock, J. Biol. Chem. **268**, 17190-17198 (1993).

[Craig *et al.* 2012] A. G. Craig, G. E. Grau, C. Janse, J. W. Kazura, D. Milner, J. W. Barnwell, G. Turner, J. Langhorne, PLoS Pathog. **8**, e1002401 (2012).

[D'Amours *et al.* 1999] D. D'Amours, S. Desnoyers, I. D'Silva, G. G. Poirier, Biochem. J. **342**, 249-268 (1999).

[Dhuri *et al.* 2020] K. Dhuri, C. Bechtold, E. Quijano, H. Pham, A. Gupta, A. Vikram, R. Bahal, J. Clin. Med. **9**, 2004 (2020).

[Eckstein 2014] F. Eckstein, Nucleic Acid Ther. **24**, 374-387 (2014).

[Ekström *et al.* 2014] P. Ekström, M. Ueffing, E. Zrenner, F. Paquet-Durand, Curr. Med. Chem. **21**, 3478-3493 (2014).

[Fain *et al.* 1999] G. L. Fain, J. E. Lisman, Invest. Ophthalmol. Vis. Sci. **40**, 2770-2772 (1999).

[Farber *et al.* 1974] D. B. Farber, R. N. Lolley, Science **186**, 449-451 (1974).

[Fesenko *et al.* 1985] E. E. Fesenko, S. S. Kolesnikov, A. L. Lyubarsky, Nature **313**, 310-313 (1985).

[Finkler *et al.* 2007] A. Finkler, R. Ashery-Padan, H. Fromm, FEBS Lett. **581**, 1873-3468 (2007).

[Fire *et al.* 1998] A. Fire, S. Xu, M. K. Montgomery, S. A. Kostas, S. E. Driver, C. C. Mello, Nature **391**, 806-811 (1998).

[Fischer *et al.* 2009] M. D. Fischer, G. Huber, S. C. Beck, N. Tanimoto, R. Mühlfriedel, E. Fahl, C. Grimm, A. Wenzel, C. E. Remé, S. A. van de Pavert, J. Wijnholds, M. Pacal, R. Bremner, M. W. Seeliger, PLoS One **4**, e7507 (2009).

[Franke-Fayard *et al.* 2004] B. Franke-Fayard, H. Trueman, J. Ramesar, J. Mendoza, M. van der Keur, R. van der Linden, R. E. Sinden, A. P. Waters, C. J. Janse, Mol. Biochem. Parasitol. **137**, 23-33 (2004).

[Frasson *et al.* 1999] M. Frasson, J. A. Sahel, M. Fabre, M. Simonutti, H. Dreyfus, S. Picaud, Nat. Med. **5**, 1183-1187 (1999).

[Fox *et al.* 1999] D. A. Fox, A. T. Poblenz, L. H. He, Oxidative/Energy Met. Neurodeg. Dis. **893**, 282-285 (1999).

[Fox *et al.* 2003] D. A. Fox, A. T. Poblenz, L. J. He, B. Harris, C. J. Medrano, Eur. J. Ophthalmol. **13**, S44-S56 (2003).

[Galluzzi *et al.* 2018] L. Galluzzi, I. Vitale, S. Aaronson *et al.*, Cell Death Differ. **25**, 486-541 (2018).

[Gavrieli *et al.* 1992] Y. Gavrieli, Y. Sherman, S. A. Ben-Sasson, J. Cell Biol. **119**, 493-501 (1992).

[Goldberg *et al.* 2016] A. F. Goldberg, O. L. Moritz, D. S. Williams, Prog. Retin. Eye Res. **55**, 52-81 (2016).

[Goll *et al.* 1992] D. E. Goll, V. F. Thompson, R. G. Taylor, T. Zalewska, Bioessays **14**, 549-556 (1992).

[Gray-Keller *et al.* 1994] M. P. Gray-Keller, P. B. Detwiler, Neuron **13**, 849-861 (1994).

[Green 1986] M. R. Green, Annu. Rev. Genet. **20**, 671-708 (1986).

[Guerini *et al.* 2003] D. Guerini, B. Pan, E. Carafoli, J. Biol. Chem. **278**, 38141-38148 (2003).

[Haber *et al.* 1993] R. S. Haber, S. P. Weinstein, E. O'Boyle, S. Morgello, Endocrinology **132**, 2538-2543 (1993).

[Hair *et al.* 2013] P. Hair, F. Cameron, K. McKeage, Drugs. **73**, 487-493 (2013).

[Hanany *et al.* 2020] M. Hanany, C. Rivotta, D. Sharon, Proc. Natl. Acad. Sci. U.S.A. **117**, 2710-2716 (2020).

[Hanscheid 2003] T. Hanscheid, Clin. Microbiol. Infect. **9**, 497-504 (2003).

[Hart *et al.* 2003] J. Hart, M. F. Wilkinson, M. E. Kelly, S. Barnes, Exp. Eye Res. **76**, 597-604 (2003).

[Hassa *et al.* 2008] P. O. Hassa, M. O. Hottiger, Front. Biosci. **13**, 3046-3082 (2008).

[Haynes 1992] L. W. Haynes, J. Gen. Physiol. **100**, 783-801 (1992).

[Hiscott *et al.* 1984] P. S. Hiscott, I. Grierson, C. J. Trombetta, A. H. Rahi, J. Marshall, D. McLeod, Br. J. Ophthalmol. **68**, 698-707 (1984).

[Hoon *et al.* 2014] M. Hoon, H. Okawa, L. D. Santina, R. O. L. Wong, Prog. Ret. Eye Res. **42**, 44-84 (2014).

[Hsu *et al.* 1993] Y. T. Hsu, R. S. Molday, Nature **361**, 76-79 (1993).

[Johnson *et al.* 2020] M. T. Johnson, A. Gudlur, X. Zhang, P. Xin, S. M. Emrich, R. E. Yoast, R. Courjaret, R. M. Nwokonko, W. Li, N. Hempel, K. Machaca, D. L. Gill, P. G. Hogan, M. Trebak, Proc. Natl. Acad. Sci. U.S.A. **117**, 17369-17380 (2020).

[Jwa *et al.* 2012] M. Jwa, P. Chang, Nat. Cell Biol. **14**, 1223-1230 (2012).

[Kaupp *et al.* 2002] U. B. Kaupp, R. Seifert, Physiol. Rev. **82**, 769-824 (2002).

[Kaur *et al.* 2011] J. Kaur, S. Mencl, A. Sahaboglu, P. Farinelli, T. V. Veen, E. Zrenner, P. Ekström, F. Paquet-Durand, B. Arango-Gonzalez, PLoS One **6**, e22181 (2011).

[Keeler 1927] C. E. Keeler, J. Exp. Zool. **46**, 355-407 (1927).

[Kim *et al.* 1994] U. Kim, Y. Wang, T. Sanford, Y. Zeng, K. Nishikura, Proc. Natl. Acad. Sci. USA **91**, 11457-11461 (1994).

[Knott *et al.* 1996] R. M. Knott, M. Robertson, E. Muckersie, J. V. Forrester, Biochem. J. **318**, 313-317 (1996).

[Koch *et al.* 1988] K. W. Koch, L. Stryer, Nature **334**, 64-66 (1988).

[Koh *et al.* 2005] D. W. Koh, T. M. Dawson, V. L. Dawson, Pharmacol. Res. **52**, 5-14 (2005).

[Körschen *et al.* 1995] H. G. Körschen, M. Illing, R. Seifert, F. Sesti, A. Williams, S. Gotzes, C. Colville, F. Miller, A. Dose, M. Godde, L. Molday, U. B. Kaupp, R. S. Molday, Neuron **15**, 627-636 (1995).

[Kraus *et al.* 1998] R. L. Kraus, S. Hering, M. Grabner, D. Ostler, J. Striessnig, J. Biol. Chem. **273**, 27205-27212 (1998).

[Krizaj *et al.* 1998] D. Krizaj, D. R. Copenhagen, Neuron **21**, 249-256 (1998).

[Krizaj 2012] D. Krizaj, Adv. Exp. Med. Biol. **740**, 873-889 (2012).

[Kulkarni *et al.* 2015] M. Kulkarni, T. Schubert, T. Baden, B. Wissinger, T. Euler, F. Paquet-Durand, J. Vis. Exp. **99**, e52588 (2015).

[Kulkarni *et al.* 2016] M. Kulkarni, D. Trifunovic, T. Schubert, T. Euler, F. Paquet-Durand, Hum. Mol. Genet. **25**, 3729-3740 (2016).

[LaVail 1976] M. M. LaVail, Exp. Eye Res. **23**, 277-280 (1976).

[Lee *et al.* 2001] H. M. Lee, Y. S. Park, W. Kim, C. Park, J. Neurophysiol. **85**, 2335-2349 (2001).

[Lehmann *et al.* 1999] K. A. Lehmann, B. L. Bass, J. Mol. Biol. **291**, 1–13 (1999).

[Leung *et al.* 2011] A. K. L. Leung, S. Vyas, J. E. Rood, A. Bhutkar, P. A. Sharp, P. Chang, Mol. Cell **42**, 489-499 (2011).

[Lewallen *et al.* 2000] S. Lewallen, V. A. White, R. O. Whitten, J. Gardiner, B. Hoar, J. Lindley, J. Lochhead, A. McCormick, K. Wade, M. Tembo, J. Mwenechanyana, M. E. Molyneux, T. E. Taylor, Arch. Ophthalmol. **118**, 924-928 (2000).

[Li *et al.* 2003] F. Li, W. Cao, R. E. Anderson, Invest. Ophthalmol. Vis. Sci. **44**, 4968-4975 (2003).

[London *et al.* 2013] A. London, I. Benhar, M. Schwartz, Nat. Rev. Neurol. **9**, 44-53 (2013).

[Macbeth *et al.* 2005] M. R. Macbeth, H. L. Schubert, A. P. VanDemark, A. T. Lingam, C. P. Hill, B. L. Bass, Science **309**, 1534-1539 (2005).

[MacCormick *et al.* 2014] I. J. MacCormick, N. A. Beare, T. E. Taylor, V. Barrera, V. A. White, P. Hiscott, M. E. Molyneux, B. Dhillon, S. P. Harding, Brain **137**, 2119-2142 (2014).

[Malanga *et al.* 2005] M. Malanga, F. R. Althaus, Biochem. Cell Biol. **83**, 354-364 (2005).

[Mank *et al.* 2006] M. Mank, D. F. Reiff, N. Heim, M. W. Friedrich, A. Borst, O. Griesbeck, Biophys J. **90**, 1790-1796 (2006).

[Mantych *et al.* 1993] G. J. Mantych, G. S. Hageman, S. U. Devaskar, Endocrinology **133**, 600-607 (1993).

[Mansergh *et al.* 2005] F. Mansergh, N. C. Orton, J. P. Vessey, M. R. Lalonde, W. K. Stell, F. Tremblay, S. Barnes, D. E. Rancourt, N. T. Bech-Hansen, Hum. Mol. Genet. **14**, 3035-3046 (2005).

[Marsh *et al.* 1995] K. Marsh, D. Forster, C. Waruiru, I. Mwangi, M. Winstanley, V. Marsh, C. Newton, P. Winstanley, P. Warn, N. Peshu, N. Engl. J. Med. **332**, 1399-1404 (1995).

[Mashimo *et al.* 2013] M. Mashimo, J. Kato, J. Moss, Proc. Natl. Acad. Sci. U.S.A. **110**, 18964-18969 (2013).

[Masaki *et al.* 2010] Y. Masaki, R. Miyasaka, A. Ohkubo, K. Seio, M. Sekine, J. Phys. Chem. B **114**, 2517-2524 (2010).

[McLatchie *et al.* 1992] L. M. McLatchie, H. R. Matthews, Proc. Biol. Sci. **247**, 113-119 (1992).

[McLaughlin *et al.* 1993] M. E. McLaughlin, M. A. Sandberg, E. L. Berson, T. P. Dryja, Nat. Genet. **4**, 130-134 (1993).

[McLaughlin *et al.* 1995] M. E. McLaughlin, T. L. Ehrhart, E. L. Berson, T. P. Dryja, Proc. Natl. Acad. Sci. U.S.A. **92**, 3249-3253 (1995).

[McNaughton 1990] P. A. McNaughton, Physiol. Rev. **70**, 847-883 (1990).

[Merkle *et al.* 2019] T. Merkle, S. Merz, P. Reautschnig, A. Blaha, Q. Li, P. Vogel, J. Wettengel, J. B. Li, T. Stafforst, Nat. Biotechnol. **37**, 133-138 (2019).

[Molday 1996] R. S. Molday, Curr. Opin. Neurobiol. **6**, 445-452 (1996).

[Molnar *et al.* 2012] T. Molnar, P. Barabas, L. Birnbaumer, C. Punzo, V. Kefalov, D. Krizaj, J. Physiol. **590**, 3465-3481 (2012).

[Morgans *et al.* 1988] C. W. Morgans, O. E. Far, A. Berntson, H. Wässle, W. R. Taylor, J. Neurosci. **18**, 2467-2474 (1998).

[Mizuno *et al.* 1984] T. Mizuno, M. Y. Chou, M. Inouye, Proc. Natl. Acad. Sci. U.S.A. **81**, 1966-1970 (1984).

[Munoz *et al.* 2017] F. M. Munoz, F. Zhang, A. Islas-Robles, S. S. Lau, T. J. Monks, Toxicol. Sci. **158**, 444-453 (2017).

[Murante *et al.* 1998] R. S. Murante, L. A. Henricksen, R. A. Bambara, Proc. Natl. Acad. Sci. U.S.A. **95**, 2244-2249 (1998).

[Nache *et al.* 2006] V. Nache, J. Kusch, V. Hagen, K. Benndorf, Biophys. J. **90**, 3146-3154 (2006).

[Nachman-Clewner *et al.* 1999] M. Nachman-Clewner, R. S. T. Jules, E. Townes-Anderson, J. Comp. Neurol. **415**, 1-16 (1999).

[Nishikura *et al.* 1991] K. Nishikura, C. Yoo, U. Kim, J. M. Murray, P. A. Estes, F. E. Cash, S. A. Liebhaber, EMBO J. **10**, 3523-3532 (1991).

[Oka *et al.* 2012] S. Oka, C. Hsu, J. Sadoshima, Circ. Res. **111**, 611-627 (2012).

[Okawa *et al.* 2008] H. Okawa, A. P. Sampath, S. B. Laughlin, G. L. Fain, Curr. Biol. **18**, 1917-1921 (2008).

[Olshevskaya *et al.* 2002] E. V. Olshevskaya, A. N. Ermilov, A. M. Dizhoor, Mol. Cell. Biochem. **230**, 139-147 (2002).

[Orrenius *et al.* 2003] S. Orrenius, B. Zhivotovsky, P. Nicotera, Nat. Rev. Mol. Cell Biol. **4**, 552-565 (2003).

[Paquet-Durand *et al.* 2006] F. Paquet-Durand, S. Azadi, S. M. Hauck, M. Ueffing, T. van Veen, P. Ekström, J. Neurochem. **96**, 802-814 (2006).

[Paquet-Durand *et al.* 2007] F. Paquet-Durand, J. Silva, T. Talukdar, L. E. Johnson, S. Azadi, T. van Veen, M. Ueffing, S. M. Hauck, P. A. R. Ekström, J. Neurosci. **27**, 10311-10319 (2007).

[Paquet-Durand *et al.* 2009] F. Paquet-Durand, S. M. Hauck, T. V. Veen, M. Ueffing, P. Ekström, J. Neurochem. **108**, 796-810 (2009).

[Paquet-Durand *et al.* 2011] F. Paquet-Durand, S. Beck, S. Michalakis, T. Goldmann, G. Huber, R. Mühlfriedel, D. Trifunovic, M. D. Fischer, E. Fahl, G. Duetsch, E. Becirovic, U. Wolfrum, T. V. Veen, M. Biel, N. Tanimoto, M. W. Seeliger, Hum. Mol. Genet. **5**, 941-947 (2011).

[Paquet-Durand *et al.* 2019] F. Paquet-Durand, V. Marigo, P. Ekström, RD genes associated with high photoreceptor cGMP-levels (mini-review). In: C. B. Rickman, C. Grimm, R. Anderson, J. Ash, M. LaVail, J. Hollyfield (eds) Retinal Degenerative Diseases, Adv. Exp. Med. Biol. **1185**, 245-249 (2019).

[Paquet-Durand *et al.* 2019] F. Paquet-Durand, S. C. Beck, S. Das, G. Huber, L. Chang, T. Schubert, N. Tanimoto, M. Garcia-Garrido, R. Mühlfriedel, S. Bolz, W. Hoffmann, U. Schraermeyer, B. Mordmüller, M. W. Seeliger, Sci. Rep. **9**, 3470 (2019).

[Parekh *et al.* 2005] A. B. Parekh, J. W. Putney Jr., Physiol. Rev. **85**, 757-810 (2005).

[Pawlyk *et al.* 2002] B. S. Pawlyk, T. Li, M. S. Scimeca, M. A. Sandberg, E. L. Berson, Invest. Ophthalmol. Vis. Sci. **43**, 1912-1915 (2002).

[Pearce-Kelling *et al.* 2001] S. E. Pearce-Kelling, T. S. Aleman, A. Nickle, A. M. Laties, G. D. Aguirre, S. G. Jacobson, G. M. Acland, Mol. Vis. **7**, 42-47 (2001).

[Peng *et al.* 2004] C. Peng, E. D. Rich, M. D. Varnum, Neuron. **42**, 401-410 (2004).

[Petesch *et al.* 2008] S. J. Petesch, J. T. Lis, Cell **11**, 74-84 (2008).

[Picones *et al.* 1997] A. Picones, J. Korenbrot, Biophys. J. **69**, 120-127 (1997).

[Pittler *et al.* 1993] S. J. Pittler, C. E. Keeler, R. L. Sidman, W. Baehr, Proc. Natl. Acad. Sci. U.S.A. **20**, 9616-9619 (1993).

[Portera-Cailliau *et al.* 1994] C. Portera-Cailliau, C. H. Sung, J. Nathans, R. Adler, Proc. Natl. Acad. Sci. U.S.A. **91**, 974-978 (1994).

[Power, Das *et al.* 2020] M. Power, S. Das, K. Schütze, V. Marigo, P. Ekström, F. Paquet-Durand, Prog. Retin. Eye Res. **74**, 100772 (2020).

[Power *et al.* 2020] M. J. Power, L. E. Rogerson, T. Schubert, P. Berens, T. Euler, F. Paquet-Durand, J. Comp. Neurol. **528**, 1113-1139 (2020).

[Raynal *et al.* 2015] N. J.-M. Raynal, J. T. Lee, Y. Wang, A. Beaudry, P. Madireddi, J. Garriga, G. Malouf, S. Dumont, E. J. Dettman, V. Gharibyan, S. Ahmed, W. Chung, W. E. Childers, M. Abou-Gharbia, R. A. Henry, A. J. Andrews, J. Jelinek, Y. Cui, S. B. Baylin, D. L. Gill, J. J. Issa, Cancer Res. **76**, 1494-1505 (2015).

[Read *et al.* 2002] D. S. Read, M. A. McCall, R. G. Gregg, Exp. Eye Res. **75**, 415-420 (2002).

[Regus-Leidig *et al.* 2014] H. Regus-Leidig, J. Atorf, A. Feigenspan, J. Kremers, M. A. Maw, J. H. Brandstatter, PLoS One **9**, e86769 (2014).

[Reichenbach *et al.* 1995] A. Reichenbach, S. R. Robinson (1995), The involvement of Müller cells in the outer retina. In: M. B. A. Djamgoz, S. N. Archer, S. Vallerga (eds) Neurobiology and clinical aspects of the outer retina. Springer, Dordrecht.

[Rosenthal 2015] J. J. C. Rosenthal, J. Exp. Biol. **218**, 1812-1821 (2015).

[Sahaboglu *et al.* 2013] A. Sahaboglu, O. Paquet-Durand, J. Dietter, K. Dengler, S. Bernhard-Kurz, P. Ekström, B. Hitzmann, M. Ueffing, F. Paquet-Durand, Cell Death Dis. **4**, e488 (2013).

[Sakamoto *et al.* 2009] K. Sakamoto, M. McCluskey, T. G. Wensel, J. K. Naggert, P. M. Nishina, Hum. Mol. Genet. **18**, 178-192 (2009).

[Sampath *et al.* 1999] A. P. Sampath, H. R. Matthews, M. C. Cornwall, J. Bandarchi, G. L. Fain, J. Gen. Physiol. **113**, 267-277 (1999).

[Saraiva *et al.* 2013] N. Saraiva, D. L. Prole, G. Carrara, B. F. Johnson, C. W. Taylor, M. Parsons, G. L. Smith, J. Cell Biol. **202**, 699-713 (2013).

[Schemann *et al.* 2002] J. F. Schemann, O. Doumbo, D. Malvy, L. Traore, A. Kone, T. Sidibe, M. Keita, Am. J. Trop. Med. Hyg. **67**, 61-63 (2002).

[Schön *et al.* 2016] C. Schön, F. Paquet-Durand, S. Michalakis, PLoS One **6**, e0156974 (2016).

[Schnetkamp 1995] P. P. Schnetkamp, J. Biol. Chem. **270**, 13231-13239 (1995).

[Sharon *et al.* 2002] D. Sharon, H. Yamamoto, T. L. McGee, V. Rabe, R. T. Szerencsei, R. J. Winkfein, C. F. M. Prinsen, C. S. Barnes, S. Andreasson, G. A. Fishman, P. P. M. Schnetkamp, E. L. Berson, T. P. Dryja, Invest. Ophthalmol. Vis. Sci. **43**, 1971-1979 (2002).

[Sidman *et al.* 1965] R. L. Sidman, M. C. Green, J. Hered. **56**, 23-29 (1965).

[Simpson *et al.* 2008] I. A. Simpson, D. Dwyer, D. Malide, K. H. Moley, A. Travis, S. J. Vannucci, Am. J. Physiol. Endocrinol. Metab. **295**, E242-E253 (2008).

[Sothilingam *et al.* 2015] V. Sothilingam, M. G. Garrido, K. Jiao, E. Buena-Atienza, A. Sahaboglu, D. Trifunovic, S. Balendran, T. Koepfli, R. Mühlfriedel, Christian Schön, M. Biel, A. Heckmann, S. C. Beck, S. Michalakis, B. Wissinger, M. W. Seeliger, F. Paquet-Durand, Hum. Mol. Genet. **24**, 5486-5499 (2015).

[Specht *et al.* 2009] D. Specht, S. B. Wu, P. Turner, P. Dearden, F. Koentgen, U. Wolfrum, M. Maw, J. H. Brandstätter, S. T. Dieck, Invest. Ophthalmol. Vis. Sci. **50**, 505–515 (2009).

[Stefl *et al.* 2006] R. Stefl, M. Xu, L. Skrisovska, R. B. Emeson, F. H. Allain, Structure **14**, 345-355 (2006).

[Stern *et al.* 1986] J. H. Stern, U. B. Kaupp, P. R. MacLeish, Proc. Nati. Acad. Sci. U. S. A. **83**, 1163-1167 (1986).

[Strynadka *et al.* 1989] N. C. J. Strynadka, M. N. G. James, Annu. Rev. Biochem. **58**, 951-958 (1989).

[Szikra *et al.* 2008] T. Szikra, K. Cusato, W. B. Thoreson, P. Barabas, T. M. Bartoletti, D. Krizaj, J. Physiol. **586**, 4859-4875 (2008).

[Takano *et al.* 2004] Y. Takano, H. Ohguro, M. Dezawa, H. Ishikawa, H. Yamazaki, I. Ohguro, K. Mamiya, T. Metoki, F. Ishikawa, M. Nakazawa, Biochem. Biophys. Res. Commun. **313**, 1015-1022 (2004).

[Takemoto *et al.* 2009] N. Takemoto, S. Tachibanaki, S. Kawamura, Proc. Natl. Acad. Sci. U.S.A. **106**, 11788-11793 (2009).

[Tan *et al.* 2012] E. S. Tan, K. A. Krukenberg, T. J. Mitchison, Anal. Biochem. **428**, 126-136 (2012).

[Tata *et al.* 2015] M. Tata, C. Ruhrberg, A. Fantin, Mech. Dev. **138**, 26-36 (2015).

[Trost *et al.* 2016] A. Trost, S. Lange, F. Schroedl, D. Bruckner, K. A. Motloch, B. Bogner, A. Kaser-Eichberger, C. Strohmaier, C. Runge, L. Aigner, F. J. Rivera, H. A. Reitsamer, Front. Cell. Neurosci. **10**, 1-13 (2016).

[UniProt 2018] The UniProt Consortium, Nucleic Acids Res. **46**, 2699 (2018).

[Untergasser *et al.* 2007] A. Untergasser, H. Nijveen, X. Rao, T. Bisseling, R. Geurts, J. A. M. Leunissen, Nucleic Acids Res. **35**, W71-W74 (2007).

[Vallazza-Deschamps *et al.* 2005] G. Vallazza-Deschamps, D. Cia, J. Gong, A. Jellali, A. Duboc, V. Forster, J. A. Sahel, L. Tessier, S. Picaud, Eur. J. Neurosci. **22**, 1013-1022 (2005).

[Virág *et al.* 2013] L. Virág, A. Robaszkiewicz, J. M. Rodriguez-Vargas, F. J. Oliver, Mol. Aspects Med. **34**, 1153-1167 (2013).

[Vita *et al.* 2019] G. Vita, G. L. Vita, O. Musumeci, C. Rodolico, S. Messina, Neurol. Sci. **40**, 671-681 (2019).

[Vyas *et al.* 2013] S. Vyas, M. Chesarone-Cataldo, T. Todorova, Y.-H. Huang, P. Chang, Nat. Commun. **4**, 2240 (2013).

[Vyas *et al.* 2014] S. Vyas, I. Matic, L. Uchima, J. Rood, R. Zaja, R. T. Hay, I. Ahel, P. Chang, Nat. Commun. **5**, 4426 (2014).

[Wang *et al.* 2016] Y. Wang, R. An, G. K. Umanah, H. Park, K. Nambiar, S. M. Eacker, B. Kim, L. Bao, M. M. Harraz, C. Chang, R. Chen, J. E. Wang, T. Kam, J. S. Jeong, Z. Xie, S. Neifert, J. Qian, S. A. Andrabi, S. Blackshaw, H. Zhu, H. Song, G. Ming, V. L. Dawson, T. M. Dawson, Science **354**, aad6872 (2016).

[Wang *et al.* 2018] T. Wang, J. Reingruber, M. L. Woodruff, A. Majumder, A. Camarena, N. O. Artemyev, G. L. Fain, J. Chen, J. Biol. Chem. **293**, 15332-15346 (2018).

[Watanabe *et al.* 1996] T. Watanabe, S. Matsushima, M. Okazaki, S. Nagamatsu, K. Hirosawa, H. Uchimura, K. Nakahara, Dev. Brain Res. **94**, 60-66 (1996).

[Wei *et al.* 2012] T. Wei, T. Schubert, F. Paquet-Durand, N. Tanimoto, L. Chang, K. Koeppen, T. Ott, O. Griesbeck, M. W. Seeliger, T. Euler, B. Wissinger, J. Neurosci. **32**, 6981-6994 (2012).

[Wettengel *et al.* 2017] J. Wettengel, P. Reautschnig, S. Geisler, P. J. Kahle, T. Stafforst, Nucleic Acids Res. **45**, 2797-2808 (2017).

[Wetzel *et al.* 1999] R. K. Wetzel, E. Arystarkhova, K. J. Sweadner, J. Neurosci. **22**, 9878-9889 (1999).

[Wolfrum *et al.* 2018] U. Wolfrum, K. Nagel-Wolfrum, Klin. Monbl. Augenheilkd. **235**, 273-280 (2018).

[Wrogemann *et al.* 1976] K. Wrogemann, S. D. J. Pena, Lancet. **307**, 672-674 (1976).

[Wutz *et al.* 2002] K. Wutz, C. Sauer, E. Zrenner, B. Lorenz, T. Alitalo, M. Broghammer, M. Hergersberg, A. de La Chapelle, B. H. F. Weber, B. Wissinger, A. Meindl, C. M. Pusch, Eur. J. Hum. Genet. **10**, 449-456 (2002).

[Yamashima 2004] T. Yamashima, Cell Calcium **36**, 285-293 (2004).

[Yau *et al.* 1984] K. Yau, K. Nakatani, Nature **309**, 352-354 (1984).

[Zhang *et al.* 2011] Y. Zhang, S. J. Matkovich, X. Duan, A. Diwan, M. Y. Kang, G. W. Dorn II, J. Biol. Chem. **286**, 26943-26951 (2011).

[Zuker 2003] M. Zuker, Nucleic Acids Res. **31**, 3406-3415 (2003).

List of Figures

List of Tables

List of Abbreviations

RP	Retinitis Pigmentosa
BBB	Blood Brain Barrier
RPE	Retinal Pigment Epithelium
ONL	Outer Nuclear Layer
INL	Inner Nuclear Layer
GCL	Ganglion Cell Layer
OPL	Outer Plexiform Layer
IPL	Inner Plexiform Layer
EC	Endothelial Cells
HC	Horizontal Cells
MC	Müller Cells
BC	Bipolar Cells
AC	Amacrine Cells
PC	Pericyte
OS	Outer Segment
IS	Inner Segment
GFAP	Glial Fibrillary Acidic Protein
cGMP	Cyclic Guanosine Monophosphate

PDE	Phosphodiesterase
GC	Guanylyl Cyclase
ASO	Antisense Oligonucleotide
CNGC	Cyclic Nucleotide Gated Channels
PARP	Poly (ADP-ribose) Polymerase
GLUT 3	Glucose Transporter 3
VGCC	Voltage Gated Ca Channels
FADD	FAS Associated Death Domain
MTP	Mitochondrial Permeability Transition
AIF	Apoptosis Inducing Factor
RNF146	Protein Ring Finger 146
ARH	poly(ADP-Ribosyl) Hydrolase
MIF	Migration Inhibitory Factor
CaMK-II	Calcium Calmodulin Dependent Protein Kinase-II
PTPC	Permeability Transition Pore Complex
IMM	Inner Mitochondrial Membrane
OMM	Outer Mitochondrial Membrane
MCU	Mitochondrial Ca^{2+} Uniporter
MICU-I	Mitochondrial Ca^{2+} Uptake-I
NCKX	Na^{+} Ca^{2+} exchanger
P	Post-natal day
LCA	Leber Congenital Amaurosis
DMD	Duchenne Muscular Dystrophy
RNaseH	Ribonuclease H
2′Ome	2′Omethylation
mRNA	mature RiboNucleic Acid
SSO	Splice-Switching Oligonucleotide
NMD	Nonsense Mediated Decay

PS	Phosphorothioate
GARP	Glutamic Acid Rich Protein
PTC	Pre-mature Termination Codon
Mm	*Mus musculus*
Hs	*Homo sapiens*
ESE	Exonic Splice Enhancers
ss count	single strand count
PCR	Polymerase Chain Reaction
TNXL	Troponin C eXtra Large
ECFP	Enhanced Cyan Fluorescent Protein
AUC	Area Under the Curve
TUNEL	Terminal deoxynucleotidyl transferase dUTP Nick End Labeling
μM	micromolar
CNBD	Cyclic Nucleotide Binding Domain
EU	European Union
RD	Retinal Degeneration
PARP	Poly (ADP-Ribose) Polymerase
PAR	Poly (ADP-Ribose)
NAD^+	Nicotinamide Adenine Dinucleotide
ADP	Adenosine DiPhosphate
ART	ADP-RibosylTransferase
AIF	Apoptosis Inducing Factor
MIF	Migration Inhibitory Factor
PKG	ProteinKinase G
HDAC	Histone Deacetylases
GLUT 3	Glucose Transporter 3
DAPI	4′,6-diamidino-2-phenylindole
PNA	Peanut Agglutinin

ADAR	Adenosine Deaminases Acting on RNA
SLO	Scanning Laser Ophthalmoscopy
OCT	Optic Coherence Tomography
DHA	Dihydroartemisinin
DPI	Days Post Infection
ERG	Electroretinogram
BRB	Blood Retinal Barrier
GFP	Green Fluorescent Protein
RBC	Red Blood Cell
NKX	Na^+ K^+ exchanger
ER	Endoplasmic Reticulum
SOC	Store-Operated Channels
SOCE	Store-Operated Ca^{2+} Entry
GCAP	Guanylyl Cyclase Activating Protein
MTP	Mitochondrial Permeability Transition
ROC	Receptor-Operated Ca^{2+} Channels

Publications

List of publications

Parts of the thesis have been published/ in the process of publication as mentioned below. The data of the respective chapters are indicated against the publication.

- *Redefining the role of Ca^{2+}-permeable channels in hereditary photoreceptor degeneration using the D- and L-cis enantiomers of diltiazem*, **S. Das**, M. Power, V. Pop, K. Groeneveld, C. Melle, L. Rogerson, T. Euler, F. Schwede, F. Paquet-Durand, V. Nache (*Submitted*). This comprise parts of results from Chapter 3.

- *Photoreceptor cell death signals: cGMP or calcium*, **S. Das**, Y. Chen, J. Yan, G. Christensen, S. Belhadj, A. Tolone, F. Paquet-Durand.(*Submitted*)

- *Isolating mouse neuroretina with its RPE for organotypic explants cultured in serum free medium*, S. Belhadj, A. Tolone, G. Christensen, **S. Das**, Y. Chen, F. Paquet-Durand, J. Vis. Exp. **165**, e61868 (2020). This comprise one of the techniques mentioned in Chapter 2.

- *Cellular mechanisms of hereditary photoreceptor degeneration*, M. Power, **S. Das**, K. Schütze, V. Marigo, P. Ekström, F. Paquet-Durand, Prog. Retin. Eye Res. **74**, 100772 (2020).

- *A retinal model of cerebral malaria*, F. Paquet-Durand, S. C. Beck, **S. Das**, G. Huber, L. Chang, T. Schubert, N. Tanimoto, M. Garcia-Garrido, R. Mühlfriedel, S. Bolz, W. Hoffmann, U. Schraermeyer, B. Mordmüller, M. W. Seeliger, Sci. Rep. **9**, 3470 (2019). This comprise parts of results from Chapter 7.

In preparation

- *A novel strategy to achieve CNGC-isoform specificity within a pharmacological therapeutic scheme for retinitis pigmentosa*, S. Wucherpfennig, W. Haq, S. Das, V. Popp, C. Melle, A. Rentsch, F. Schwede, F. Paquet-Durand, V. Nache. (*in preparation*)

Awards

- Best Poster Award at "Hot Topics in Signal Transduction and cGMP", Tübingen, Germany in October 2018.
- Travel Fellowship Award for International Society for Eye Research ISER XXIII Biennial Meeting in Belfast, Northern Ireland in September 2018.
- Laboratory exchange grant by Graduate Training Centre of Neuroscience/ International Max Planck Research School and Centre for integrative neuroscience (CIN), University of Tübingen to Prof. Rob Collin's Laboratory, Department of Human Genetics, Radboud University Medical Centre (Radboudumc), Nijmegen, Netherlands from August 01-31, 2017.
- Research Fellowship by ProRetina-Stiftung Germany from August 1, 2016 to October 31, 2017 with conveyor no. Pro-Re/Prom-Stip/Paquet-Durand – Das.I-2016 entitled "Targetierung der CNG-Ca^{2+} Kanäle: Evaluation von Pharmakologischen und Genetischen 'knock-down' Ansätzen zur Behandlung der Retinitis Pigmentosa (Targeting CNG-Ca^{2+} channels: Evaluation of pharmacological and genetic 'knock-down' approaches for the treatment of retinitis pigmentosa)".

Statement of Contribution

Apart from the contributions mentioned in the following, the thesis comprise my original work. Light-induced Ca^{2+} response under two-photon was done in collaboration with Prof. Dr. Thomas Euler, Centre for Integrative Neuroscience, Tübingen. The experiments, light-induced Ca^{2+} response on cones, were done by Dr. Michael Power in Prof. Euler's laboratory. The data analysis of this experiment was done by Dr. Luke Rogerson and Prof. Dr. Thomas Euler. Figure 3.11 is prepared by Prof. Dr. Thomas Euler. This is a part of the manuscript which is submitted and they are the co-authors.

Assessment of the effects of D- and L-cis-diltiazem on heterotetrameric rod CNGA1:B1a and cone CNGA3:B3-channels expressed in *Xenopus* oocytes were done in collaboration with Dr. Vasilica Nache, University of Jena. The experiments, data analysis and the preparation of the Figure 3.10 was done by Dr. Vasilica Nache and her group members. This is a part of the manuscript which is submitted and they are the co-authors.

Site directed RNA editing was done in collaboration with Prof. Dr. Thorsten Stafforst, Department of Biochemistry, University of Tübingen. The preparation of RNA editing ASOs and the experiments on cell line were performed in Prof. Stafforst's laboratory. This is an ongoing collaborative project at this stage.

Master Students Marlly Archury and Alexander Günter contributed with immunostaining and data analysis for CNGB1 and PARP on my experimental sections as a part of their master project under my co-supervision. Laboratory of Prof. Dr. Ulrich Schraermeyer provided their help with the demonstration of sample preparation and electron microscopy.

Acknowledgments

I am very happy to be a part of this wonderful institution as well as wonderful people and receive a very good exposure for learning and discussion. For providing me with this opportunity I earnestly thank the director of our institute Prof. Dr. Marius Uffing and my doctoral supervisor Prof. Dr. François Paquet-Durand. I would like to thank my supervisor for his help and support for my project, collaborations and guiding me through the grant applications for my doctoral program to Deutscher Akademischer Austauschdienst (DAAD), ProRetina and the Deutsche Forschungsgemeinschaft (DFG).

I am very thankful to Prof. Dr. Bernd Wissinger and Prof. Dr. Thomas Euler for being in my thesis committee, guiding me through the project and providing me with valuable inputs for greater understanding of the field.

I would like to especially thank Dr. Tobias Bonifert for introducing me to the field of antisense technology and guide me through in the very initial phase with his expertise. I would like to thank Dr. Nicole Weisschuh, Dr. Peggy Reuter, Dr. Julia Felden and Dr. Tina Bayer for discussions and their guidance for troubleshooting in the experiments. I would like to take the pleasure to thank Prof. Dr. Rob Collin for welcoming me in his laboratory in Radboudumc, Department of Human Genetics, Nijmegen and Dr. Alex Garanto for helping me with his experience.

I would like to thank Mr. Norman Rieger for taking care of animals, Ms. Klaudija Massarini, Ms. Sylvia Bolz, Ms. Christine, Ms. Katrin Junger and Ms. Manuela Kübler for their technical guidance and support. I would like to thank Prof. Dr. Ulrich Schraermeyer, Dr. Sylvie Julien-Schraermeyer and Ms. Antonina for their special help in electron microscopy.

It is my immense pleasure to thank Prof. Dr. Thorton Strafforst for collaboration on site-directed RNA editing in the mouse tissue. I thank Dr. Jacquiline Wettengel, Dr. Tobias Merkle and Ms. Laura Pauss for various scientific and technical discussions in the project.

I would like to thank my friends and colleagues Dr. Michael Power, Ms. Soumaya Belhadj, Ms. Arianna Tolone, Ms. Yiyi Chen, Mr. Gustav Christensen, Mr. Alexander Günter, Ms. Marlly Archury and Ms. Maria Pia-Polito for making a very friendly and supportive laboratory for scientific discussions as well as moral support through the time during my accident.

I am very happy to thank Dr. Rudra Sekhar Manna, my life partner and a very good friend, who is a physicist himself and my sister Ms. Rituparna Das to be by my side during difficult times. I would like to thank my both father(s) Mr. Soumen Das and Mr. Asit Baran Manna, my mother(s) Mrs. Ruma Das and Mrs. Kalpana Manna, my brother-in-law(s) Mr. Chandra Sekhar Manna and Mr. Suvra Sekhar Manna, my sister-in-law(s) Mrs. Anindita Maiti and Mrs. Rituparna Jana for their understanding, trust and continuous motivation.

Last but not the least, I would like to give a very special and big thanks to Dr. Arijit Mukhopadhyay for his continuous motivation and support throughout my journey.

I would like to thank ProRetina and DFG (Deutsche Forschungsgemeinschaft) for funding my project, Graduate Training Centre and Centre for Integrative Neuroscience, Tübingen to finance me for laboratory exchange in Radboudumc, Department of Human Genetics, Nijmegen and ISER to give me a travel grant for attending the conference.

Soumyaparna Das

Tübingen, date 15.12.2020